

**SAKARYA UNIVERSITY
INSTITUTE OF SCIENCE AND TECHNOLOGY**

**IMPROVEMENT OF METAL-EPDM RUBBER
ADHESION BY PLASMA SURFACE
MODIFICATION**

M.Sc. THESIS

Fatma MIHÇI

**Field of Science : NANO SCIENCE AND NANO
ENGINEERING**

Supervisor : Assoc. Prof. Dr. Uğursoy OLGUN

January 2018

SAKARYA UNIVERSITY
INSTITUTE OF SCIENCE AND TECHNOLOGY

IMPROVEMENT OF METAL-EPDM RUBBER
ADHESION BY PLASMA SURFACE
MODIFICATION

M.Sc. THESIS

Fatma MIHÇI

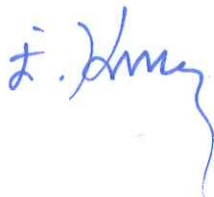
Field of Science : NANO SCIENCE AND NANO
ENGINEERING
Supervisor : Assoc. Prof. Dr. Uğursoy OLGUN

This thesis has been accepted unanimously by the examination committee on
29.01.2018

Prof. Dr.
İsmail KIRAN
Head of Jury

Assoc. Prof. Dr.
Uğursoy OLGUN
Jury Member

Prof. Dr.
Sefer Cem OKUMUŞ
Jury Member



DECLARATION

I declare that all the data in this thesis was obtained by myself in academic rules, all visual and written information and results were presented in accordance with academic and ethical rules, there is no distortion in the presented data, in case of utilizing other people's works they were refereed properly to scientific norms, the data presented in this thesis has not been used in any other thesis in this university or in any other university.

Signature

Fatma MIHÇI

28.03.2018

ACKNOWLEDGEMENTS

I express my sincere gratitude to Assoc. Prof. Dr. Uğursoy Olgun (Department of Chemistry) for his great contribution and support. I have benefited from his knowledge and experience during this master thesis. I also gratefully thank to Assist. Prof. Dr. Ekrem Altuncu (Material Science and Metallurgy Engineering) and Dr. Ali Erkin Kutlu (R&D Director, Standard Profil) for their fruitful discussions, support and encouraging me at all stages of the study. I would like to thank to Yusuf Güner, Galip Soyalp and Kübra Kılınaz (Standard Profil) for their great support during the experimental analyses. I also gratefully thank to Standard Profil Research and Development Laboratory in Düzce for sharing with me all test facilities, also for financial support and Thermal Analysis Laboratory located in Sakarya University for surface energy measurements.

This master thesis is supported by SAÜ Scientific Research Commission (BAP) (project number: 2018-50-01-002).

TABLE OF CONTENTS

ACKNOWLEDGEMENTS	i
TABLE OF CONTENTS	ii
LIST OF SYMBOLS AND ABBREVIATIONS	vii
LIST OF FIGURES.....	x
LIST OF TABLES.....	xv
SUMMARY.....	xvi
ÖZET.....	xvii

CHAPTER 1.

INTRODUCTION	1
1.1. Interface Bonding between Metal and Rubber.....	1
1.2. Interface Bonding Methods Used in Past and Today	3
1.3. Literature Survey Regarding Interface Bonding Between Metal and Rubber	4
1.4. Ethylene Propylene Diene Rubber (EPDM)	6
1.4.1. EPDM rubber compounding.....	9
1.4.1.1. Filler systems.....	10
1.4.1.1.1. Carbon black.....	10
1.4.1.1.2. Silica and silicates.....	10
1.4.1.1.3. Other filler systems.....	11
1.4.1.2. Stabilizer systems.....	11
1.4.1.3. Vulcanization system.....	11
1.4.1.4. Special materials.....	12
1.5. Importance of Interface Bonding Mechanism in Weather-Strip Industry	12

CHAPTER 2.

RUBBER TO METAL INTERFACE ADHESION.....	15
2.1. Rubber and Adhesive Characteristics in Terms of Interface Adhesion... 15	15
2.2. Theories of Adhesion.....	19
2.2.1. Mechanical theory.....	19
2.2.2. Electrostatic (electronic) interaction theory (acid-base theory)... 21	21
2.2.3. Diffusion theory.....	21
2.2.4. Wetting theory.....	22
2.2.5. Chemical bonding.....	23
2.2.6. Thermodynamic theory of adhesion.....	25
2.2.6.1. Surface tension or surface free energy (solid, liquid) and contact angle.....	25
2.2.6.2. Wetting, wetting criteria, and wettability.....	27

CHAPTER 3.

ADHESION BONDING PROMOTERS.....	29
3.1. Silane Adhesion Promoters and Its Chemistry.....	29
3.2. Bonding Mechanism to the Inorganic and Organic Substrates.....	32
3.3. How to Choose a Silane Coupling Agent.....	34
3.4. Nonsilane Adhesion Promoters.....	34

CHAPTER 4.

SURFACE PLASMA AND NANOTECHNOLOGY APPLICATIONS.....	35
4.1. Atmospheric Plasma.....	35
4.2. Material Processing with Atmospheric Plasma.....	37
4.2.1. Bulk materials treatments.....	38
4.2.2. Surface treatments.....	38
4.2.3. Surface coating.....	39
4.3. Coating Application by Atmospheric Pressure Plasma Polymerization..	41
4.4. Nanotechnology Surface Applications.....	42
4.4.1. Surface modification with nanoparticles.....	43

CHAPTER 5.

MATERIAL AND METHOD.....	46
5.1. Materials.....	46
5.1.1. Rubber.....	46
5.1.2. Metal.....	47
5.1.3. Interface coating materials.....	48
5.2. Interface Treatment and Adhesion Processes.....	48
5.2.1. Surface treatments by thermal ageing.....	48
5.2.2. Surface treatments by cold plasma.....	50
5.2.3. Interface coating application process.....	51
5.2.4. Interface adhesion process.....	51
5.3. Analysis and Measurement Methods of Interface.....	52
5.3.1. Wettability.....	53
5.3.2. Surface roughness.....	53
5.3.3. Coating thickness.....	54
5.3.4. T-peel strength.....	54
5.3.5. Weight change.....	55
5.3.6. Microscopic analysis.....	55
5.3.7. FT-IR analysis.....	55
5.3.8. Thermogravimetric analysis.....	55
5.3.9. Thermal analysis.....	56
5.3.10. Design of experiment (DEO) analysis.....	56

CHAPTER 6.

RESULTS.....	58
6.1. Surface Characterization of the Chemosil Coating on the Aluminum Surface.....	58
6.1.1. Ageing of Chemosil coating.....	58
6.1.1.1. Wettability characteristics of the thermally aged surfaces.....	58
6.1.1.2. Surface morphology change of the aged surfaces.....	62
6.1.1.3. Surface roughness change of the thermally aged	

surfaces.....	65
6.1.1.4. T-Peel strength test	69
6.1.1.5. Weight change after T-Peel strength test	73
6.1.1.6. FTIR analysis	76
6.1.1.7. Simultaneous thermal analysis (STA) of the Chemosil..	78
6.2. Plasma Effect on the Aluminum Surface in Terms of Interface Adhesion.....	79
6.2.1. Contact angle (CA) / Surface wettability	79
6.2.2. T-Peel strength test	80
6.2.3. FTIR Analysis	84
6.3. Surface Characteristics of the Improved Coating Materials	85
6.3.1. Wettability analysis.....	85
6.3.2. Surface morphology analysis	86
6.3.3. Coating thickness analysis	88
6.3.4. Surface roughness analysis.....	89
6.3.5. T-Peel strength test	90
6.3.6. Weight change after T-Peel strength test	91
6.3.7. Visual evaluation of the interface after T-Peel strength test.....	93
 CHAPTER 7.	
CONCLUSION	96
 REFERENCES.....	102
RESUME	106

LIST OF SYMBOLS AND ABBREVIATIONS

AA	:Aluminum alloy
AL	:Aluminum
APPT	:Atmospheric pressure plasma torch
APS	:Air plasma spray
ASTM	:American society for testing and materials
BTSE	:Bis-1,2-(triethoxysily)ethane
CB	:Carbon black
CR	:Chloroprene rubber
CTP	:N-Cyclohexylthiophthalimide
CVD	:Chemical vapor deposition
DAN	:6-diallylamino-1, 3, 5-triazine-2,4-dithiol monosodium salt
DBD	:Dielectric barrier discharge
DC	:Duty cycle / direct current
DCPD	:Dicyclopentadiene
DEO	:Design of experiment
DSC	:Differential scanning calorimetry
DTA	:Differential thermal analysis
DMA	:Dynamic mechanical analysis
EDS	:Energy-dispersive X-ray spectroscopy
EELS	:Electron energy loss spectroscopy
ENB	:Ethylidene norbornene
EPM	:Ethylene propylene monomer
EPDM	:Ethylene propylene diene terpolymer / Ethylene propylene diene rubber
ESCA	:Electron spectroscopy for chemical analysis

Eqn.	:Equation
EVA	:Ethylene vinyl acetate
f_{pe}	:Frequency of the electrons
f_{pi}	:Frequency of the ions
FTIR	:Fourier transform infrared spectrophotometer
G'	:Storage modulus
G''	:Loss modulus
GC	:Gas chromatography
GRC	:Glass run channel
HD	:Helium
HDMSO	:1, 4-hexadiene
HMDSN	:Hexamethyldisiloxane
HREELS	:Hexamethydisilazane
ICP	:High resolution electron energy loss spectroscopy
MIPs	:Inductive coupled plasma
MBPS	:Microwave induced plasmas
MS	: γ -methacryloxypropyltrimethoxysilane
NBR	:Mass spectroscopy or spectrometry
NMR	:Butadiene acrylonitrile rubber
NP	:Nuclear magnetic resonance
NR	:Nanoparticle
OH	:Natural rubber :Hydroxide / hydroxyl
OWB	:Outer waist belt
PAA	:Polyacrylic acid
PAM	:Polyacrylamide
PBD	:Polybutadiene
PCB	:Polychlorinated biphenyls
PCT	:Plasma cycle time
PECVD	:Plasma enhanced chemical vapor deposition
Pd	:Palladium
PEO	:Polyethylene oxide

phr	:Parts per hundred rubber
PM-IRRAS	:Polarization modulation-infrared reflection-adsorption spectroscopy
PMMA	:Poly(methyl methacrylate)
PSSNa	:Polysodium styrene sulfonate
PVC	:Polyvinyl chloride
PVD	:Physical vapor deposition
QD	:Quantum dot
R	:Radius
Ra	:Roughness, average in micro-meter & micro-inches
RBS	:Rutherford backscattering spectrometry
RF	:Radio frequency
SAM	:Self-organizing monolayer layer
SAMs	:Self-organizing monolayer layers
SB	:Scotch brite®
SBR	:Styrene-butadiene rubber
SEM	:Scanning electron microscopy
Si	:Silisyum
SIMS	:Secondary ion mass spectroscopy
SBR	:Stiren bütadien rubber
ShA	:Shore durometer hardness A
ShD	:Shore durometer hardness D
SPM	:Scanning probe microscopy
STA	:Simultaneous thermal analyzer
T	:Temperature
TEM	:Transmission electron microscopy
TEOS	:Tetraethoxysilane
TES	:6- (3-triethoxysilypropylamino) -1, 3, 5-triazine-2, 4-dithiol
TGA	:Thermogravimetric analysis
TMCSO	:Tetramethylcyclotetrasiloxane
TMDSO	:Tetramethyldisiloxane
TOF-SIMS	:Time of flight secondary ion mass spectrometry

UV	:Ultraviolet
VELS	:Vibrational electron energy loss spectroscopy
VOCs	:Volatile organic compounds
wt.	:Weight
WCA	:Water contact angle
ZDA	:Zinc diacrylate
γ	:Surface tension
γ_{LV}	:Surface free energy of liquid and vapor in the equilibrium state
γ_{SL}	:Surface free energy of solid and liquid in the equilibrium state
γ_{sv}	:Surface free energy of solid and vapor in the equilibrium state
θ	:Wetting or contact angle between solid-liquid interface

LIST OF FIGURES

Figure 1.1.	Commercially used diene containing monomers [28].....	9
Figure 1.2.	Position of the weather-strip profiles on a vehicle.....	12
Figure 1.3.	Schematic display of the roll forming and extrusion line [20].....	14
Figure 2.1.	Schematic display of a coil coating line.....	17
Figure 2.2.	Rubber to metal bonding interface adhesion reaction mechanism...	18
Figure 2.3.	Surface irregularity types occurred as a result of mechanical surface abrasion [34].....	21
Figure 2.4.	Electrical double layer at polymer-metal interfaces [31].....	21
Figure 2.5.	Diffusion theory of adhesion [34].....	22
Figure 2.6.	Examples of good and poor wetting by an adhesive spreading across a surface [31].....	23
Figure 2.7.	The structure of γ -glycidoxypropyltrimethoxysilane [1].....	24
Figure 2.8.	Schematic display of chemical bonding theory occurring at the interface [31].....	25
Figure 2.9.	Schematic of the contact angle that form a liquid drop on a solid surface [34].....	26
Figure 2.10.	Sessile drop method for calculation of contact angle (θ) or wetting angle [1].....	27
Figure 3.1.	Silane coupling agents –dual reactivity [31].....	30
Figure 3.2.	General structure of silane coupling agents [31].....	31
Figure 3.3.	Mechanism of organosilane deposition and reaction on a metal and further use [34].....	33
Figure 4.1.	Electrons and ions frequency in cold plasmas [40].....	36
Figure 4.2.	Commonly used monomers for the deposition of SiO ₂ coatings [42].....	41
Figure 4.3.	Schematic comparison between conventional polymers	

	and plasma polymers [42].....	41
Figure 4.4.	Shapes of different particulates [36].....	42
Figure 5.1.	Rigid and lanced aluminum alloy plates a) uncoated aluminum alloy substrate b) Chemosil coated aluminum alloy substrate c) lanced and uncoated aluminum alloy substrate.....	47
Figure 5.2.	Muffle furnace and metal sample hanger respectively.....	49
Figure 5.3.	The plasma treatment unit and plasma nozzle [47].....	50
Figure 5.4.	Coating application process to the surfaces of Aluminum and EPDM based rubber compound.....	51
Figure 5.5.	Sample holder that is used in the molding step.....	52
Figure 5.6.	Hot pressing machine.....	52
Figure 5.7.	KRUS contact angle-measuring system.....	53
Figure 5.8.	Mahr MarSurf PS1 surface roughness measurement device.....	54
Figure 5.9.	T-peel strength test of the interface of EPDM based rubber compound and AI strip.....	54
Figure 6.1.	Statistical parameters for surface energy of the thermally treated samples.....	59
Figure 6.2.	Statistical parameters for surface energy after removal of the effect of the factors' interaction.	59
Figure 6.3.	Statistical parameters for surface energy after removal of the statistically insignificant factors.....	60
Figure 6.4.	Interaction plot of the factors; time and temperature on the surface energy.....	61
Figure 6.5.	Pie chart of the factors; time and temperature on the surface energy.....	61
Figure 6.6.	Contour Plot of surface energy change after thermal treatments from 100°C to 360°C for 2, 4, 8, 16, 64 min. ageing conditions respectively.....	62
Figure 6.7.	Microscope images of the thermally aged samples at 100°C, 165°C, 230°C, 295°C and 360°C from top to down after 2, 8 and 64 min. thermal ageing from left to right respectively.....	63
Figure 6.8.	Statistical parameters for surface roughness of the thermally	

	treated samples.....	65
Figure 6.9.	Statistical parameters for surface roughness after removal of the effect of the factors' interaction.....	66
Figure 6.10.	Statistical parameters for surface energy after removal of the statistically insignificant factors.....	66
Figure 6.11.	Interaction plot of the factors; time and temperature on the surface energy.....	67
Figure 6.12.	Pie chart of the factors; time and temperature on the surface energy.....	67
Figure 6.13.	Contour Plot of surface roughness change after thermal treatments from 100°C to 360°C for 2, 4, 8, 16, 64 min. ageing conditions respectively	69
Figure 6.14.	Statistical parameters for T-peel Strength of the thermally treated samples.....	69
Figure 6.15.	Statistical parameters for T-peel Strength after removal of the statistically insignificant factors.....	70
Figure 6.16.	Interaction plot of the factors; time and temperature on the response of T-peel strength.....	71
Figure 6.17.	Pie chart of the factors; time and temperature on the surface energy.	71
Figure 6.18.	Contour Plot of T-Peel Strength after thermal treatments from 100°C to 360°C for 2, 4, 8, 16, 64 min. ageing conditions respectively.	72
Figure 6.19.	Images of the interface adhesion failures between Chemosil coated aluminum and EPDM surfaces after T-peel strength test. (a) Cohesion failure of EPDM at 100°C for 2, 4, 8, 16 and 64 min. and 165°C for 2 and 4 min., (b) Partially adhesion and cohesion failure at 165°C for 8 min., (c) Adhesion failure at 165°C for 16 and 64 min.....	73
Figure 6.20.	Statistical parameters for weight loss of the thermally treated samples.....	73
Figure 6.21.	Interaction plot of the factors; time and temperature on the	

	response of the weight loss.....	74
Figure 6.22.	Pie chart of the factors; time and temperature on the response of the weight loss.....	75
Figure 6.23.	Contour Plot of weight loss change after thermal treatments from 100°C to 360°C for 2, 4, 8, 16, 64. min. ageing conditions respectively.....	75
Figure 6.24.	Infrared spectra of untreated and thermally treated Chemosil coated aluminum surfaces under the following conditions: at 100°C and 165°C for 8 min.....	77
Figure 6.25.	Infrared spectra of untreated and thermally treated Chemosil coated aluminum surfaces under the following conditions: at 100°C and 165°C for 64 min.....	77
Figure 6.26.	Simultaneous thermal analysis of the Chemosil coating. The blue DSC thermal curve and the black TGA weight loss curve are displayed above..	78
Figure 6.27.	Wetting angle change of the uncoated dry aluminum and primer cCoated dry aluminum surfaces after plasma application...	80
Figure 6.28.	T-Peel strength forces of aluminum surfaces with EPDM.....	81
Figure 6.29.	Interface appearance of the samples after molding operation (a) uncoated rigid aluminum, (b) uncoated lanced aluminum, (c) Uncoated rigid and sand blasted Aluminum, (d) Uncoated rigid and plasma treated Aluminum, (e) Primer coated rigid Aluminum, (f) Primer coated rigid, plasma treated Aluminum.....	82
Figure 6.30.	EPDM coverage on the metal surface after T-peel test (%) by weight.	83
Figure 6.31.	Interface images of the coated and coated/plasma treated surfaces after T-Peel Strength test.....	83
Figure 6.32.	FTIR Infrared spectra of plasma treated / untreated primer coated aluminum surfaces.....	83
Figure 6.33.	Images of the coated aluminum surfaces with improved coating materials.....	84

Figure 6.34. Contact angle distribution of the improved coating materials 2A, 3A, 4A, 1B, 2B, 3B, 4B, 5B and 6B respectively under microscope.....	86
Figure 6.35. Surface morphology images of the improved coated materials of 1A, 2A, 3A, 4A, 1B, 2B, 3B, 4B, 5B and 6B respectively under microscope.....	87
Figure 6.36. Coating thickness distribution of the improved coating.....	89
Figure 6.37. Surface roughness distribution of the improved coating materials..	90
Figure 6.38. T-peel strength forces of the interfaces coated with improved coating materials.....	91
Figure 6.39. Weight changes of the (a) aluminum stripe and (b) EPDM based rubber plate after T-peel test.....	92
Figure 6.40. Images of the interfaces of “A” series coating applied between aluminum stripe and EPDM based rubber plate after T-peel test.....	95
Figure 6.41. Images of the interfaces of “B” series coating applied between.....	95

LIST OF TABLES

Table 2.1.	Bondability characteristics of different rubber types.....	15
Table 2.2.	Companies of rubber to metal interface adhesive products.....	16
Table 2.3.	Theories of adhesion [1]	19
Table 2.4.	Examples of energies of lifshitz-Van Der Walls interactions and chemical bonds [1]	23
Table 3.1.	Silane coupling agents; matching organic group to polymer type.....	31
Table 4.1.	List of thin film deposited by atmospheric plasma [42]... ..	40
Table 4.2.	Characteristics of different functional groups available for QD fictionalization [36]... ..	44
Table 5.1.	Component of the C073 compound.....	47
Table 5.2.	Improved coating mixtures' contents and their codes.....	49
Table 5.3.	Surface thermal treatment conditions.....	49
Table 5.4.	Experimental run performed based on factorial design platform in Minitab.....	57
Table 6.1.	Evaluation of the interfaces after T-peel test in terms of their adhesion ability to EPDM and AL.....	95

SUMMARY

Keywords: EPDM, Aluminum, Adhesion Strength, Nano Coating

In this study, the effect of different surface qualities and various adhesive grades on interface adhesion between EPDM (Ethylene-Propylene-Diene monomer) based rubber and AL alloy in 5754 grade was investigated. The EPDM-AI interface is widely used in outer waist belt (OWB) and glass run channel (GRC) roof profiles in automotive weather-strip profiles. In the current study, alternatives coatings of the current commercial Chemosil coating were studied. In this scope, all experiments were carried out with a widely used EPDM-based rubber compound in 80 ShA \pm 5 ShA hardness. The study consists of three categories in total. In the first step of the work, the surface characteristics of the existing coating material were examined and the optimum surface parameters required for adhesion were defined. In the second phase of the study, surface was modified at nano level via plasma application and its effect on the adherence strength was evaluated. In the final phase, the surface characteristics of the newly developed coatings that some of them are at nano level were examined and the results compared with Chemosil.

Surface characteristics of the coatings were evaluated by the analysis of CA, roughness, morphology under microscope, coating thickness, weight change FTIR, STA. Moreover, interface adhesion strength was defined by T-peel test.

METAL-EPDM KAUÇUK ARAYÜZEY YAPIŞMANIN PLAZMA YÜZEY MODİFİKASYONU İLE İYİLEŞTİRİLMESİ

ÖZET

Anahtar kelimeler: EPDM, Alüminyum, Yapışma Kuvveti, Nano Kaplama

Bu çalışmada bir EPDM (Ethylene-Propylene-Diene Monomer) bazlı kauçuğun 5754 sınıfı alüminyum alaşım metal plakasına yapışma mukavemetine, değişik yüzey kalitelerinin ve değişik yapıştırıcı cinslerinin yapışmaya olan etkisi araştırılmıştır. Söz konusu EPDM-AI arayüzeyi otomotiv sızdırmazlık profilleri içerisinde dış sıyrıcı ve cam kanal çatı profillerinde yaygın olarak kullanılmaktadır. Bu çalışmada ise mevcut durumda kullanılan Chemosil ticari kaplamasının alternatifleri üzerine çalışılmıştır. Bu kapsamda yaygın olarak kullanım gösteren 80 ShA \pm 5 ShA sertlikte tek tip EPDM bazlı kauçuk hamuru ile tüm denemeler gerçekleştirilmiştir. Çalışma toplamda üç kategoriden oluşmaktadır. Çalışmanın ilk etabında mevcut kaplama malzemesinin yüzey karakteristikleri incelenmiştir ve yapışma için olması gerekli optimum yüzey parametreleri tanımlanmıştır. Çalışmanın ikinci etabında ise yüzey plazma uygulaması ile nano boyutlarda aktive edildi ve yapışma kuvveti üzerine etkisi değerlendirildi. Çalışmanın son etabında ise bazıları nano boyutta olan yeni geliştirilen kaplamaların yüzey karakteristikleri incelenerek sonuçlar Chemosil ile kıyaslanmıştır.

Kaplamaların yüzey karakteristikleri ıslatma açısı, pürüzlülük, morfoloji, kaplama kalınlığı, ağırlık değişimi, FTIR ve STA gibi analiz yöntemleri ile değerlendirildi. Ayrıca arayüzey yapışma kuvveti de T-peel testi ile belirlendi.

CHAPTER 1. INTRODUCTION

1.1. Interface Bonding between Metal and Rubber

The use of rubber today finds a very wide range of application area such as; isolating vibration, reducing shock and seal in solids, liquids and gases. In the automotive sector, rubber to metal bonded dynamic applications such as engine mounts, bumper cross beams, door modules, suspension bushing, body mounts, torsional dumpers, helicopter rotor bearings, seismic bearings, transmission and axle seals are used in numerous areas. Moreover, rubber to metal bonded parts are also used in the different industries such as aerospace industries, biomedical applications and microelectronics. Correspondingly, rubber usages increases day by day in the different areas [1, 2].

The interest to the adhesion bonding technology in the combination of similar or dissimilar structural components increases each passing day. When two materials are brought in contact, the proper or adequate adhesion strength between them is of great importance, so it is necessary to device ways to attain the requisite adhesion strength between similar or dissimilar materials including the different combinations of metallic materials, polymers, composites materials and ceramics. Therefore, it is important that the interface phenomenon occurring between the different substrates is well-defined [1].

Two solid or liquid phases in contact have atoms/molecules on both sides of an imaginary plane called the interface. The adhesion bonding formed in the interface must have intrinsic adhesion forces and the magnitude and nature of those forces are

very important. The intrinsic adhesion refers the direct molecular forces of attraction between the adhesive and the substrates. Whereas, 'measured adhesion' refers the strength or toughness of an adhesive joint. The intrinsic adhesion between the adhesive and adhered arises from the fact that all materials have forces of attraction acting between their atoms and molecules, and a direct measure of these interatomic and intermolecular forces is surface tension. For this reason, it is important to determine the structure of the adhesive and adhered as atomic and molecular [1, 3, 4].

The molecular origin of the work of adhesion are the intermolecular attractive interactions. When two smooth polymer surfaces approach each other within a distance of a few nanometers, they jump into contact because of such intermolecular interactions as the universal van der Waals interactions and other types of specific molecular interactions such as polar interactions hydrogen bonding and acid-based interactions. In this way, interface is performed as a result of intermolecular interaction of the adherent and adhesive which takes properties of both materials in the near-interface region [1].

Adhesion is influenced mainly surface characteristics of the substrate and influenced by many factors such as type of adherents and adhesives, surface pre-treatment, adhesive thickness and bonding and testing conditions. Many issues have been unfolded because the subject of the adhesion is interdisciplinary. Despite working on interface adhesion phenomenon since long time, no single global theory or model can explain all the phenomena or mechanism due to adhesion is very complex phenomenon since it involves multidisciplinary knowledge of metallurgy, surface science, adhesion science, rubber chemistry and process engineering [1, 3].

Among the advantages of a robust interface formation, increased load bearing capacity, improved joint stiffness, more uniform stress distribution over a large area, good fatigue resistance, high strength in shear, low stress concentration at the edges, energy absorption reducing noise, vibration and so on properties take place. There is

a dual propose of proper adhesive choice at the interface; providing mechanical strength and seals the joints against moisture and debris ingress [1, 5, 6].

1.2. Interface Bonding Methods Used in Past and Today

Rubber to metal bonding was discovered as the result of the accidental bonding of the rubber to the brass during vulcanization. A breakthrough discovery was made by the development of the bonding agent codded as 220 in 1950s by the Lord [3]. The published studies regarding to rubber to metal bonding process are limited despite there is a long history of research and development. In terms of adhesive improvement, same situation is valid. There are a few reports about how to improve adhesive performance due to know-how belongs to adhesive manufacturers. [7].

Among the methods used in the rubber to metal bonding in the past, mechanical bonding and usage of ebonite take place. Mechanical bonding is still in use today, but it performs unstable interface. Ebonite is composed of mixture of the 30-40 phr (parts per hundred rubber) elemental Sulphur and natural rubber (NR). Normally in the composition of soft rubber compounds, Sulphur, which forms crosslinking between rubber molecules, is available less than 4 phr. Hard rubber or ebonite is formed when the Sulphur level I between 25-45 phr. Bonding with ebonite has very various disadvantages. One of the significant disadvantage, ebonite causes to quite weak bonding at high temperatures due to it is thermoplastic. Based on the Sulphur amount in the composition, ebonite exhibits thermoplastic transition temperature; i.e., softening between 70-80 °C.

Another method for interfacial bonding, the use of special metal alloys, which react and combine with Sulphur. For example, usage of the bismuth and arsenic with copper and zinc alloys. The alloys are electrically deposited to the metal surface and make bonding with the rubber during the vulcanization. Moreover, in the bonding of the rubber and iron or steel, electrodeposited brass is used. Bonding is realized as a result of the chemical interaction between Sulphur in the composition of the rubber and brass. However, this method requires machinery investment. The usage of the

isocyanates in the triphenylmethane triisocyanate is another bonding method. However, isocyanates has high sensitivity against of moisture and steam. It is difficult in terms of processability.

1.3. Literature Survey Regarding Interface Bonding Between Metal and Rubber

In literature studies up to now on metal to rubber bonding, the creation of interface bonding mechanism as the result of crosslinking has been proven in many of the studies. The release of the active groups on the surface as the results of the creation of the new chemical groups via plasma polymerization or removal of the pollution layer caused by carbon atoms and oils and also removal of the other contaminations from the surface have substantial impact on the adhesion phenomenon. Correspondingly, it was observed that the important parameter for the strong interface adhesion is the chemical composition and structure of the layers forming the interface. Among the techniques used to activate metal surface, plasma has been proven as the best technique to activate the surface [8].

Wang et al. have aimed to create self-organizing monolayer layers (SAMs) on the aluminum surface using the 6- (3-triethoxysilypropylamino) -1, 3, 5-triazine-2, 4-dithiol (TES) coupling agent to provide aluminum and EPDM interfacial adhesion via crosslinking. The functional structure designed at the EPDM-aluminum interface consists of two parts; (i) TES self-assembly monolayer is bound to aluminum through its ethoxy silyl functional group, (ii) and the thiol function group is strongly cross-linked to EPDM rubber. [9].

Roucoules et al. have aimed to form the interfacial covalent bond between interface coating material on the AI surface and elastomer (EPDM) during the cross-linking process occurring between elastomer (EPDM) and peroxide. This coating material including imide double bond has been generated via plasma polymerization on the aluminum surface by using monomer of maleic anhydride. The interfacial covalent bond formation has been aimed with incorporation of these double bonds during the cross-linking process between EPDM and peroxide [10].

Airoudj et al. have investigated the effect of the plasma duty cycle during plasma polymer deposition on the adhesion strength occurred at the interface of the EPDM/aluminum. The cross-linking degree between the EPDM and the plasma layer and the double bond density on the surface occurred as a result of the plasma polymerization were directly influenced by the plasma duty cycle. Alongside the intended functional structure at the low duty cycle, a thicker alkaline functionalized layer and strong interfacial adhesion have been achieved [11].

Roucoules et al. have aimed to create functional structures via plasma polymerization on both EPDM and aluminum surfaces. In this way, it was intended to thermally reversibly bond with the Diels-Alder reaction at the interface. The diene functional structure with maleic anhydride plasma polymerization in cyclohexane has been created on the aluminum surface. The maleic anhydride film layer formed by plasma polymerization on the EPDM surface reacts with the amine-terminated nucleophile [12].

Kang et al. have aimed to form nano-scale film from the 6-diallylamino-1, 3, 5-triazine-2,4-dithiol monosodium salt (DAN) via polymer plating on high ductile spheroidal-graphite cast iron. This film was intended for direct interface bonding as a result of cross-linking with EPDM [13].

Petersen et al. have investigated the formation of controlled interface chemical modification with allylamine atmospheric plasma polymerization, which leads to the formation of primary amino groups (new chemical structures) on the aluminum surface with the aim of increasing interface adhesion strength between aluminum and epoxy resin [14].

Batan et al. have conducted a study on the activation of the aluminum surface by using atmospheric plasma, vacuum plasma and immersion methods with bis-1,2-(triethoxysily)ethane (BTSE) (water based). It was found that atmospheric plasma oxidizes the surface more than other methods [15].

Diaz et al. have investigated the cleaning of the aluminum alloy (AA6063) surface via atmospheric pressure plasma torch (APPT). The effectiveness of the plasma on the surface activation have been evaluated based on the effect of the parameters such as the distance (2, 6 and 12 mm) between sample and torch, speed (1 and 10 m/min) and ageing duration (1, 24 and 48 hours) on the contact angle and surface energy. It was observed that increased surface wetness and stronger interfacial adhesion were obtained by high velocity and the decrease in plasma density and temperature at the minimum distance [16].

Saleema et al., has investigated the resistance of aluminum AA6061-T6 surfaces, which were oxidized with atmospheric pressure helium-oxygen plasma and activated via plasma after mechanical pre-abrasion, against time in terms of interface adhesion with two component epoxy resin. When the effectiveness of plasma treatment versus time (15, 45, 75 sec.) was assessed, the highest bond strength and the lowest contact angle were obtained after 15 sec. plasma application time. It was observed that the mechanical pre-abrasion increased the interface adhesion strength in terms of environmental resistance [17].

Williams et al., evaluated the effectiveness of helium and oxygen plasma in interface activation studies to improve adhesion between the aluminum-aluminum interfaces against sandblasting, sandblasting / plasma, sol-gel, and combinations thereof. Plasma has been found as the most effective method [18].

Sperandio et al., have investigated the effect of atmospheric plasma on the aluminum surface using plasma gas at different rates and the effectiveness of the oxidized surface in terms of interface adhesion strength [19].

1.4. Ethylene Propylene Diene Rubber (EPDM)

Ethylene-propylene rubbers are available in two different types; EPM and EPDM. Ethylene propylene monomer (EPM) is the copolymer of ethylene and propylene and it has saturated polymer chain and can only be cross-linked using peroxide cure

systems as it is fully saturated. Ethylene propylene diene monomer (EPDM) is the terpolymer of ethylene, propylene and non-conjugated diene with residual unsaturation in the side chain. The third monomer in the EPDM includes double bond. This enables a sulfur crosslinking. [20, 21, 22].

Although EPM can only be cured with peroxides; EPDM can be cured with both peroxide and sulfur. In the case of high heat requirements, EPDM should be cured with peroxide. Peroxide curing also provides compression set properties that are superior to those of Sulphur-cured EPDM compounds [21].

EPDM type rubbers are mostly used in the applications of automotive such as weather-strips, hose, tubing, insulation, and window gasket and wire-and-cable covers, single ply roofing and many other fields. EPDM is selected in the sealing industry due to its notable resistance against high and low temperatures, solar ageing, ozone and high elasticity under compression, high insulating, wide hardness range and low density.

Although, EPDM is resistance against of polar solvents such as ketones and alcohols, it has poor resistance against of aliphatic, aromatic, and chlorinated hydrocarbons. The price of the EPDM is competitive compared the other types of the rubbers due to EPDM can be highly loaded with low-cost fillers, including clays, silica, carbon black, and talc [1, 21, 23].

Ethylene, propylene and diene quantities are used in different ratios in the EPDM compounding formulation. The increase in the amounts of these gives EPMD compounding different properties. As the ethylene content increases, the polymer crystallinity increases. On the other hand, as the ethylene content decreases and propylene content increase, the polymer is increasingly amorphous. According to this change in the ethylene and propylene in the formulation, EPDM polymers are classified as semi-crystalline and amorphous. Semicrystalline grades generally have ethylene contents of 62 wt. % or greater, while amorphous grades generally have

ethylene contains of less than 62 wt. %. In the EDPM grades currently used commercially, ethylene content varies from 40 to 80 wt. % [21].

Amorphous or semi crystalline types of EPDM affects properties such as temperature resistance, hardness, elasticity, tensile strength, modulus and hardness on the final product. Amorphous grades of EPDM have more flexibility at low temperatures, lower in hardness. On the other hand, semi-crystalline grades have properties of higher green strength, higher tensile and modulus, and higher hardness. As the shortcomings of semi-crystalline grades, they have less flexibility at low temperatures and compression set [21].

In the EPDM compounding formulation, non-conjugated diene is used as third monomer in different proportions. It is known that as the diene increases in the EPDM formulation, the cure rate increases. For the effective Sulphur curing, approximately min 2% (by weight) diene is required. In the case of faster curing rate is required such as continuous cure lines and production of sponge materials, in which the blowing rates must be matched with very fast cure rate, diene levels greater than 6% (by weight) are preferred [21].

As the diene monomer used in the formulation of EPDM, there different types available commercially; ethylidene norbornene (ENB), which is in use most commonly, dicyclopentadiene (DCPD) and 1, 4-hexadiene (HD). Figure 1.1. shows the structures of these monomers. As it is seen from the structures, these monomers are consisting of two double bonds, one of which is consumed during the polymerization reaction, while the other remains in the resulting polymer [21].

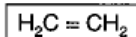
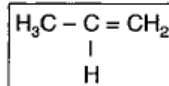
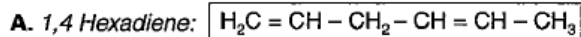
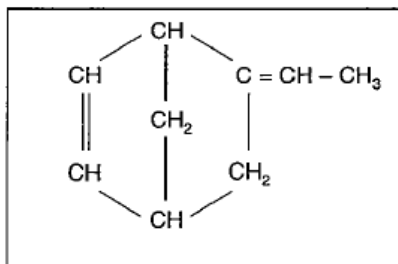
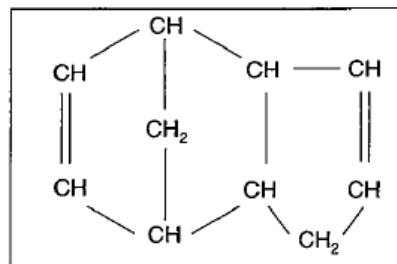
I. Ethylene:**II. Propylene:****III. Diene Containing Monomer:****B. Ethylidene Norbornene (ENB):****C. Dicyclopentadiene (DCPD):**

Figure 1.1. Commercially used diene containing monomers [21].

1.4.1. EPDM rubber compounding

Compounding is revealed within the tire and rubber industry, the art and science of selecting various compounding ingredients to optimize properties to meet a given service application or set of the performance parameters of the final product. The final products could be tires, conveyor belts, large dock fenders, building foundations, automotive engine components, and a wide range of domestic applications in different rubber compound formulations [21, 24].

Rubbers are used in the form of vulcanized with the vulcanizing agent such as sulfur in most cases and peroxide. Since rubber has many different application areas from automotive to domestic usage, numerous different functional and material properties are needed. Therefore, rubber recipes are prepared using different additives to meet this requirement. Rubber compounding is a multidisciplinary science including materials physics, organic polymer chemistry, inorganic chemistry, and chemical reaction kinetics [24, 25].

The rubber compound formulation also referred as recipe is divided into five categories;

- Polymers: Natural rubber, synthetic polymers.
- Filler systems: Carbon black, clays, silicas, calcium carbonate.
- Stabilizer systems: Antioxidants, antiozonants, waxes.
- Vulcanization system components: Sulfur, accelerator, activators.
- Special materials: Secondary components such as pigments, oils, resins, processing aids, and short fibers [24].

1.4.1.1. Filler systems

Filler systems referred also as reinforcing agents are carbon black, clays, silica, calcium carbonate and reinforcing resins. They are added to compound formulation to fulfill the materials and functional properties such as tensile strength and abrasion resistance [21, 24].

1.4.1.1.1. Carbon black

Carbon black (CB) comprises about 30% of most rubber compounds. It is derived from combustion or thermal decomposition of hydrocarbons. It has excellent properties such as smallest particle size, highest oil resistance, color strength, cost effectiveness and UV performance. Since proving high UV resistance properties, CB is widely used as black pigment for thermoplastic applications [21, 26].

1.4.1.1.2. Silica and silicates

Silica in the rubber recipe provides properties of improved in tear strength, reduction in heat buildup, and increase in compound adhesion in multicomponent products such as tires. While selecting the proper silica for the rubber compounds, fundamental properties of silica such as ultimate particle size and extent of hydration should be taken into consideration [24].

1.4.1.1.3. Other filler systems

Other filler systems include kaolin clay (hydrous aluminum silicate), mica (potassium aluminum silicate), talc (magnesium silicate), limestone (calcium carbonate), and titanium dioxide. Clays used in the formulation provides improved tear strength, an increase in modulus, improved component-to-component adhesion in multicomponent products, and improved aging properties. Calcium carbonate is mostly used as a low cost filler and titanium dioxide is used where the appearance is important [24].

1.4.1.2. Stabilizer systems

Carbon-carbon double bonds provides unsaturated nature to the elastomer causing non-resistance against of oxygen, ozone, and thermal degradation. That is why, it is important to antidetergents including antioxidants, antiozonants and waxer. These include chemical classes such as p-phenylene diamines, substituted phenols, and quinolones [21, 24].

1.4.1.3. Vulcanization system

Vulcanization describes the process by which physically soft-compounded rubber materials are converted into high-quality engineering products. A typical vulcanization system is consisting of activators, vulcanizing agents and accelerators [32]. Activators are chemical additives, which provides activation of the accelerator. The vulcanization activator systems are consisting of zinc oxide and stearic acid. As the vulcanizing agents, sulfur, insoluble sulfur and peroxides are mostly used in the rubber formulation. Accelerators are used in to formulation to accelerate the cure and crosslink density and reduce vulcanization time. Mostly used accelerators are sulfenamides, thiazoles thiurams, dithiocarbamates, and guanidines [21, 24].

1.4.1.4. Special materials

Filler systems, stabilizers systems and vulcanization systems are primary additives in the compounds formulation. There are also secondary additives such as processing aids, resins and coloring agents.

1.5. Importance of Interface Bonding Mechanism in Weather-Strip Industry

Rubber to metal interface bonding process is widely used in the production of the weather-strip in automotive industry. Weather strips are consisting of dynamic seals and static seals on vehicle body. Dynamic seals are door, trunk, dust and hood profiles. Static seals are glass run channels and inner/outer belt seals as shown in Figure 1.2. Weather strips are used to seal window, door, hood, decklid, and sun-roof openings from noise, dust, dirt and rain. Additionally, they retain heat in the winter/air conditioning in the summer, maintains clean glass surface by inner and outer waist belts and sustains ice release properties between surface for ease of opening power windows and doors. Weather-strips around the trunk, the hood, and the door openings provide a buffer between the metal frame and the closure panel, reducing metal on the metal noise [27].

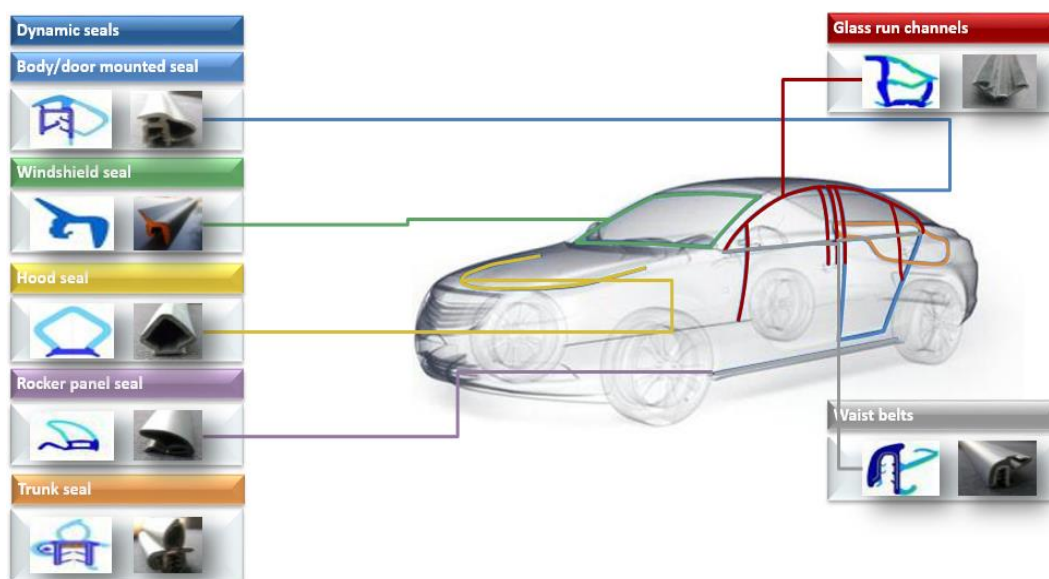


Figure 1.2. Position of the weather-strip profiles on a vehicle.

Performance and service life of these weather strip profiles play active role based on their qualifications; strength properties in internal / external working conditions, compressibility performance, resistance against of UV and hot-cold-moisture atmosphere, abrasion and corrosion resistance. Design capability, material selection, process and assembly capability are effective factors in the success of a weather strip. Rubber based profiles proceed with extrusion process have different geometries and designs based on their position on the vehicle body as shown in Figure 1.2. [28].

In the production of automotive weather strip profiles by means of a co-extrusion process, EPDM based rubber materials are widely used and preferred due to their qualifications of high resistance against of ozone and severe atmospheric conditions, high elasticity, low density, wide range of hardness (30 ShA-50 ShD), wide service range (-40 °C / 120 °C), easy processability. EPDM is the main raw material in the compound formulation and constitutes on average 30% of the composition. The other components in the formulation are carbon black, mineral oils, mineral fillers, various accelerators and processing aids [20, 29].

Weather strip profiles are produced in different designs and dimensions in the extrusion die. The process occurs as following; the specially formulated solid state EPDM mixture is melted (180-220 °C) to the two-sided thin sectioned, rigid or laced strips made of aluminum alloy (AA5754) simultaneously in the extrusion die. [30].

Metal carrier provides structural integrity through the weather strip. Aluminum alloys as metal carrier are widely used in the production of weather strip due to low cost, lightweight and resistance properties against of corrosion. In the manufacturing process, an elastomeric material of ethylene propylene diene monomer (EPDM) based rubber extrudes over and bonded to support carriers in an extrusion line. Extrusion line process is consisting of accumulator, roll former, extruder, rubber cure oven, cooler and air knife, and chopper as illustrated in Figure 1.3. In the working principle of the extrusion line, metal carrier coil is unwound and fed through a series of rollers, and then is pre-formed by roll-formers according to the engineering design of the profile cross section. Then the formed metal carrier is fed to the extruder and

combined with EPDM rubber. In the extruder, EPDM rubber is mixed and heated by screw feed mechanism. The custom-engineered die at the end of the extruder reveals the weather strip profile at the desired dimensions. In many cases, extrusion line does not include a pre-treatment process of the metal surface. Hence, metal parts are supplied as coated. During this extruder process, first intimate contact with coated metal and EPDM rubber occurs under heat and compression. Correspondingly, crosslinking of the EPDM rubber formulation in itself and between coating on the metal and EPDM is occurred. Therefore, the extruder temperatures play important role in terms of curing of both EPDM and coating material on the metal surface. If the higher temperatures occur, interface adhesion is deteriorated due to degradation of the coating material [27].

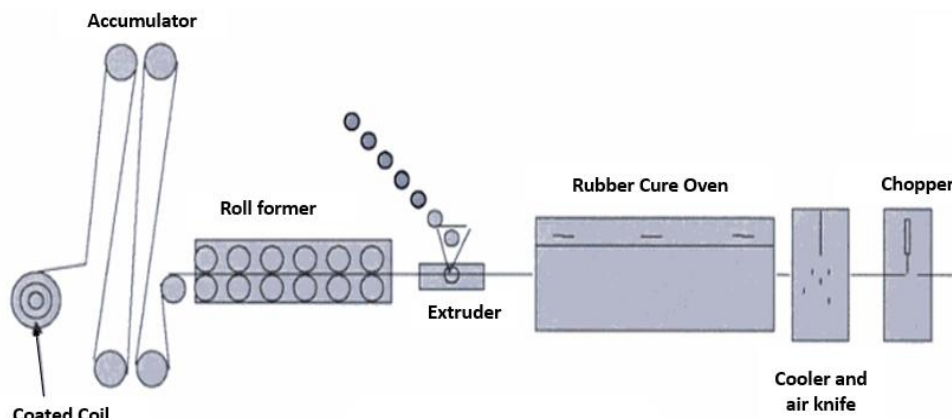


Figure 1.3. Schematic display of the roll forming and extrusion line [27].

Especially in the analysis of user complaints and production scraps, it is demonstrated that aluminum alloy and EPDM rubber interface properties are the primary parameters affecting performance. In these profiles, where good adhesion is not obtained, the EPDM is separated from the metal surface and therefore weather strip profiles loses its functional and appearance properties that are expected itself, thus having a critical level in terms of competitiveness and quality level and production productivity [11]. Therefore, EPDM-aluminum interface surface characteristics were deeply investigated in this master thesis. Moreover, it is aimed to improve coating materials including Nano sized materials as the alternative coating materials to the commercial coating of Chemosil.

CHAPTER 2. RUBBER TO METAL INTERFACE ADHESION

2.1. Rubber and Adhesive Characteristics in Terms of Interface Adhesion

There are numerous commercial rubber to metal interface adhesion products. In terms of interface adhesion force, selection of the rubber type is also a crucial parameter. Generally, there is a hierarchy between the rubber types according to their ability to bond with the adhesive. This hierarchy is attributed based on their polarity, chemical reactivity, solubility and molecular symmetry. Table 2.1. shows the bondability characteristics of different rubber types.

Table 2.1. Bondability characteristics of different rubber types

Easiest to bond	Nitrile (acrylonitrile-butadiene) rubber (NBR) Polychloroprene (CR) Styrene butadiene rubber (SBR) Natural rubber or polyisoprene (NR or IR) Ethylene propylene diene rubber (EPDM)
Most difficult to bond	Isobutylene-isoprene (butyl) rubber (IIR)

The second crucial parameter in the rubber to metal bonding process is a suitable choice of adhesive. In general, there are many factors that are effective in selecting the appropriate adhesive system; type of rubber, surface preparation of substrates, adhesive preparation, adhesive application and molding process to perform the bonding. Besides, adhesive should have wet substrate, spread equivalent / uniform on the surface and compatible with the rubber type used. Frequently, adhesives are chosen empirically due to their adhesion mechanism at the interface is not well understood [3, 7].

Today, many companies produce adhesives for rubber-metal bonding. Some of known companies and their adhesive products for rubber to metal interface are shown in Table 2.2.

Table 2.2. Companies of rubber to metal interface adhesive products.

Company	Tradename
Lord Chemical Products Division of Lord Corporation	Chemlock
Henkel KGaA (Lord licensee)	Chemosil
Morton International	Thixon
Metallgesellschaft	Megum
Par Chemie	Parlok
Compounding Ingredients Limited (CIL)	Cilbond
Metalok	Metalok
Proquitec	Adetec

Another important point for an equal, uniform and wet substrate adhesive in the interface is the adhesive application method. There are eight different application methods available; brushing, dipping, electrostatic, flow coating, coil coating, roller, sponging, spraying. The choice of application method depends on the size and shape of the parts and the number of parts to be coated and whether the coating will be entire surface or partially [1]. The most common method is coil coating, which is the continuous application of a primer and an adhesive to one or both sides of a metal coil. As depicted in Figure 2.1., a cleaned and treated metal coil is uncoiled, run through a roll coat setup, and followed by a bake cycle to dry/set the primer. The coating and baking steps are repeated for the topcoat adhesive application. There are numerous advantages of this coating method; 100% transfer efficiency of the primer and the coating, fast line speed proving large quantity of coated substrate quickly, ability of coating both surface at one time, controlling of the wet and dry film thickness within a very tight tolerance, controlling over the cure state [3, 27].

The adhesion mechanism of the rubber to metal interface is not very well understood until now. Primers and adhesives used with the purpose of rubber to metal bonding are custom formulated products.

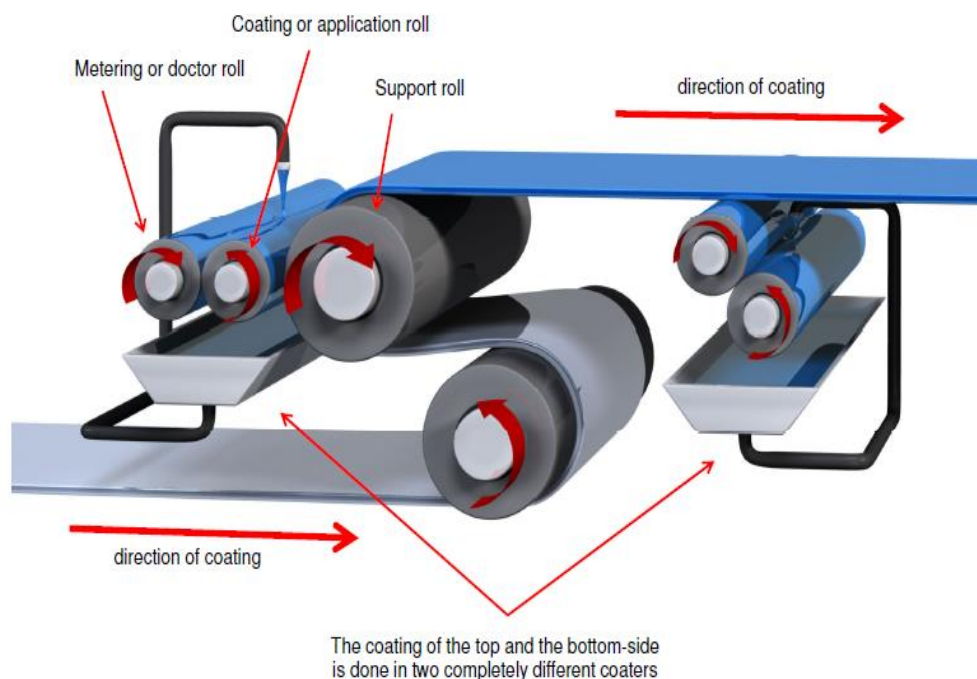


Figure 2.1. Schematic display of a coil coating line.

Primers including halogenated rubber and resin enable wetting of the metal surface. Moreover, organic resin forms chemical bonding with the metal during the vulcanization and provide barrier against of corrosion migration. Polymers are used in the formulation with the purpose of forming better coating film. During the interface adhesion, resin and rubber form interpenetrating network of polymer chains [3, 7].

Polymer ingredients available in the formulation of adhesive are used to provide compatibility with the rubber and ingredients in the primer formulation. Most of those rubbers are halogenated polymer based. Adhesives also include powerful curatives to provide reaction between polymer used in the adhesive and rubber.

The rubber to metal bonding process also has a complex mechanism because many reactions occur simultaneously. All these must occur in a very short time due to the necessity of rubber to be cured within the time of curing. Reactions occurred at the interface is shown in Figure 2.2.

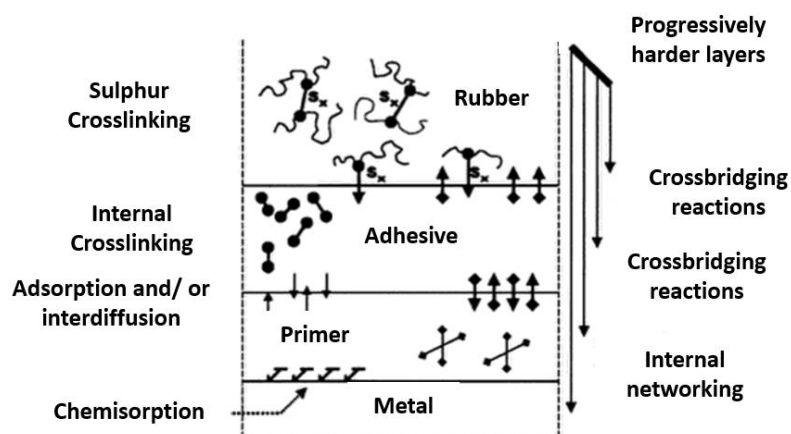


Figure 2.2. Rubber to metal bonding interface adhesion reaction mechanism [3].

In the process of rubber to metal bonding, each three organic layers; primer, adhesive and rubber, are either cross-linked or cured during the molding step. Each three organic layer interacts with its top and bottom layer via same chemical ingredients, which provide internal crosslinking. Crosslinking reaction occurs via heat reactive resins or crosslinking agents, which are added to the formulation externally. Figure 2.2. illustrates the vulcanization bonding process occurring between rubber and metal. The first reaction named chemisorption occurs at the primer and metal interface. Organic resins available in the primer formulation form covalent bonding with metal oxides, which take place at the metal surface. The next reaction occurs via diffusion or migration of the curative agents available in the adhesive into the primer layer during the vulcanization and this enables chemical bonding between primer and adhesive. Moreover, the polymeric film formers in the primer diffuse and knit with the adhesive layer due to compatibility properties of the polymers used in the primer and adhesive formulation. The final link occurs at the adhesive and rubber interface via diffusion of the curative agents available in the adhesion layer into the rubber during the vulcanization process. The bonding reaction occurring at the final interface is named as cross bridges. Moreover, this can be distinguished from the crosslinking reaction occurring within rubber. In addition, Sulphur available in the rubber formulation diffuses to the adhesive layer and this enables additional cross bridge [3].

2.2. Theories of Adhesion

Adhesion mechanism is the interatomic and intermolecular interaction at the interface of two similar or dissimilar substrates and depends on surface characteristic of materials in question. Because it is crucial to know the surface mechanisms and interfacial variables [7]. Surface chemistry, physics, rheology, polymer chemistry, mechanics of materials, polymer physics, fracture analysis are important in terms of adhesion characteristics. It is impossible to explain the bonding mechanism, which occurs at the interface with a single bonding mechanism. Adhesion phenomena at the interface is a complex structure and includes more than one surface mechanism. In the literature, bonding mechanisms at the interface are as follows; (i) diffusion, (ii) mechanical, (iii) molecular and chemical and (iv) thermodynamic adhesion. Table 2.3. shows the 5 different mechanism, which occurs at the interface [1, 8, 23].

Table 2.3. Theories of adhesion [1]

Adhesion Type	Scale of Action
Mechanical theory	Microscopic
Electrostatic (electronic) interaction theory (acid-base theory)	Molecular
Diffusion theory	Molecular
Adsorption / surface reaction	
Wetting theory	Molecular
Chemical bonding	Atomic
Acid-base theory of adhesion	Molecular
Thermodynamic theory of adhesion	
Surface tension or surface free energy (solid, liquid) and contact angle	Molecular
Work of adhesion	Molecular
Wetting, wetting criteria, and wettability	Molecular

2.2.1. Mechanical theory

In mechanical theory, adhesion occurs by penetration between the pores, cavities and other surface irregularities on the surface. In other words, adhesion occurs with mechanical interlocking of a polymer adhesive into the pores and other superficial asperities of a substrate. The fact behind this is that the adhesive is replaced by trapped air at the interface. Accordingly, the surface roughness and porosity of the surface are important in terms of wettability and mechanical interlocking. It is open

to debate that the mechanism providing adhesion is whether mechanical interlocking or increase at adhesive contact surface [1, 23].

Different type of surface irregularities are available as a result of abrading the surface as shown in Figure 2.3. Type A and C could only improve the adhesion strength for given directions of the applied force [14]. Type B can form more suitable and stable mechanical interlocking. Because of increased surface roughness, mechanical interlocking, formation of a clean surface, formation of a highly reactive surface and an increase contact area could be improved [23].

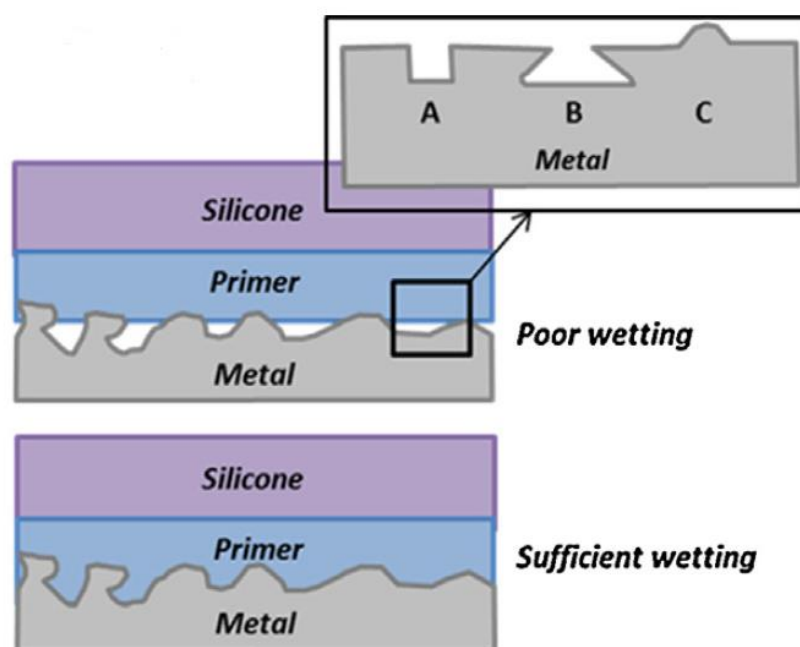


Figure 2.3. Surface irregularity types occurred as a result of mechanical surface abrasion [34].

The mechanical interlocking model can be effectively applied in situations where the substrate are impermeable to the adhesive and where the surface of the substrate is sufficiently rough. In the literature, there are proven data for and against it. So bonding durability could be improved or declined as a result of surface roughness increase [1].

2.2.2. Electrostatic (electronic) interaction theory (acid-base theory)

Electrostatic interaction theory is valid for the incompatible interfaces such as polymer and metallic substrates. Based on this theory, interface adhesion occurs as a result of electrostatic effect between adhesive and adherent. Due to unlike electronic band structure of the adhesive and adherent, electron transfer occurs at the interface and interfacial adherence occurs by mutual sharing of the electrons.

As shown in Figure 2.4, development of electrostatically charged double layers at the interface as a result of interactions of different two substrates which have different charges of positive and negative. This theory is not directly effective or major contributor on the interface adhesion [1, 23].

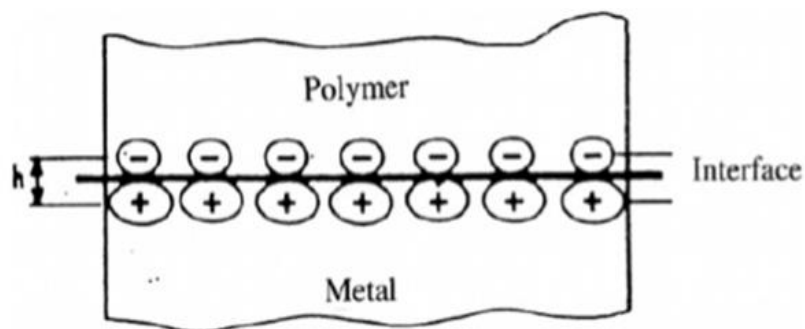


Figure 2.4. Electrical double layer at polymer-metal interfaces [31].

2.2.3. Diffusion theory

In interdiffusion theory, adherent and adhesive materials, which are mutually miscible and compatible polymers, adhere with macromolecular interdiffusion at the interface as shown in Figure 2.5. This theory applies to cases where the adherent and adhesive are long chain polymers [1, 23].

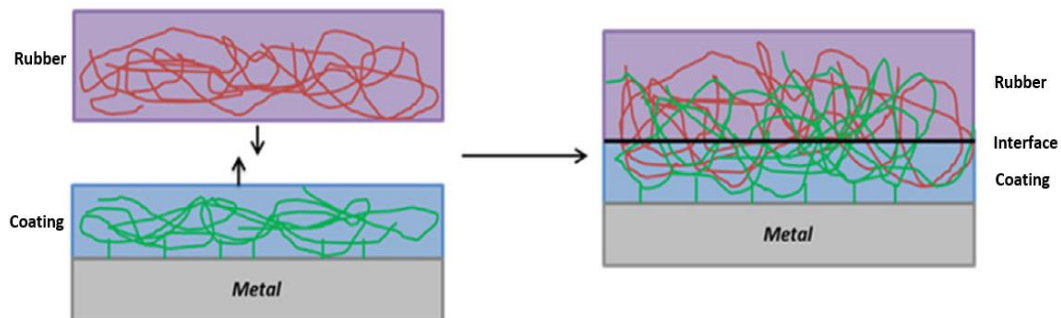


Figure 2.5. Diffusion theory of adhesion [34].

Inter-diffusion is optimal when the solubility characteristic of both polymers are equal. The parameters effecting the inter-diffusion are the chain length of the macromolecule, the concentration c , and the temperature T .

Diffusion model of adhesion does not contribute to adhesion if the substrate polymers are crystalline or highly cross-linked or if contact between two polymeric phases occurs far below their glass transition temperature or adhesive and substrate are not soluble [1].

2.2.4. Wetting theory

According to this theory, adhesion occurs through the molecular contact of two materials and by surface forces developing between them. The main step in the bonding is the formation of interfacial forces between the two surfaces; adhesive and adherent. Therefore, it is known as wetting that continuous contact between two surfaces occurs. To provide wetting on the adherent surface, surface tension of the adhesive must be lower than adherent. Figure 2.6. illustrates the complete and incomplete wetting stages of the same adherent to different surface properties. Good wetting could be occurred as a result of exhibiting good flow through valleys and crevices on the adherent surface. On the other hand, poor wetting occurs between the adhesive and the adherent in the presence of air bubbles or solvent residue. In cases of poor wetting, interfacial defects are observed. The main criterion for achieving a good interface wetting is that the adherent surface energy is higher than the adhesive [23].

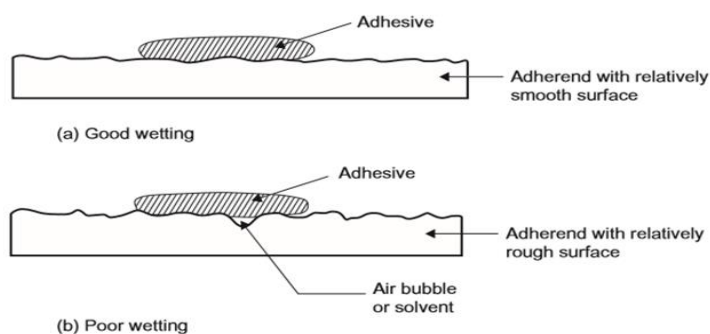


Figure 2.6. Examples of good and poor wetting by an adhesive spreading across a surface [23].

2.2.5. Chemical bonding

Chemical bonding creates an enhanced interface between two similar or dissimilar surfaces. The bonding that occurs at the interface is usually primary bonding, such as ionic, covalent and metallic bonding. Table 2.4. shows the energies of these chemical bonds. The chemical bonding at the interface occurs between chemical grouping on the adhesive surface and a compatible chemical group in the adherent. Whichever of these bonds occurs at the interface is entirely related to the chemical structure of the surfaces. Moreover, interfacial strength depends on number and type of chemical bonds. Atomic or molecular transport, by diffusion process, is involved in chemical bonding.

Covalent and ionic bonds are the strongest among the chemical bonds. In addition to chemical bonds in the interface bonding mechanism, mechanical interlocking, diffusion or electrostatic mechanisms can contribute to the bonding.

Table 2.4. Examples of energies of lifshitz-Van Der Walls interactions and chemical bonds [1].

Type	Example	E (kJ/mole)
Covalent	C-C	350
Ion-ion	$\text{Na}^+ \cdots \text{Cl}^-$	450
Ion-dipole	$\text{Na}^+ \cdots \text{CF}_3\text{H}$	33
Dipole-dipole	$\text{CF}_3\text{H} \cdots \text{CF}_3\text{H}$	2
London dispersion	$\text{CF}_4 \cdots \text{CF}_4$	2
Hydrogen bonding	$\text{H}_2\text{O} \cdots \text{H}_2\text{O}$	24

Covalent bond formation usually occurs on cross-linked adhesives and thermoset coatings. The presence of mutually reactive chemical groups are required to form this bond. This bond usually forms the strongest and most durable interface. Methods such as corona and flame treatment can be used for the formation of the functional structures required on the surface to initiate covalent bond formation.

Particularly for dissimilar interfaces, coupling agents are used as chemical bridges to create compatibility between two surfaces and to improve joint strength.

In addition to the improvement in joint strength, a significant enhancement of the environmental resistance of the interface or durability of the adhesive joints, in particular to moisture, can be achieved in the presence of such coupling agents at elevated temperatures. Silane based coupling agents are most commonly used. Figure 2.7. illustrates the structure of the silane-coupling agent.

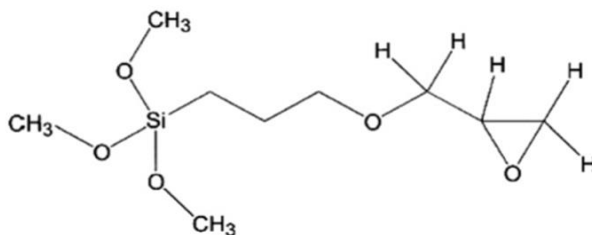


Figure 2.7. The structure of γ -glycidoxypropyltrimethoxysilane [1].

Silane based coupling agents have a unique hybrid chemical structure which can react chemically at both ends, with the substrate on one side and the polymer on the other side as shown in Figure 2.8. In silane species, organofunctional structures are more widely used between polymeric and inorganic surfaces. The general structure of silane is $X_3Si(CH_2)_nY$. Where X is a hydrolyzable (generally alkoxy) group capable of reacting with the substrate and Y is the organofunctional group selected for bonding to polymer. Oxone bonds are created with the hydroxyl groups of inorganic surfaces, which are reversible in nature, and it may also interact with the polymer matrices to form covalent bonds with the reactive functional groups of the

polymer or form interpenetration polymer networks, or combination of the two [1, 23].

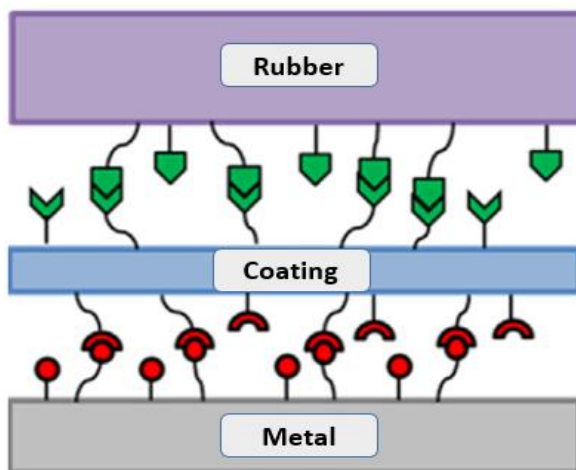


Figure 2.8. Schematic display of chemical bonding theory occurring at the interface [31].

2.2.6. Thermodynamic theory of adhesion

2.2.6.1. Surface tension or surface free energy (solid, liquid) and contact angle

The adhesion formed in the interface must have intrinsic adhesion forces and the magnitude and nature of those forces are very important. The intrinsic adhesion between the adhesive and adherent arises from the fact that all materials have forces of attraction acting between their atoms and molecules, and measurement of interatomic and intermolecular forces gives surface tension. The molecular origin of the work of adhesion are the intermolecular attractive interactions. When two smooth polymer surfaces approach each other within a distance of a few nanometers, they jump into contact because of such intermolecular interactions as the universal van der Waals interactions and other types of specific molecular interactions such as polar interactions, hydrogen bonding and acid-base interactions. Van der Waals forces directly relate to fundamental thermodynamic parameters, such as the free energies of the adhesive and substrate, and allow a reversible work of adhesion of the materials to be calculated for the materials in contact. This means that work of adhesion can be calculated by contact angle and surface tension of the liquid [1, 4].

The tension in the surface layer is the result of the attraction of the bulk material for the surface layer and this attraction tends to reduce the number of molecules in the surface region resulting in an increase in intermolecular distance. This increase requires work to be done and returns work to the system. This explains why surface tension exists and why there is a surface free energy.

As shown in Figure 2.9., according to the Young's equation, most liquid surfaces are wetted at a certain level and show surface angle. The surface angle in the static system can be measured in the equilibrium state. Interfacial tension is determined as γ , which represents the level of equilibrium at the intersection of the three phases. The L, S and V subscripts represent the solid, liquid and vapor phases, respectively. γ^o indicates that the solid phase is in balance with the vapor phase of the liquid. That is, the film is adsorbed on the solid surface. Young shows this with equation 2.1.

$$\gamma_{LV} \cdot \cos\theta = \gamma_{SV} - \gamma_{SL} \quad (2.1)$$

Where, γ_{LV} is the surface free energy of liquid and vapor in the equilibrium state (mJ/m^2) (or the surface tension of the liquid, mN/m), γ_{sv} the surface free energy of solid and vapor in the equilibrium state, γ_{SL} the surface free energy of solid and liquid in the equilibrium state and θ is the wetting or contact angle between solid-liquid interface [1, 4].

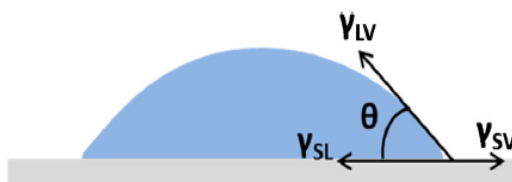


Figure 2.9. Schematic of the contact angle that form a liquid drop on a solid surface [34].

The contact angles also known as wetting angle indicates the intersection of three interphases, separating different material phases in the equilibrium state and determines three phase interface morphologies.

Surface energies are associated with formation of adhesive bond. The angle of contact θ formed on the surface of the adhesive applied to the solid surface is related to the surface energies as described in the Young's equation.

As shown in Figure 2.10., the contact angle (wetting angle) can be measured by the sessile drop method by using series of test liquids. To calculate the contact angle, eqn. 2.2 is used. Where h is the height of the drop on the solid surface, r is the radius of the spherical segment [1].

$$\text{Contact angle } (\theta) = \sin^{-1} \frac{2rh}{r^2 + h^2} \quad (2.2)$$

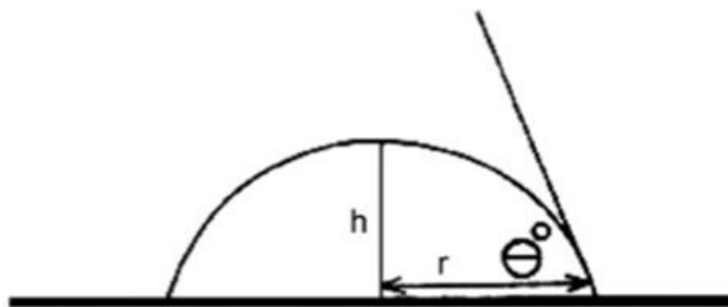


Figure 2.10. Sessile drop method for calculation of contact angle (θ) or wetting angle [1].

2.2.6.2. Wetting, wetting criteria, and wettability

For a good interfacial adhesion, it is necessary to make the adhesive homogeneous on the adherent surface. The basic principle of homogeneous diffusion is related to the surface energies of the adhesive and adherent. In addition, this diffusion is called wetting. The wetting of both surfaces, i.e. metal by primer and primed metal by the rubber essential for obtaining homogeneous interfaces [31].

Adhesives that have surface energies less than that of the adherent will readily wet the surface and form good bonds. This situation is explained in eqn. 2.3.

$$\gamma_{SV} \geq \gamma_{SL} + \gamma_{LV} \quad (2.3)$$

The different surface free energies between the adhesive and the adhesive release the extent of wetting. Wetting between two different surfaces are occurred as a result of (a) acid-base interactions, (b) weak hydrogen bonding or (c) van der Waals forces (dipole-dipole and dispersion forces).

The surface energy of the adhesive is lower than the surface energy of the adherent, the adhesive spreads on the surface, and in this case, the energy change that occurs is called the spreading coefficient or spreading energy as shown in eqn. 2.4. If S is positive, it indicates that the adhesive is completely homogeneous on the surface, whereas negative indicates that it is partially diffused [1].

$$S = \gamma_{sv} - \gamma_{LV} - \gamma_{SL} \geq 0 \quad (2.4)$$

CHAPTER 3. ADHESION BONDING PROMOTERS

Adhesion promoters or coupling agents enhance the interfacial adhesion between the organic polymer and the inorganic substrate. Organic and inorganic materials can not establish a strong interface bonding due to their different properties such as compatibility, chemical reactivity, surface properties and coefficient of thermal expansion. For this reason, an adhesion promoter is used at this stage to bond the different surfaces to each other. The use of adhesion promoters chemically and physically affects the adhesion of the interface as well as acts as a "glue" or compatibility bridge to increase the bonding strength of the different interfaces.

Adhesion promoters have dual functionality in molecular structures. A central metal atom such as silicon, zirconium, titanium and aluminum (especially the metal atom containing the methoxy, ethoxy or hydroxyl groups) gives the inorganic reactivity to adhesion promoters. In addition, organofunctional groups attach to the metal atom via alkylene, arylene, or other types of organic bridges in order to provide organic reactivity to the adhesion promoters.

Inorganic reaction groups self-condense to give the oligomeric structure to adhesion promoters. The oligomeric adhesion promoters have dual or multi-functionality and structural integrity. Thus, a strong and stable chemical bond is formed between two different organic and inorganic structures. Organosilane coupling agents within adhesion promoters are predominant chemical type of adhesion promoters [23, 31].

3.1. Silane Adhesion Promoters and Its Chemistry

Silane coupling agents are used as bonding or bridging agents between organic (such as an organic polymer, coating, adhesive) and inorganic phases (such as glass, metal,

or mineral). Correspondingly, they provide adhesion between two different types of materials as shown in Figure 3.1. Silane adhesion promoter used in interfacial bonding has unique physical and chemical properties. At the interfaces where silane is used, increased bonding strength and resistance against of humidity and other severe environmental conditions are observed.

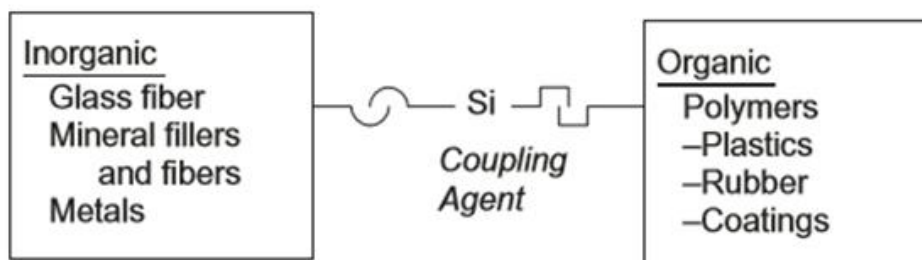
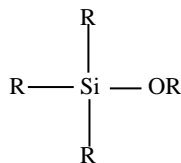


Figure 3.1. Silane coupling agents –dual reactivity [23].

Silicon and carbon are in the same element family in the periodic table. However, silicon shows significant differences in terms of chemical reactivity. Silicon is more electropositive than carbon and therefore does not form stable double bonds and is capable of special, useful chemical reactions. Silane has a unique structure that contains both organic and inorganic reactivity in a single molecule structure, allowing it to be used as adhesion promoters. The structure of adhesion promoters with silicon-based chemical functionality consists of four different or the same substituents attached to a single silicon atom.

As shown in Figure 3.2., most common structure of the silane-coupling agent is consisting of three inorganic-reactive alkoxy groups, methoxy or ethoxy and one organic group. Organic group could be reactive (amino, epoxy, methacrylate, etc.) or unreactive (methyl, buthyl, octyl, phenyl, etc.). There are coupling agents in different organofunctional structures. Table 3.1. shows mostly used coupling agents. There is a correlation between the physical and chemical properties of both coupling agents and the polymer species [23].



R = alkyl, or organofunctional group

OR' = methoxy or ethoxy

Figure 3.2. General structure of silane coupling agents [23].

Table 3.1. Silane coupling agents; matching organic group to polymer type [23].

Chemical Type	Chemical Name	Polymer
Amine	Aminopropyltriethoxysilane	Acrylic, nylon, epoxy, phenolics, urethanes, melamines, PVC, nitrile rubber
Diamine	Diaminopropyltrimethoxysilane	Acrylic, nylon, epoxy, phenolic, melamines, urethanes, nitrile rubber, PVC,
Methacrylate	3-Methacryloxypropyltrimethoxysilane	Unsaturated polyesters, acrylics, Polyolefin, EVA,
Epoxy	3-Glycidoxypropyltrimethoxysilane	Epoxy, PBT, urethanes, acrylics, polysulfides
Methyl	Methyltrimethoxysilane	Hydrophobing agents for mineral surfaces
Isobutyl	Isobutyltrimethoxysilane	Hydrophobing agents for mineral surfaces, masonry water repellent
Phenyl	Phenyltrimethoxysilane	Hydrophobing, dispersing aid for mineral surfaces, blend, hydrophobe, thermal stability
Octyl	Octyltrimethoxysilane	Hydrophobing for mineral surfaces; dispersion of minerals in polyolefins; masonry water repellent
Vinyl	Vinyltrimethoxysilane	Graft to polyethylene for moisture, crosslinking, EPDM rubber, SBR, polyolefin

3.2. Bonding Mechanism to the Inorganic and Organic Substrates

The inorganic reactive groups attached to the silicon atom of the silane coupling agent structure are usually rapidly and dynamically bonded to inorganic substrates containing silicon, aluminum, or most heavy metals. When the coupling agent is attached to the inorganic surface, surface chemistry and surface reactivity characteristics of the inorganic substrate anymore exhibits the surface characteristics of the coupling agent. Thus, the treated surface exhibits the characteristics of the surface properties of the organic groups bound to the coupling agents [23].

Organosilane adhesion exhibits different adhesion properties to the inorganic substrates. The difference adhesion characteristics are arising from structure of the oxide layer and the concentration of hydroxyl functions available at the inorganic surface. For that reason, sufficient and suitable surface treatments play a critical role on the inorganic surface prior to application of adhesion material [31].

The organosilane structure is consisting of three hydrolysable groups and one organic functional group. Functional groups such as vinyl and amino act as coupling agent. This promotes the adhesion to the organic substrate. The reaction of silane coupling agents between organic and inorganic substrates involves four steps as following. In addition, reaction are illustrated in Figure 3.3.

- a. First step hydrolysis reaction of alkoxy group in the presence of water or ethanol, converting siloxane groups into silanol groups.
- b. Second step condensation reaction occurs between silanol groups, which leads to the formation of oligomers.
- c. Formation of the hydrogen bonds as a result of reaction between reactive hydrogen groups on the silanol groups and hydroxyl groups on the inorganic substrate.
- d. Interfacial reactions during the curing step. (i) Interfacial condensation of the functional groups occurs and water is released. (ii) Interfacial chemical reactions

with the organic substrate. The organic functional groups of the silane reacts with organic surface (polymer) during the vulcanization process [23, 31, 32, 33]

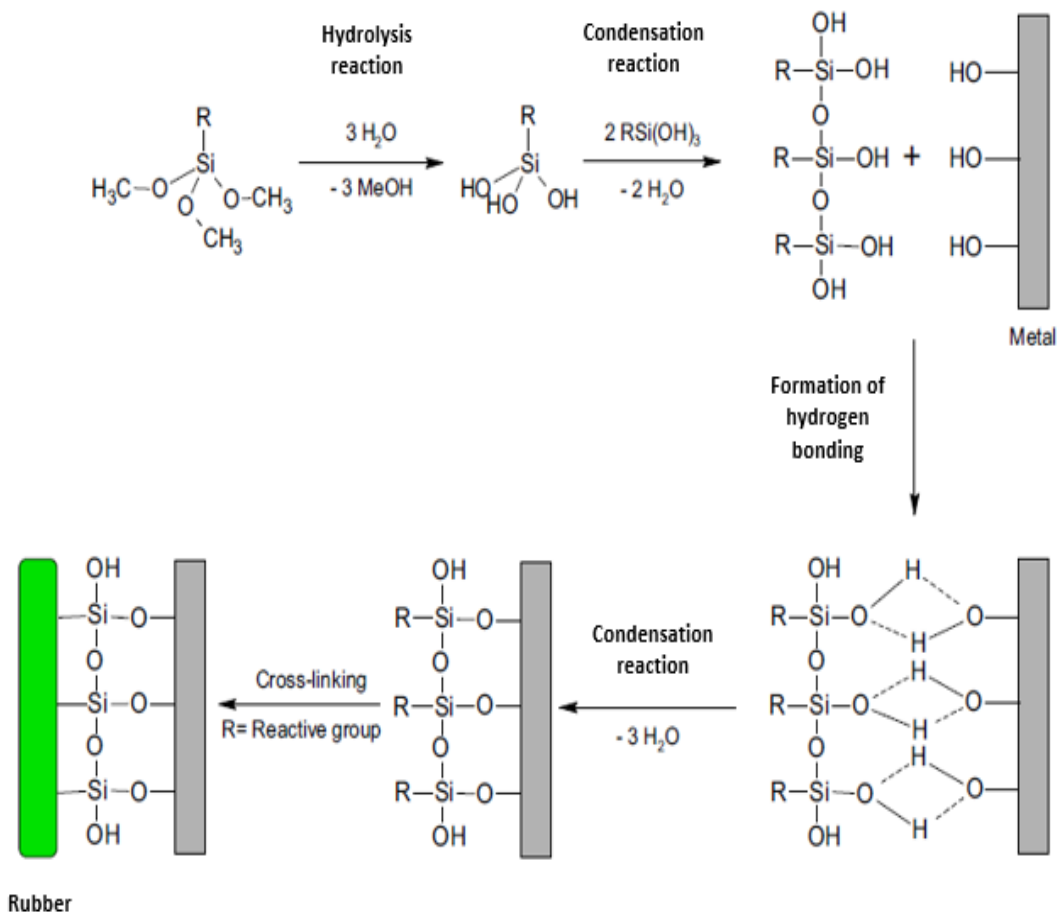


Figure 3.3. Mechanism of organosilane deposition and reaction on a metal and further use [31].

The interaction of the silane-coupling agent with the organic polymer is more complex with respect to the interaction with the inorganic substrate. Therefore, matching of the bonding mechanism between thermoset polymer and coupling agent should be considered. The intended / desired bonding takes place when the organofunctional groups of coupling agents are involved in the curing mechanism or reactively attach to the polymer structure i.e., in the curing mechanism of the epoxy resin, either epoxysilane or aminesilane could participate [23].

3.3. Choosing a Silane Coupling Agent

In choosing a good silane-coupling agent, the type of the organic groups of the organism should be taken into account first. The organofunctional group on the silicon atom determines which type of polymer can be bonded to the coupling agent. Meanwhile, chemical nature of the organic material determines the effectiveness of the coupling agent [23].

3.4. Nonsilane Adhesion Promoters

Adhesion promoters used except silane have the same concept of chemistry with silane. They are only based on the other kind of metallic element. They have inorganic reactivity on metallic atom, and organofunctional groups such as methacrylate, carboxylate. Organo-titanates, organo-zirconates and zircoaluminates are the other types of adhesion promoters. Especially in metallic applications, the high metallic structure of zircoaluminates provides fast / easy reactivity with metal. Similarly, organo-titanates are known as excellent wetting agents and provide an intimate contact between the adherent and the adhesive. Another type of adhesion promoters are based on maleation of polypropylene, polyethylene and other thermoplastic polymers. This polymer backbone in the coupling agent structure is interpenetrating into ethylene, propylene and other thermoplastic polymers. Accordingly, bonding between adhesion promoters and polymers occurs through van der Waals or other atomic forces. The carboxyl group on the coupling agent enables interaction and bonding to inorganic substrates such as metal [23].

CHAPTER 4. SURFACE PLASMA AND NANOTECHNOLOGY APPLICATIONS

Plasma is the fourth state of the matter and chemically active media. Plasma gas is generated by applying thermal or electric current or electromagnetic radiation energy into neutral gas, a fraction of gas particles can be converted (ionized) into charged particles to form plasma. Hence, they consist of positive (and negative) ions and electrons, as well as neutral species, which are in fundamental and excited states. It is partially or fully ionized gas. Much of the visible matter in the universe is in the plasma state. Therefore, 97% of the universe is consisting of plasma. [34, 35].

Plasma systems can generate low or very high temperatures based on their activation and working power. Hence, they are classified as cold (atmospheric or glow discharge) which involve high chemical reactivity or thermal plasmas (arc and inductive coupled plasma ICP discharges). Plasma technology finds application in a quite wide range area such as surface coating and treatment, waste destruction, gas treatments, chemical synthesis, machining due to wide temperature range. In terms of surface treatment application, several treatments can be made such as cleaning (grease removal decontamination); etching; functionalization (electrical conductivity, chemical barrier); activation (adherence or anti adherence properties) [34, 36].

4.1. Atmospheric Plasma

Atmospheric plasma also referred as “high pressure” plasma is operated at ambient temperature and at non-equilibrium. Application capabilities of non-equilibrium atmospheric plasmas are quite broad due to their gas temperatures ranging from room temperature to 1000°C. Plasma process is clean and environmental-friendly, which can easily applied to in-line production applications mostly in surface

treatment and thin film deposition. This technology found a great interest due to its low cost application and elimination of constraints compared to vacuum based plasma technologies. One of the main advantages of the plasma is that, they can be applied to any kind of substrates: from steel or glass, to highly temperature sensitive materials such as plastics, or even textiles.

Vacuum based plasma technologies used widely in past are not appropriate in terms of continuous in-line manufacturing due to difficulty of movement the sample in and out of vacuum system. Moreover, contrary to vacuum plasmas, atmospheric plasmas avoid the use of expensive pumping systems, the building of complex transfer chambers from air to vacuum and vice versa, with a high-pressure gap. Therefore, different types of atmospheric plasma processes were developed. The plasma parameters, such as current, power, gas flow and composition, and voltage are easy to control in terms of processing. The excitation frequency of the plasma is important due to influencing the behavior of the electrons and the ions. Figure 4.1. shows an example of the variation range for f_{pe} (frequency of the electrons) and f_{pi} (frequency of the ions) in cold plasmas. Correspondingly, atmospheric plasma sources are classified into three groups based on their excitation mode.

- the direct current (DC) and low frequency discharges,
- the plasma which are ignited by radio frequency (RF) waves,
- the microwave discharges [33, 34].

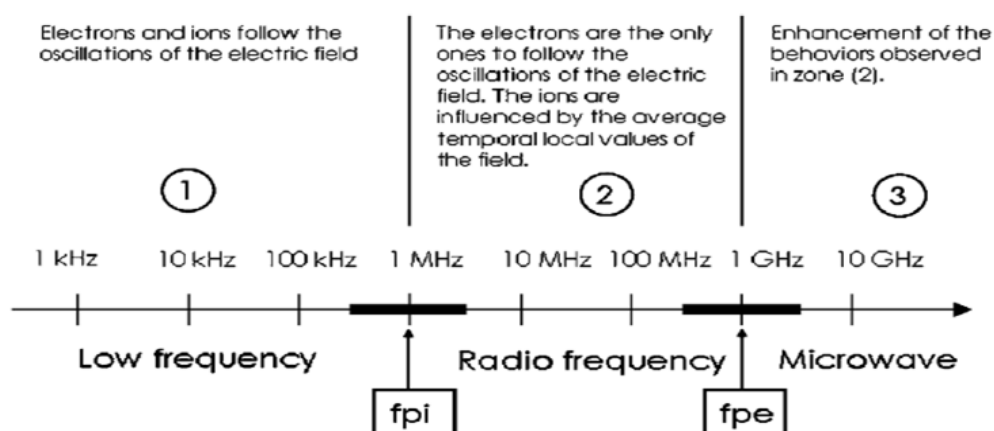


Figure 4.1. Electrons and ions frequency in cold plasmas [34].

Direct current (DC) and low frequency discharges are worked with a continuous or pulsed mode based on their design. In the continuous working mode: the arc plasma torches are fed by a DC power supply and temperature varies from 8 000 K to 15 000 K, which enables high temperature applications. The arc is ignited between the cathode and the anode and ionizes the plasma gas. The pulsed working mode is consisting of three types; corona discharge, dielectric barrier discharge (DBD), the one derived from corona process and micro plasma. In the corona discharge, DC power is pulsed and plasma creates lighting crown around the wire. The most popular cold atmospheric plasma sources are based on DBD, which is a device consisting of two plane-parallel metal electrodes covered at least one of them with a dielectric layer. Plasma gas flows in the gap. The gas is ignited by a power source [34, 37].

Radio frequency (RF) sources can work with a high or low power supply based on their design. This effects the application properties of the plasma [34].

Microwave induced plasmas (MIPs) are consisting of a microwave power source (power supply, magnetron and circulator to protect the magnetron from the reflected power), microwave equipment (wave-guides, tuning system), an ignition system and gas injections. In the working principle, microwaves are guided along the system and transmitted energy to the plasma gas electrons. Thus, the gas partially ionized and became plasma, which supports microwave propagation [34]. There are some disadvantages of using MIP systems; (i) high power is often required for plasma generation and (ii) the size of the plasma can be enlarged waveguide dimensions [37].

4.2. Material Processing with Atmospheric Plasma

Application of cold atmospheric plasma in surface processing and film deposition widely takes place during the last decades. Primary applications include surface pretreatment, cleaning, activation or passivation, deposition of films and post-treatments of coated surfaces in order to change the chemical composition or

crystallinity of the coating. Material processing can be divided into three categories [34, 37].

- Bulk material treatments
- Surface treatments
- Surface coating

4.2.1. Bulk materials treatments

In the bulk material treatments, high temperature plasma type is used. Therefore, the plasma sources are arc or microwave plasmas. Fine particle treatments, toxic waste treatments, material machining treatment (for example welding or cutting) and metallurgical treatments could be done by using atmospheric plasma technique [34].

4.2.2. Surface treatments

Surface treatment process is consisting of cleaning (removal of the decontaminants and grease), etching, functionalization (electrical conductivity, protection against corrosion, chemical barrier) and activation (adherence or anti adherence properties). As the surface cleaning process, halogenated solvents were widely used in past. Since strict environmental rules on the use of hazardous and toxic solvents, plasma surface cleaning process is improved. It is easy to clean the surface from oil, dust, oxides, biological and chemicals agents by using low temperature plasmas (cold plasma). Surface etching consists of removing the organic materials from the treated surface. Adherence and anti-adherence surface activation can be made by plasma. Surface activation occurs by grafting chemical functions (plasma active species) on the surface to provide adherence or anti adherence properties to the surface. Surface adherence properties are defined by used gas in the plasma systems. For example, ArCF₄ plasma makes the surface fluorination and hydrophobic, and leads to anti-adherence properties. On the other hand, oxygen, nitrogen, argon and so on based plasmas lead to the grafting of polar and hydrophilic functions (oxygen groups) and

provides increased surface energy and correspondingly decreased contact angle [34, 37].

4.2.3. Surface coating

Surface properties of the materials are modified by many technologies to deposit the appropriate coatings with the purposes of chemical barrier, corrosion resistance and electrical conductivity while the intrinsic bulk properties remain unchanged. Plasma discharge technology is a promising coating application process due to inhibiting numerous challenges such as control of the chemistry and structure of the layer, adhesion of the layer on a substrate, deposition rate, geometric concerns, minimizing energy injected and so on [34, 38].

In the coating deposition history, there are mainly two kinds of methods available; physical (PVD) and chemical vapor (CVD) deposition techniques. PVD consists of a physical process to deposit thin coatings by the condensation of a vaporized form of a solid precursor. In the chemical vapor deposition technique, gaseous or vapor of a liquid carried by gas precursors reacts with another molecule in the gas phase at high temperature environment or substrate to create the molecule of interest that will deposit to form the coating. The disadvantage side of this technique is the thermal constraints [38].

Two kinds of atmospheric plasma coatings are developed:

- Air plasma spray (APS)
- Plasma enhanced chemical vapor deposition (PECVD)

The working principle of APS coating technique consists of the injection of the coating material in the form of fine powder suspended in the carrier gas into plasma jet, where powder particles are accelerated and heated. Then the high velocity molten or semi molten particles strike the substrate surface where they are flattened and then dramatically frozen. Plasma jet temperature reaches up to temperatures of 15 000 K and this provides broad range of application of different materials. On the other hand,

this technique does not find wide application due to the fundamentals of this process are not completely identified [34].

In the PECVD coating technique, the precursors mostly, gas (or liquid carried by gas) are introduced to the reaction chamber where chemically reactive (plasma) media is available to activate the coating reactions. The reactive species are carried to surface and they are absorbed. Moreover, plasma reactive media provides that coating process proceeds at much lower temperatures compared to conventional CVD in which the gas and surface reactions occur by thermal activation [34, 38].

The silicone oxide based coatings are widely used in the many industrial applications due to their good wettability, chemical, thermal, and optical properties. Table 4.1. illustrates the lists of coating that are deposited by atmospheric plasma technology in the literature. The first column identifies the coating obtained, the second describes the used technology (mostly DBD), and the last column shows the used precursors. Correspondingly, Figure 46.2. shows the commonly used monomers for the deposition of silica like coatings. HMDSO and TEOS are the one that is mostly used in popular studies [38].

Table 4.1. List of thin film deposited by atmospheric plasma [38].

Coating	Technology	Precursor(s) used
SiO ₂	DBD	HMDSO/N ₂ + N ₂ O
SiO ₂	DBD	HMDSO/Ar or Ar + air
SiO ₂	DBD	HMDSO/N ₂ + BTSE/ AR or Ar + O ₂
TiO ₂	DBD	TiCl ₄ /N ₂ O
TiO ₂	Single and multi plasma jet	Titanium (IV) diisopropoxide bis(2,2,6,6-tetramethyl-3,5-heptanedionate [Ti(O-i-Pr) ₂ (thd) ₂]/He+N ₂

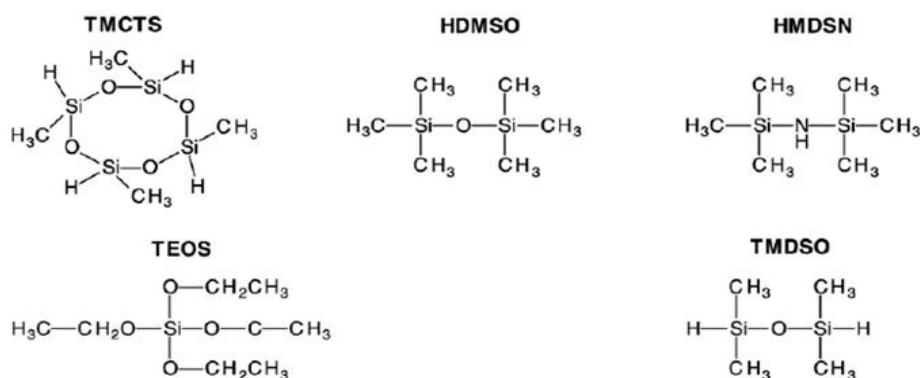


Figure 4.2. Commonly used monomers for the deposition of SiO₂ coatings [38].

4.3. Coating Application by Atmospheric Pressure Plasma Polymerization

The plasma polymerization process (plasma synthesis of coatings) consists of generating active radicals from precursors (monomer) in the gas phase and takes place at atmospheric pressure. These radicals are generated by a collision with a high-energy particle (electrons, ions, or metastable) or can be generated by irradiation using UV light [38].

The structure of the polymer revealed as a result of plasma polymerization, is different from that of conventional polymers due to plasma-polymerized coatings, which are often formed by random radical recombination. As shown in Figure 4.3., they exhibit a higher degree of crosslinking and branching. Moreover, they are not characterized by repeating units [38].

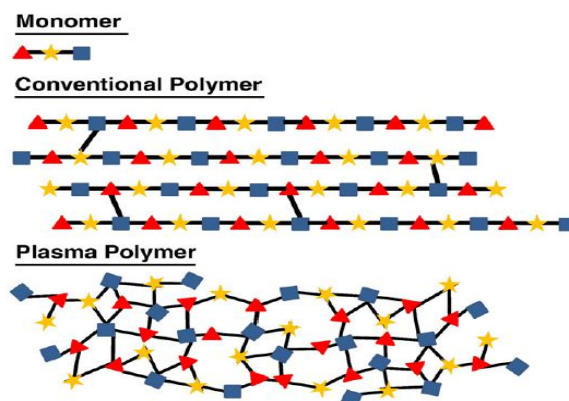


Figure 4.3. Schematic comparison between conventional polymers and plasma polymers [38].

4.4. Nanotechnology Surface Applications

Nanomaterials are a part of material science and available in different geometrical dimensions with sizes less than 100nm. Carbon nanotubes, nanofibers, nanoclays, nanocomposites, nanoporous materials, nanowires and nanoparticles (NPs) are within the family of nanomaterials. NPs are often available as embedded in a solid, liquid, or gas matrix. NPs occur as naturally (e.g., lipoprotein and volcanic particles), incidentally (carbonnanoparticle from diesel combustion), or as a result of custom engineering (catalyst). Moreover, they have different particle shapes such as spherical, rounded, cylindrical, cubic, acicular, angular, polygonal, flake, fibrous, porous, dendritic, aggregate as shown in Figure 4.4. They are often prepared in different forms; core-only NP, core-shell NP, hollow (or shell-only) NP. NPs are used application field at commercial stages due to their various properties such as high surface area which leads to increase reactivity, reduced percolation threshold, improved hardness and so on [39].

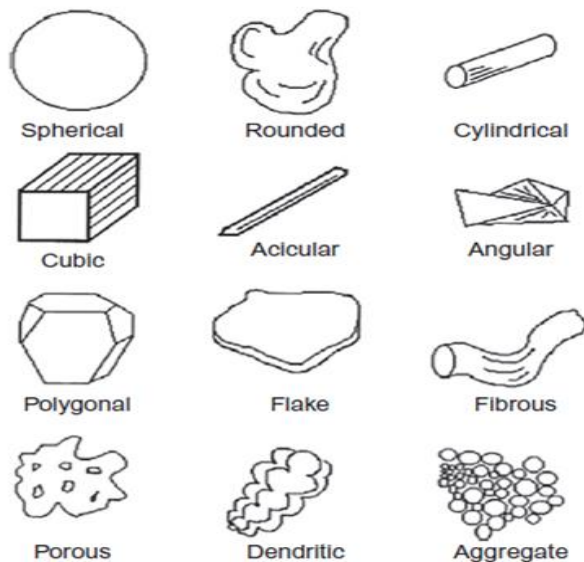


Figure 4.4. Shapes of different particulates [39].

NPs can be classified based on their composition, properties, synthesis process, and applications. In terms of composition, they can also be divided into four groups; inorganic metals, inorganic semiconductors, inorganic insulators including oxides and sulfides, and organics and polymers. Synthesis processes methods of NPs

include bottom-up (e.g., physical method), top-down (e.g., chemical process), or a combination thereof (e.g., biological process). All those synthesis methods use different media (gas, liquid, solid) and energy sources (sputtering, laser, microwave, convection, and sonochemical). Moreover, NPs have a variety of application sector; (i) energy: Pd NPs for automotive catalyst, TiO₂- based dye-sensitized solar cell, (ii) environment: TiO₂- based photocatalyst; magnetic NPs for remediation, (iii) microelectronics: Al₂O₃-based chemical-mechanical polishing, (iv) biomedical: NP-based drug delivery, (v) and others: light materials [39].

4.4.1. Surface modification with nanoparticles

NPs have unique qualifications compared to conventional adhesion filler due to their small size and large surface area. Surface modification of NPs occurs as a result of noble metal NPs' modification by thiols, disulfides, amines, nitriles, carboxylic acids, and phosphines. Carboxylates, silanes and phosphonates are used in the case of metal oxides. Modification of the NPs provides compatibility with a second phase such as metal and polymer and enables self-organization. Coating of the surfaces with modified NPs enables hydrophobic and hydrophilic and other characteristic (e.g., -COO- provides stability against agglomeration and aggregation) surfaces based on the functionality created on the surface. Table 4.2. illustrates different functional characteristics [39, 40].

Silica based NPs are widely used at the interface coating applications between rubber and metal with the purpose of adhesion. Silica NPs are organosilicone compounds consisting of hydrolysable group on silicone (siloxane) and an organofunctional group. They have numerous modification types with different functional groups; carboxylate, amine, amine/phosphonate, poly(ethylene glycol), octadecyl, and carboxylate/octadecyl groups. Surface composition of NPs is critical. Active groups on the surface of silica NPs after modification enables interaction with the polymer surface and acting as ligands for the metal ions. Therefore, functionalized silica NPs have tendency to adhere both polymer and metal surface and this enhances the interfacial adhesion [32, 39].

Table 4.2. Characteristics of different functional groups available for QD fictionalization [39].

Functionality	Property
Charged group (-OSO ₃ ⁻ , -SO ₃ ⁻ , -COO ⁻ , -PO ₃ ⁻ , (adsorption N ⁺ (CH ₃) ₃ Cl ⁻ , etc.)	Colloidal stability, electrostatic interactions of polyelectrolytes, biomolecules)
Reactive groups (-COOH, -CHO, -CH ₂ Cl, -OH, -NH ₂ , -SH, epoxide, ecatal, activated ester, tosylate, etc.)	Covalent immobilization on plain supports (silica wafers); grafting of biomolecules; chemical modification of preformed particles
Hydrophilicity (PEO, PAA, PAM, PMMA, PSSNa, hydroxyethylcellulose, etc.)	Steric stabilization, depletion of biomolecules, stealth effect
Sensitivity to stimulus (T, pH, ionic strength, reaction rates; light or UV, electric or magnetic fields, stress, etc.)	Shape, swelling behavior (microgels); ionic charge, recognition
Dye label (color, fluorescence)	Detection of a molecular interaction
Conductive polymers (Pyrrole, aniline)	Conductivity, optical absorbance
Complexation (PEO, PMAA, metal chelates, etc.)	Protein purification, oriented immobilization (proteins etc.)
Ligand (oligosaccharide, lipid, peptide, nucleic,	Recognition of antigen, specific cells, DNA, RNA, antibody, protein, protein, lectin, etc.

PEO, polyethylene oxide; PAA, polyacrylic acid, PAM, polyacrylamide; PMAA, polymethacrylicacid; PSSNa, polysodium styrene sulfonate.

In the literature, numerous functionalized nanoparticles have been investigated between similar or dissimilar substrates and effect of the NPs in the adhesion materials has been investigated. Some of the investigations and findings are summarized below.

Baurer at al., have worked on the modification of silica, alumina, and titania nanoparticles by trialkoxysilanes as well as reinforcement of epoxy adhesives. In addition, adhesion characteristics have been investigated between modified nanoparticles and epoxy resin formulations. The surfaces of the silica, alumina and

titania NPs have been modified by glycidyloxypropyltrimethoxysilane and incorporated in epoxy Novolac adhesives. In the result of the study, it was observed that, crosslinking reactions occurred during heat curing due to polymerization-active surface coverage of nanoparticles [40].

Zihai et al., have investigated the influence of different NPs; nano- Al_2O_3 (average size of 80 nm in diameter), nano- CaCO_3 (40~80 nm), nano- SiO_2 (10~20 nm) on the adhesion force between epoxy adhesive and steel substrate. In addition, the effect of the surface abrasion has investigated. In the results, it was demonstrated that, epoxy adhesive modified by 2% nano- Al_2O_3 and abraded with 150# improved the adhesion 5 times. Moreover, the adhesive characteristics of the epoxy adhesives showed increase with additives of NPs [41].

Mohseni et al., have examined the influence of amino and vinyl-silane-based treatments on the performance of an epoxy coated AA 1050 aluminum substrate. Wettability results showed increase at the surface energies of the silane treated specimens and this leads to more hydrophilic surface [42].

CHAPTER 5. MATERIAL AND METHOD

In this study, adhesion mechanisms of different types of coating materials and their comparisons in terms of interface adhesion force with Chemosil coating occurred between EPDM based rubber material and aluminum strip were evaluated. The Chemosil coating material was taken as the reference coating material due to it has a very wide range applications in the Al-EPDM interface applications. Therefore, Chemosil coating surface characteristics were first evaluated by using several methods. Then, the different types of coating materials and their combinations were compared with Chemosil coating material in terms of their surface characteristics and interface adhesion mechanisms. Moreover, the effect of the cold plasma treatment on un/coated aluminum alloy in terms of interface adhesion was investigated between EPDM based rubber material and aluminum alloy within this master thesis.

5.1. Materials

5.1.1. Rubber

EPDM based rubber material specially formulated by Standard Profil Automotive Company was used as the upper substrate of the interface. Different compound formulations in very wide hardness ranges from 55 ShA to 95 ShA are available. They are classified under different compound codes based on their hardness ranges. In this study, C073 grade of compound, which mostly has application as the carrier compound around the Al strip, was used in the dimensions of 113 x 36 x 6.3 mm and in hardness of 80 ± 5 ShA. The components used in the compound formulation is shown in Table 5.1.

EPDM is the main raw material in the compound formulation and constitutes on average 30% of the composition. The other components in the formulation are carbon black, mineral oils, mineral fillers, various reaction accelerators and processing aiding's.

Table 5.1. Component of the C073 compound.

Component	Percentage in the compound
Rubber-EPDM	29,5 %
Carbon black	27,5 %
White fillers	27,5 %
Oil	10 %
Small Chemicals (ZnO, Activators and CaO)	4 %
Sulphur and accelerators	1,5 %

5.1.2. Metal

In this study, aluminum alloy substrates at 5754 grade and 100x31x0,60 mm in dimensions were used. 5754 grade of aluminum alloy is into aluminum -magnesium family (5xxx series). This grade aluminum alloy is widely used in automotive industry due to their advantages of low cost, lightweight, high resistance against of corrosion. Aluminum alloy strips are available in rigid and lanced shapes as shown in Figure 5.1. Besides, Chemosil coated rigid aluminum alloy substrate was used as the reference coated aluminum strip within this study.

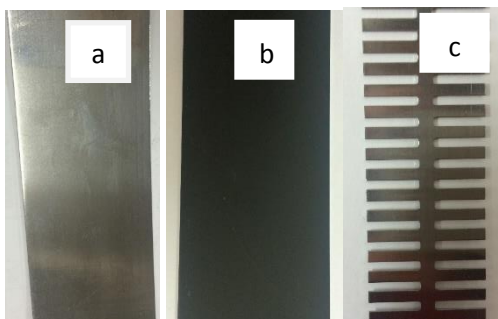


Figure 5.1. Rigid and lanced aluminum alloy plates a) uncoated aluminum alloy substrate b) Chemosil coated aluminum alloy substrate c) lanced and uncoated aluminum alloy substrate.

5.1.3. Interface coating materials

- Reference Coating Material, Chemosil

Chemosil coating material and its primer were supplied from Lord (Waalwijk, Netherlands). Chemosil NL 411 elastomer bonding agent as cover coat and Chemosil® 211 primer and/or bonding agent as lower coat(primer) were used in this study as the reference interface coating material. Chemosil NL 411 elastomer bonding agent is a versatile bonding agent suitable for use as a cover coat material over Chemosil 211 primer, or as a one-coat bonding agent for bonding a variety of elastomer compounds to metal substrates during the vulcanization process. It is composed of a mixture of dispersed polymers, cross-linking agent and suspended solids in an organic solvent system. LORD Chemosil 211 primer is a heat-activated bonding agent designed for use as a substrate primer under other Chemosil cover coat bonding agents. It is composed of a mixture of polymers, organic compounds and mineral fillers dissolved or dispersed in an organic solvent system.

- Improved Coating Materials

In this study, different types of interface coating materials and their mixtures were used. As shown in Table 8.2., they were coded and each code represent to different coating and their mixtures. It was aimed to see their single and combination effects at the interface.

5.2. Interface Treatment and Adhesion Processes

5.2.1. Surface treatments by thermal ageing

Aluminum strips coated with Chemosil were exposed to thermal ageing in the muffle furnace (Thermolyne®) in a preselected die temperature range and time combinations as shown in Table 5.3. The selection was intentionally made to simulate extrusion-processing condition of the Chemosil coated aluminum surface.

They were placed to muffle furnace as horizontally on specially designed metal sample hanger to avoid them from touching one another as shown in Figure 5.2.

Table 5.2. Improved coating mixtures' contents and their codes.

Coating Code	Content of the Coating
1A	MER
2A	MER + BYK
3A	MER + 1895COST
4A	MER + TLA
1B	211
2B	211 + BYK + (NL411)
3B	211 + 1895COST + (NL411)
4B	211 + TLA + (NL411)
5B	211 + (NL411)
6B	PF

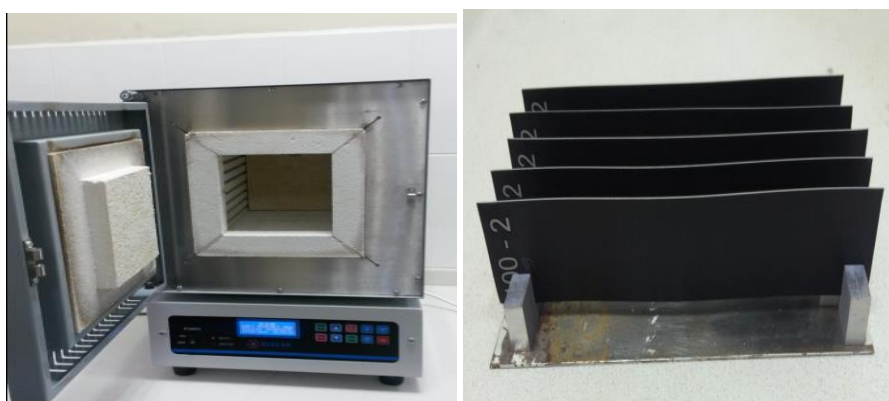


Figure 5.2. Muffle furnace and metal sample hanger respectively.

Table 5.3. Surface thermal treatment conditions.

	Treatment time (min)				
	2	4	8	16	64
Treatment at 100 °C	2	4	8	16	64
Treatment at 165 °C	2	4	8	16	64
Treatment at 230 °C	2	4	8	16	64
Treatment at 295 °C	2	4	8	16	64
Treatment at 360 °C	2	4	8	16	64

5.2.2. Surface treatments by cold plasma

The atmospheric plasma treatment was carried out using the PlasmaTreat™ Open air atmospheric plasma system. This jet system is an example of the blown arc type and uses dry and filtered compressed air as the ionized working gas at a pressure of 700–300 mbar. Plasma surface treatments were applied to the metal surface via plc controlled with 1kW air plasma rotary nozzle torch (Plasmatreat® RD1004) in Figure 5.3. Plasma treatment parameters selected were treatment frequency 21 kHz, 80% voltage, 80% plasma cycle time (PCT) and 3500 mbar air pressure. On the surface, after the plasma pre-cleaning process is performed first, the surface activation process is completed. The water contact angle (WCA) was obtained using a Kruss DSA25 Instrument. 4 μ l drops were allowed to sit on the surface for a maximum of 10 s before the WCA was measured. Each WCA value presented here is based on at least three measurements at different points on the sample. Primarily, the effect of the cold plasma at different application time (1, 2, 5 and 10 sec.) on the aluminum alloy substrate was analyzed based on contact angle. The effect that plasma treatment had on the morphology of the surface was evaluated following a treatment of 5 s at a fixed gap distance of 12 mm.



Figure 5.3. The plasma treatment unit and plasma nozzle [47].

The ability of the adhesion of un/coated, un/treated, rigid/lanced and sanded aluminum alloys to the EPDM based rubber plates were evaluated after cold plasma application to the surface of the aluminum alloy plates for 5 sec. In this scope, experiments were performed in six different combinations as follows: a. Uncoated

rigid aluminum, b. Chemosil coated rigid aluminum, c. Uncoated and sanded rigid aluminum, d. Uncoated and plasma applied rigid aluminum, f. Chemosil coated and plasma applied rigid aluminum , g. Uncoated lanced aluminum.

5.2.3. Interface coating application process

The selected interface coating materials were applied to the AI strip surface by brush as shown in Figure 5.4. They were left to dry for 7 days in laboratory conditions.

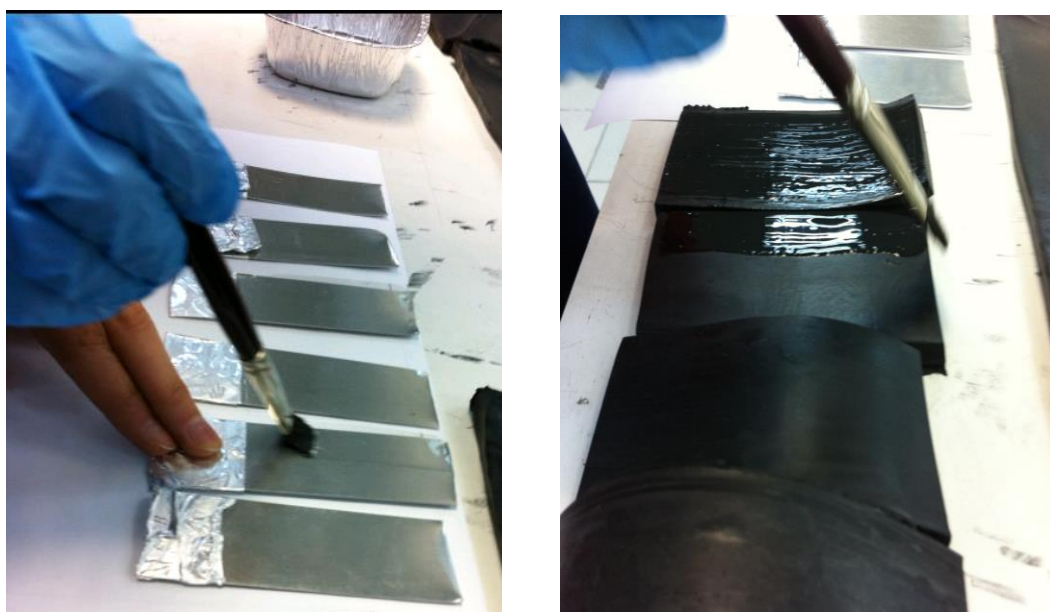


Figure 5.4. Coating application process to the surfaces of Aluminum and EPDM based rubber compound.

5.2.4. Interface adhesion process

Interface adhesion of the EPDM based rubber and Aluminum strip was performed based on the international test standard of the ASTM 1876 to be able to carry out T-peel strength test accordingly. The coated AI strips were first placed to the specially designed sample holder as shown in Figure 5.5. Then EPDM based rubber compounds were placed to the top of the AI strips and they were hot pressed at 200 °C for 4 min under 400 kN as shown in Figure 8.6.



Figure 5.5. Sample holder used in the molding step.



Figure 5.6. Hot pressing machine.

5.3. Analysis and Measurement Methods of Interface

Different measurements were carried out in order to characterize the interface mechanism of the different kind of coating materials and Chemosil coating material as the reference before and after interface treatments. The diversity basically depends on the lack of the literature to define the current case and a quantifiable measurement is sought.

5.3.1. Wettability

Contact angle and surface energies of the surfaces were measured by using KRUS contact angle-measuring system as shown in Figure 5.7. Test liquids of 3 ml high purity water and diiodomethane drops are selected respectively. Surface energy measurements are conducted by Kruss analysis software using the Laplace-Young method.

The water contact angle (WCA) was obtained using a Kruss DSA25 Instrument. 4 μl drops were allowed to sit on the surface for a maximum of 10 s before the WCA was measured. Each WCA value presented here is based on at least three measurements at different points on the sample.

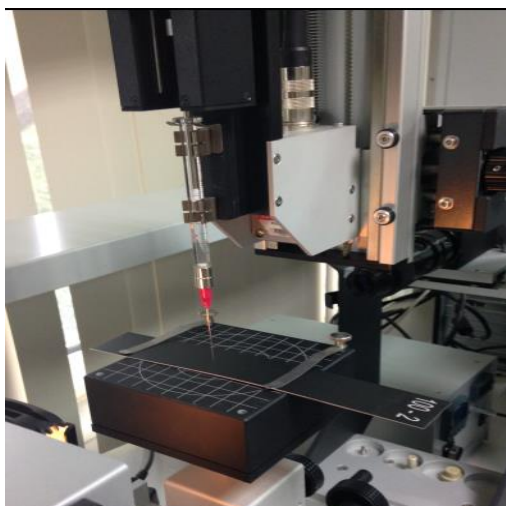


Figure 5.7. KRUS contact angle-measuring system.

5.3.2. Surface roughness

A surface profiles, a Mahr MarSurf PS1 shown in Figure 5.8., was used to determine roughness of the surfaces. The profiler in 2-micrometer radius measuring tip moves along a single direction with a scanning length of 17.5 mm and scan velocity 0.5 mms^{-1} . The measurement was performed from three different area of the surface to discriminate the deviation and average roughness values “ R_a ” was calculated for each surface.



Figure 5.8. Mahr MarSurf PS1 surface roughness measurement device.

5.3.3. Coating thickness

Coating thickness measurements were carried out via coating thickness gauge (Huatec®). Measurements were taken from different areas of the surface to be able to eliminate the deviations and observe stability of the coating thickness along the surface. Thereby, 10 measurements were performed for each surface.

5.3.4. T-peel strength

Interface adhesion of the Al and EPDM based rubber has been measured by T-peel strength test at a peel rate of 100 mm/min using Zwick Roell Dynamometer as shown in Figure 5.9. The test was carried out based on the ASTM 1876 test standard. Interface adhesion was performed between EPDM based rubber plate (113 x 36 x 6.3 mm) and Al alloy plate (100 x 31 x 0.6 mm) after samples were hot pressed at 200 °C for 4 min and conditioned for 72 hours at 23±5 °C and 60 ± 5 RH respectively.



Figure 5.9. T-peel strength test of the interface of EPDM based rubber compound and Al strip.

5.3.5. Weight change

Weight change on both EPDM based rubber plates and Al plates were evaluated after T-peel strength test. The remaining materials on the substrates were calculated as percentage coverage based on their weight change after separation. Hence, their interface separation types as adhesive or cohesive were defined.

5.3.6. Microscopic analysis

Morphological changes of the surfaces were observed under Eclipse E200 light microscope at 1000X magnification.

5.3.7. FTIR analysis

FTIR-ATR spectra was performed to determine the changes of the chemical composition of the untreated and plasma treated Chemosil coated aluminum alloy surfaces after T-peel strength test. Moreover, it was carried out to see the functional structures of the improved coating mixtures. A Perkin Elmer FTIR spectrophotometer was used to carry out infrared (IR) spectra of the surfaces.

5.3.8. Thermogravimetric analysis

Netzsch Simultaneous Thermal Analyzer (STA) incorporates TGA and DSC was conducted simultaneously to observe the amount of weight change, heat flow rate (caloric reactions/endothermic and exothermic reactions) and most off all thermal degradation behavior of the Chemosil coating material due to decomposition reactions occurred as a function of increasing temperature. Samples were heated from 40°C to 900°C at a constant rate of 40/10.0 (K/min) under N₂ atmosphere.

5.3.9. Thermal analysis

Simultaneous Thermal Analyzer (STA) (Netzsch®) incorporates TGA and DSC was conducted simultaneously to observe the amount of weight change, heat flow rate (caloric reactions/endothermic and exothermic reactions) and most off all thermal degradation behavior of the coating materials as a function of increasing temperature. Samples were heated from 40°C to 900°C at a constant rate of 40/10.0 (K/min) under N₂ atmosphere.

5.3.10. Design of experiment (DEO) analysis

Measurements were analyzed by full factorial design of experiment for factorial design platform in Minitab to observe the effect of the factors and effect of the interactions of the factors on the responses. Because, if one factor was analyzed by keeping all the remaining factors separately, this would not reveal the interaction of the factor's effects. In this full factorial design, an experimental run was performed for two factors; time and temperature and five levels for each factors. The experimental run was created as shown in Table 5.4. In the design table, standard order, run order, factor levels and response values are available. Totally, 25 run was performed to generate the design for two factors and five levels for each. Single replicate design is used.

Hypothesis test in General Linear Model was conducted to check whether each of the factors and their interactions investigated in the experiment are significant or not. Based on the P values of the factors and interactions of the factors, statistically insignificant factors were removed from the model and General Linear Model was re-created. If the P values is higher than 0.05, this shows that related factors do not have statistically significant effect on the response. Moreover, the interaction plots were also evaluated to see the interaction cases of the factors and their levels. Moreover, pie charts was carried out to see the effect of each factor on the response and effect of the model error as percentage. Finally, results were exhibited on the Contour Plot to see the effect of each level of the factors on the response. Thus, it

was concluded that how the factor's levels can be minimized or maximized to determine which of several factors are important and affecting the responses.

Table 5.4. Experimental run performed based on factorial design platform in Minitab.

Std Order	Run Order	Pt Type	Blocks	Temperature	Time
17	1	1	1	295	4
1	2	1	1	100	2
14	3	1	1	230	16
21	4	1	1	360	2
11	5	1	1	230	2
22	6	1	1	360	4
12	7	1	1	230	4
19	8	1	1	295	16
8	9	1	1	165	8
4	10	1	1	100	16
13	11	1	1	230	8
25	12	1	1	360	64
7	13	1	1	165	4
5	14	1	1	100	64
24	15	1	1	360	16
6	16	1	1	165	2
2	17	1	1	100	4
20	18	1	1	295	64
15	19	1	1	230	64
10	20	1	1	165	64
18	21	1	1	295	8
23	22	1	1	360	8
16	23	1	1	295	2
9	24	1	1	165	16
3	25	1	1	100	8

CHAPTER 6. RESULTS

The empirical phase of this master thesis is consisting of three categories. In the first phase, surface characteristics of the thermally aged Chemosil coated aluminum plates have been investigated and optimum processing parameter values have been defined based on their interface adhesion performances. In the second phase, the effect of plasma treatment on the pure and coated aluminum surfaces have been investigated based on their ability to adhere to the EPDM plate. In the final phase, surface characteristics of the newly developed coating materials have been defined and their adhesion performance to both aluminum and EPDM surfaces have been analyzed.

6.1. Surface Characterization of the Chemosil Coating on the Aluminum Surface

6.1.1. Ageing of Chemosil coating

Chemosil coated aluminum surfaces have been thermally aged in different time and temperature combinations. Their surface characteristics have been investigated with the following methods.

6.1.1.1. Wettability characteristics of the thermally aged surfaces

The effect of the thermal ageing on the wettability characteristics of the Chemosil coated aluminum surface was evaluated in terms of surface energy change. The surface energy measurements were carried out based on DEO design matrix as shown in Table 5.4. General Linear Model is selected to defined the statistically significant factors on the response. Figure 6.1. shows the statistical parameters. P value should be greater than 0.05 for the factor to be statistically significant in the

design DEO model. When two factors, which are time and temperature and their interactions are included, the model does not give P values due to most of the factors or interactions are negligible on the response. Correspondingly, F-test could not be defined as shown in Figure 6.1. Therefore, in the first step, the effect of the interaction should be removed from the model.

Source	DF	Seq SS	Adj SS	Adj MS	F	P
Temperature	4	4436.24	4436.24	1109.06	**	
Time	4	178.64	178.64	44.66	**	
Temperature*Time	16	754.56	754.56	47.16	**	
Error	0	*	*	*		
Total	24	5369.44				

** Denominator of F-test is zero or undefined.

Figure 6.1. Statistical parameters for surface energy of the thermally treated samples.

The effect of the temperature and time interaction is removed from the model and General Linear Model is re-carried as shown in Figure 6.2. To be able to define the statistically significant factors on the responses, P values are analyzed. The P value of the effect of the temperature is less than 0.05. This demonstrates that the factor of the temperature is statistically significant on the response of surface energy. On the other hand, P values for the time is $0.463 > 0.05$, which shows that this factor is not effective and statistically significant on the response. Therefore, it should be removed from the model.

Source	DF	Seq SS	Adj SS	Adj MS	F	P
Temperature	4	4436.24	4436.24	1109.06	23.52	0.000
Time	4	178.64	178.64	44.66	0.95	0.463
Error	16	754.56	754.56	47.16		
Total	24	5369.44				

S = 6.86731 R-Sq = 85.95% R-Sq(adj) = 78.92%

Figure 6.2. Statistical parameters for surface energy after removal of the effect of the factors' interaction.

The new General Linear Model is re-created after eliminating the statistically insignificant factors as shown in Figure 6.3. When R-square adjusted parameter is checked, it is seen that the new design can explain the 79.14% percent of the model. As the insignificant factors are eliminated from the model, R-square adjusted parameter is increased from 78.92 % to 79.14 %. This demonstrates that the new design model can give us more reliable results.

Source	DF	Seq SS	Adj SS	Adj MS	F	P
Temperature	4	4436.2	4436.2	1109.1	23.77	0.000
Error	20	933.2	933.2	46.7		
Total	24	5369.4				

S = 6.83081 R-Sq = 82.62% R-Sq(adj) = 79.14%

Figure 6.3. Statistical parameters for surface energy after removal of the statistically insignificant factors.

Figure 6.4. illustrates the interaction plot of the time and temperature on the response of the surface energy. When the interaction plot is examined, findings are as follows. For the temperature increase from 100°C to 165°C, there is no effect of the interaction for each level of the time increase on the response. When the temperature is increased to 230°C, interaction of the factors only occurred for 4 min. As the temperature is more increased to 295°C and 360°C respectively, there is no interaction observed for the different time levels. There is only one interaction occurred in the whole model. As also demonstrated in the General Linear Model, the interaction of the factors is not statistically significant on the response.

The effect of the factors is also exhibited on the pie chart as percentage. From the Figure 6.5., it is seen that the factor of temperature affects the 98.1% of the model. The effect of the time is negligible due 0.4% effect. In addition, error percent of the model is low as 1.6%. This was also demonstrated in General Linear Model.

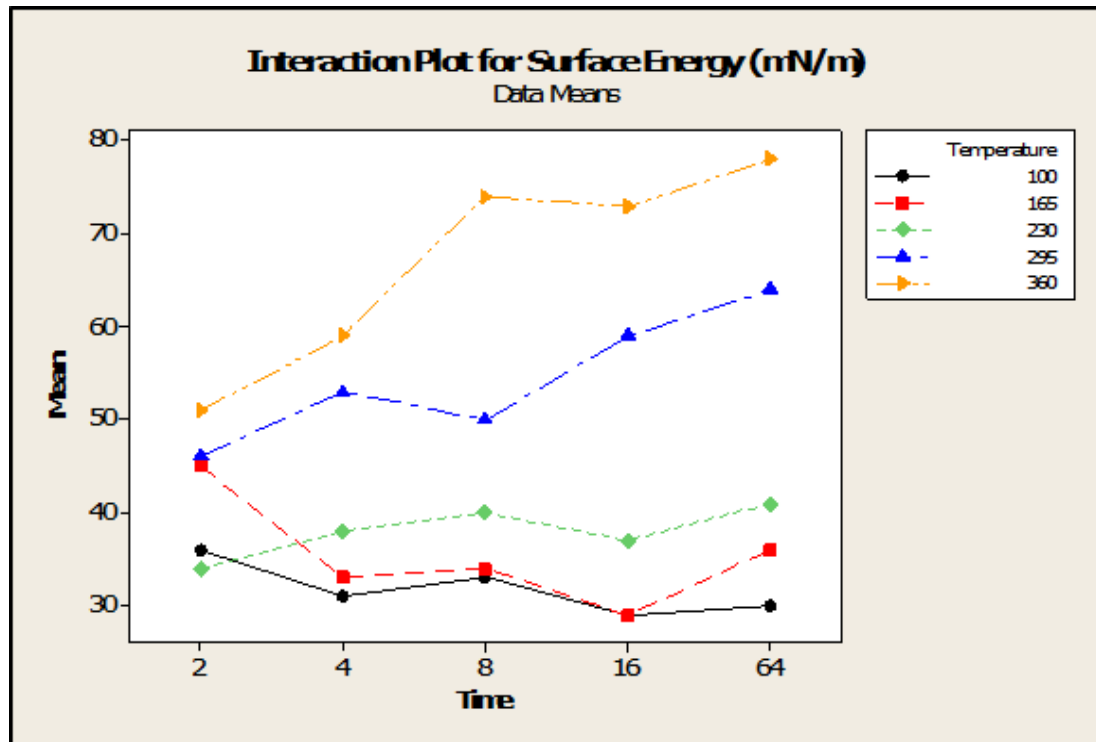


Figure 6.4. Interaction plot of the factors; time and temperature on the surface energy.

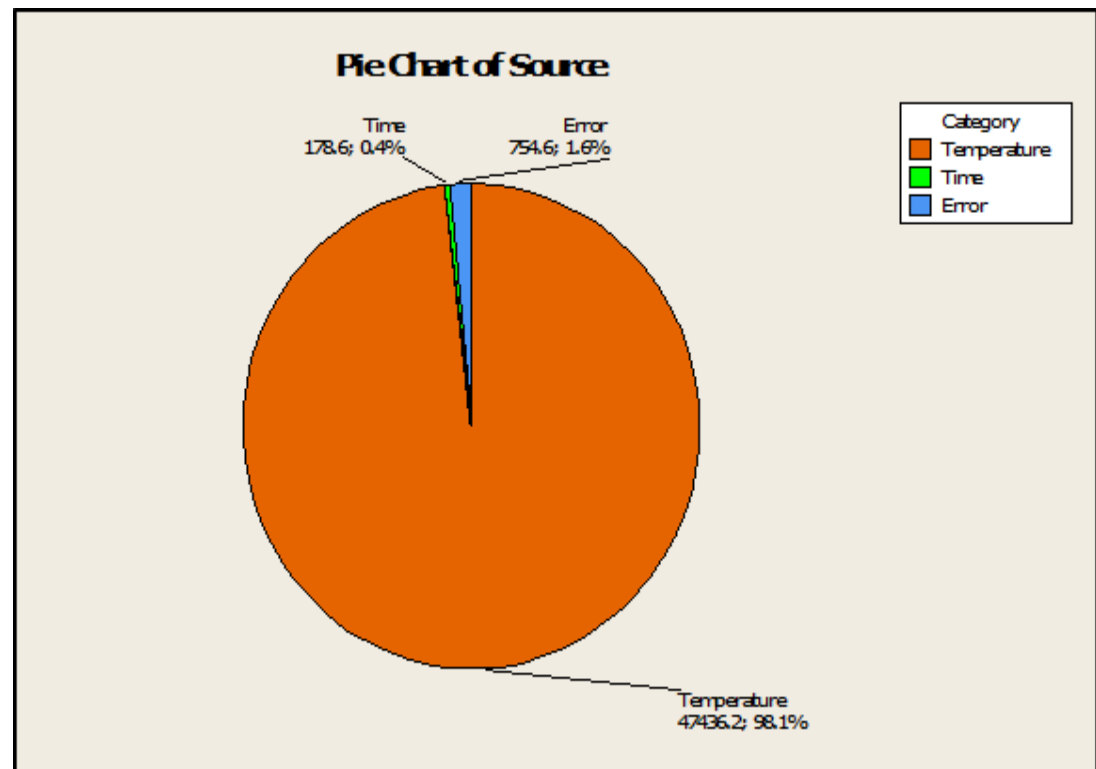


Figure 6.5. Pie chart of the factors; time and temperature on the surface energy

Results are exhibited on the Contour Plot to see the effect of each level of the factors on the response. It is obviously seen from the Figure 6.6., the surface energy exhibits continuously increase as an increasing function of temperature. On the other hand, time is not an effective parameter on the surface energy. It is known that, adhesion characteristics of the interface increases as a function of increased surface energy. Hence, it can be easily concluded that, low processing time is sufficient to increase surface energy at any processing temperature. The sufficient surface energy of the interface will be defined based on the T-Peel strength test results in the following sections.

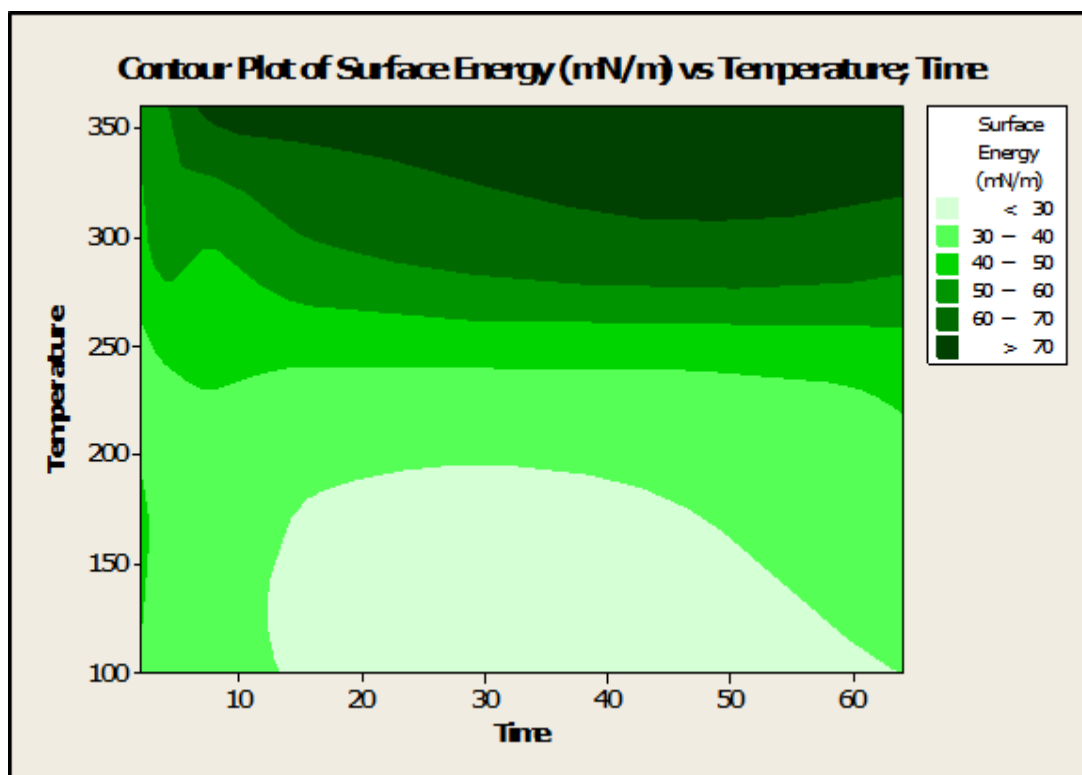


Figure 6.6. Contour Plot of surface energy change after thermal treatments from 100°C to 360°C for 2, 4, 8, 16, 64 min. ageing conditions respectively.

6.1.1.2. Surface morphology change of the aged surfaces

The morphology and roughness are well known impacts in controlling of surface energy and correspondingly interphase adhesion characteristics. The surface morphology changes after thermal ageing in different time and temperature combinations were evaluated under microscope. Figure 6.7. shows the surface

morphology changes at 100°C, 165°C, 230°C, 295°C and 360°C from top to bottom after 2, 16 and 64 min. thermal ageing from left to right respectively. The areas were divided into 4 categories based on their morphological changes after thermal ageing.

At the area 1, wider and deeper porous structure was observed at low temperatures such as 100°C and 165°C and short thermal ageing times such as 2 and 8 min. This wide and deep porous structure occurred at the beginning of thermal ageing is estimated due to removal of the volatile components and temperature activated curative agents from the coating material. Moreover, with increasing ageing time at 100°C and 165°C temperatures, surface pore abundance increase shown on area 2.

Area 3 illustrates the completion of the removal of the volatile components and initiating of the chemical degradation of the components available in the coating formulation at 230°C for 8 min and 295°C and 360°C for 2 min thermal ageing condition. Thereby, pore diameter decreases and pore abundance increases on the surface. When thermal ageing temperature reaches to 360°C for 8 and 64 min, surface consists of rather small diameter pores and color of the surface varies visibly from black to opaque. This change is shown on area 4. At this stage, it could be interpreted that, component available in the coating formulation is completely exposed to chemical degradation.

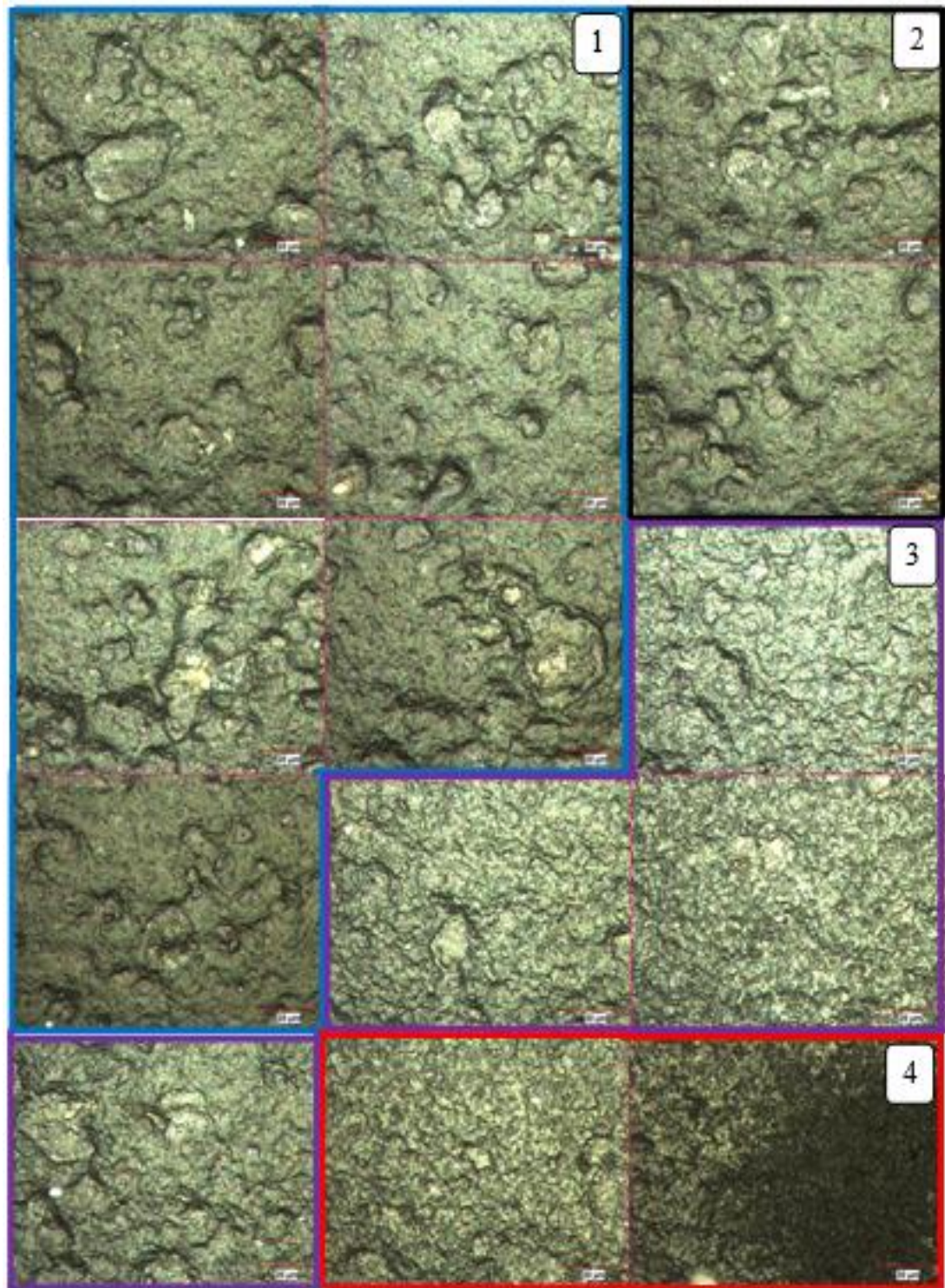


Figure 6.7. Microscope images of the thermally aged samples at 100 °C, 165°C, 230°C, 295°C and 360°C from top to down after 2, 8 and 64 min. thermal ageing from left to right respectively.

6.1.1.3. Surface roughness change of the thermally aged surfaces

The surface roughness changes after thermal ageing in different time and temperature combinations were evaluated by profilometer. Correspondingly, obtained values were analyzed by design of experiments in Minitab to observe individual effect of the temperature, time and their correlations as well as main effect of each particular factor on roughness. The experiment was carried out based on the design matrix of the DEO as shown in Table 6.4. The effect of factors and their interactions were evaluated based on the General Linear Model. As shown in Figure 6.8., F-test is zero or undefined due to statistically insignificant values are available in the model. Those values should be eliminated from the model.

Source	DF	Seq SS	Adj SS	Adj MS	F	P
Temperature	4	0.0785186	0.0785186	0.0196297	**	
Time	4	0.0076602	0.0076602	0.0019151	**	
Temperature*Time	16	0.0368334	0.0368334	0.0023021	**	
Error	0	*	*	*		
Total	24	0.1230122				

** Denominator of F-test is zero or undefined.

S = *

Figure 6.8. Statistical parameters for surface roughness of the thermally treated samples.

The effect of the temperature and time interaction was eliminated from the model and General Linear Model was re-carried to be able to define the statistically significant factors on the response as shown in Figure 6.9. The P value of the effect of the temperature is less than 0.05. This demonstrates that the factor of the temperature is statistically significant on the response of surface roughness. On the other hand, P values for the time is $0.524 > 0.05$ which shows that this factor is not effective and statistically significant on the response. Therefore, it should be removed from the model.

Source	DF	Seq SS	Adj SS	Adj MS	F	P
Temperature	4	0.078519	0.078519	0.019630	8.53	0.001
Time	4	0.007660	0.007660	0.001915	0.83	0.524
Error	16	0.036833	0.036833	0.002302		
Total	24	0.123012				

S = 0.0479800 R-Sq = 70.06% R-Sq(adj) = 55.09%

Figure 6.9. Statistical parameters for surface roughness after removal of the effect of the factors' interaction.

In the final model, time and time*temperature interaction which were defined as statistically insignificant were removed from the system. P-values of the temperature is changed from 0.001 to 0.000 and the R-square adjusted values is increased from 55.09% to 56.60% as expected as shown in Figure 6.10. Now, the new designed model can answer the 56.60% percent of effect of the factors on the response.

Source	DF	Seq SS	Adj SS	Adj MS	F	P
Temperature	4	0.078519	0.078519	0.019630	8.82	0.000
Error	20	0.044494	0.044494	0.002225		
Total	24	0.123012				

S = 0.0471665 R-Sq = 63.83% R-Sq(adj) = 56.60%

Figure 6.10. Statistical parameters for surface energy after removal of the statistically insignificant factors.

Figure 6.11. illustrates the interaction plot of the time and temperature on the response of the surface roughness. When the interaction plot was examined, findings are as follows. For the temperature increase from 100°C to 165°C, there is interaction for 4 min. and 64 min. This means that both temperature and time increase affects the response. When the temperature is increased to 230°C, an interaction is available for 16 min. As the temperature is more increased to 295°C, more complicated interaction is occurred. Finally, temperature is increased to 360 °C, interaction was occurred at 16 min. At this interaction points, it is expected to see noticeable changes in surface roughness. In any case, as illustrated in General Linear Model's findings, these interactions are not statistically significant in terms of DEO model.

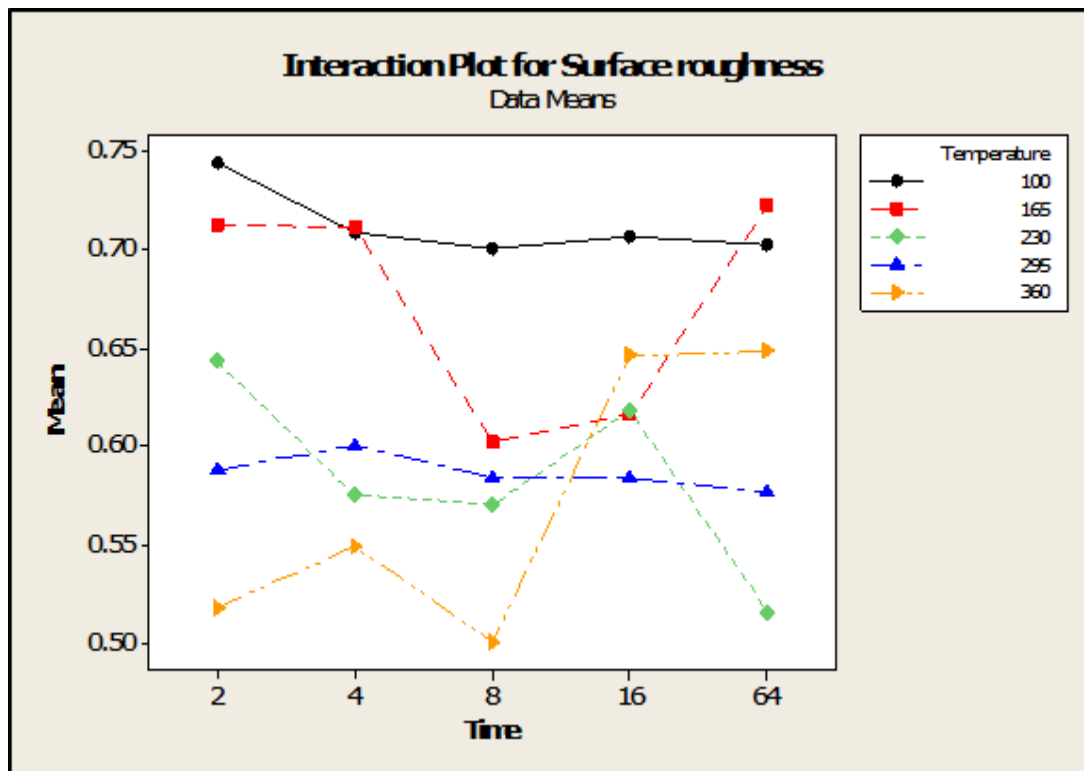


Figure 6.11. Interaction plot of the factors; time and temperature on the surface energy.

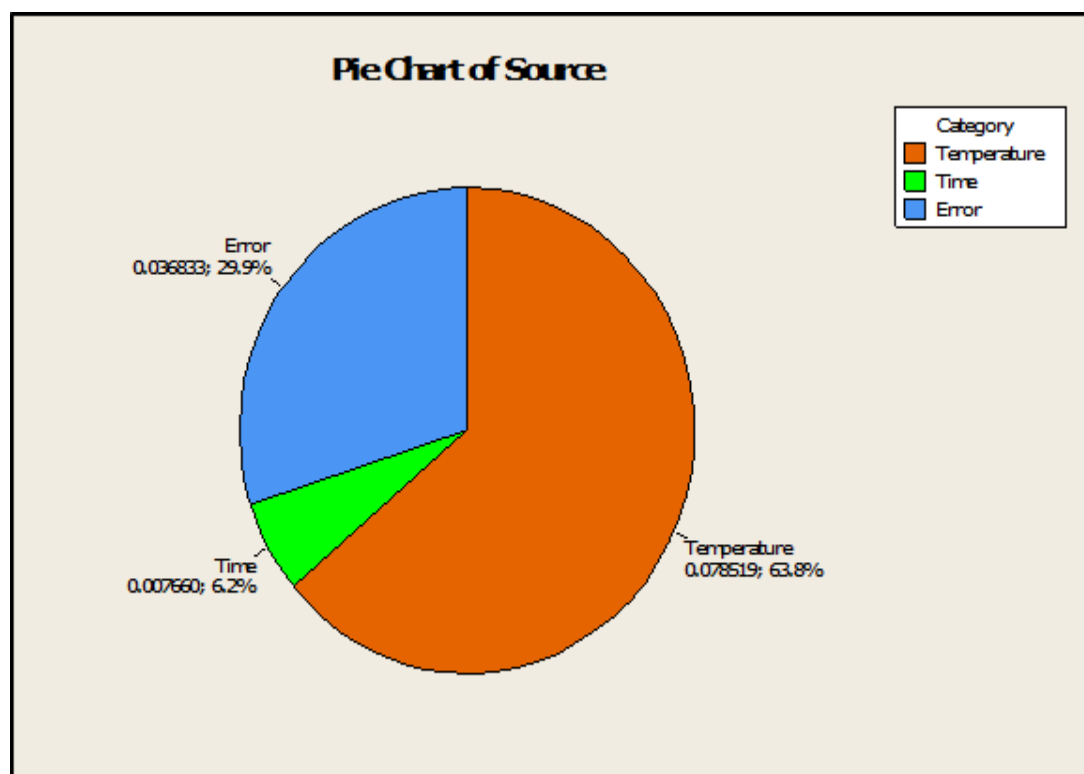


Figure 6.12. Pie chart of the factors; time and temperature on the surface energy.

As explained in the results of the General Linear Model, time is not an effective parameter on the response. This finding was also demonstrated by pie chart as shown in Figure 6.12. Based on the pie chart graph, temperature affects the 63.8 % percent of the model. The error percent is 29.9%. Based on the R-square adjusted value (56.60%) in the findings of the General Linear Model, the high error percentage is expected.

Figure 6.13. illustrates the effect of temperature and time to the surface roughness by Contour Plot graph. As carried out in microscopic analysis, areas in the Contour Plot were divided into 4 categories. Similar surface changes were obtained with microscopic analysis. Surface roughness exhibited increase at the areas of 1, 2 and 4. The increase surface roughness at the areas 1 and 2 could be related to the increased surface porosity in wideness and deepness due to removal of the volatile components and temperature activated curative agents from the coating material as explained in microscopic analysis findings. The third surface roughness increase was observed at the area 4 due to porosity abundance increases as the result of exposing quite high temperature to the surface (360 °C). At the area 3, surface became more smooth with increasing time and temperature due to completion of the removal of the volatile components and reaming porous were filled with degraded components or spreading of the degraded components.

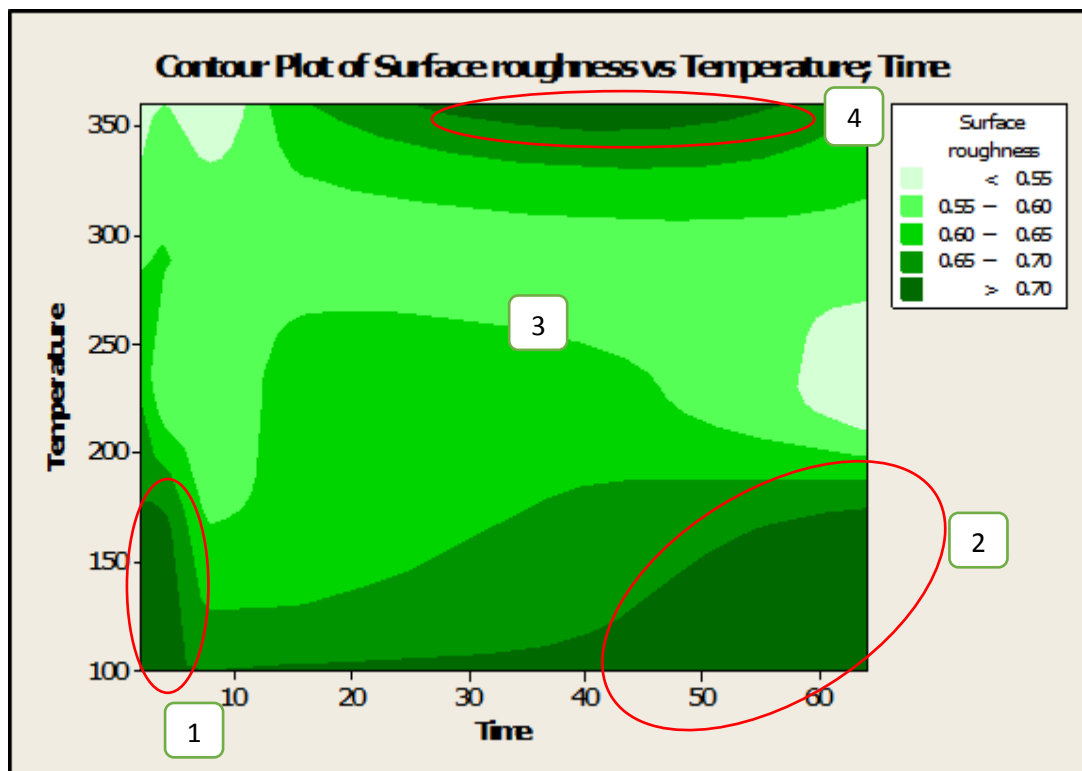


Figure 6.13. Contour Plot of surface roughness change after thermal treatments from 100 °C to 360 °C for 2, 4, 8, 16, 64 min. ageing conditions respectively.

6.1.1.4. T-Peel strength test

The effect of thermally ageing conditions of the coated aluminum surface at different temperature and time combinations were evaluated in terms of interface adhesion performance of the Chemosil to both EPDM and AL via T-peel test based on the ASTM 1876 test standard. General Liner Model was carried out to eliminate statistically insignificant factor's effect. The factor of time was removed from the model due to P-value is greater than 0.05 as shown in Figure 6.14. Current case explains the 64.09 % of the DEO model according to R-square adjusted value.

Source	DF	Adj SS	Adj MS	F-Value	P-Value
Temperature	4	769852	192463	21.41	0.000
Time	4	64068	16017	1.78	0.182
Error	16	143821	8989		
Total	24	977742			

Model Summary

S	R-sq	R-sq(adj)	R-sq(pred)
94.8095	85.29%	77.94%	64.09%

Figure 6.14. Statistical parameters for T-peel Strength of the thermally treated samples.

The effect of the temperature was only remained in the model due to its P-values, which is less than 0.05. The effect of the time and interaction of the time*temperature are eliminated from the system as shown in Figure 6.15. In the current case, the eliminated model can explain the 66, 78 % percent of the whole system. Before elimination of the statistically insignificant factors, R-square adjusted value was 64, 09 %. As expected, R-sq. adjusted values exhibited increase as a result of insignificant factors were eliminated from the model.

Source	DF	Adj SS	Adj MS	F-Value	P-Value
Temperature	4	769852	192463	18.52	0.000
Error	20	207890	10394		
Total	24	977742			

Model Summary

S	R-sq	R-sq(adj)	R-sq(pred)
101.953	78.74%	74.49%	66.78%

Figure 6.15. Statistical parameters for T-peel Strength after removal of the statistically insignificant factors.

Figure 6.16. illustrates the interaction plot of the time and temperature on the response of the T-peel strength. When the interaction plot was examined, findings are as follows. For the temperature increase from 100°C to 165°C, interactions are available for 4 min and 8 min ageing time. As the temperature was more increased to 230 °C, 295°C and 360°C respectively, there was no interaction observed for the different ageing time levels. It is worth to illustrate that, T-peel strength curves of the 295 °C and 360 °C were overlapped for the whole ageing times. This demonstrates that there is no significant effect of the temperature on the response after 230 C ageing condition. From the graph, it was also easily seen that, there is a dramatic decline on the T-peel strength after 165 C for 8 min. Moreover, there is a huge decline after 64 min ageing for 100 °C and 165 °C. Those results lead the way where to focus in the whole system for the further analysis. Therefore, in the FTIR analysis, these temperature and time ranges were analyzed.

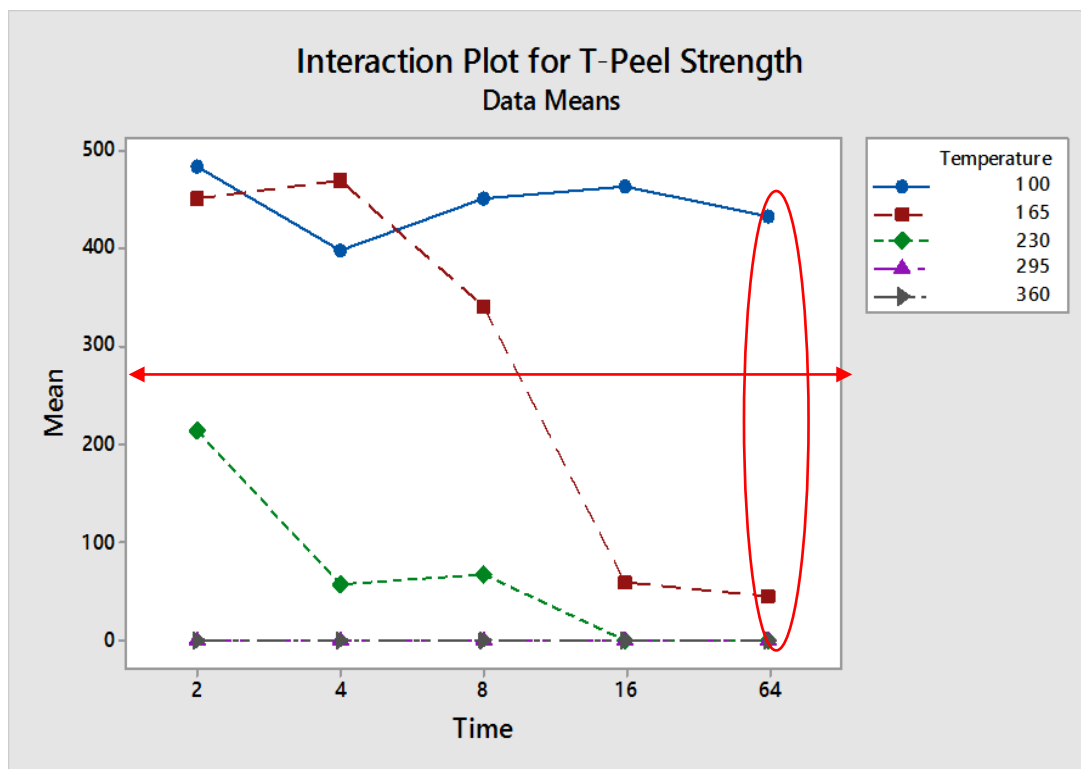


Figure 6.16. Interaction plot of the factors; time and temperature on the response of T-peel strength.

The effect of the factors was also exhibited on the pie chart as percentage. From the Figure 6.17., it was seen that the factor of temperature affects the 78.7% of the model. Time affects the model 6.6 % and the error percentage of the model is 14.7%. Those results verify the findings in General Linear Model.

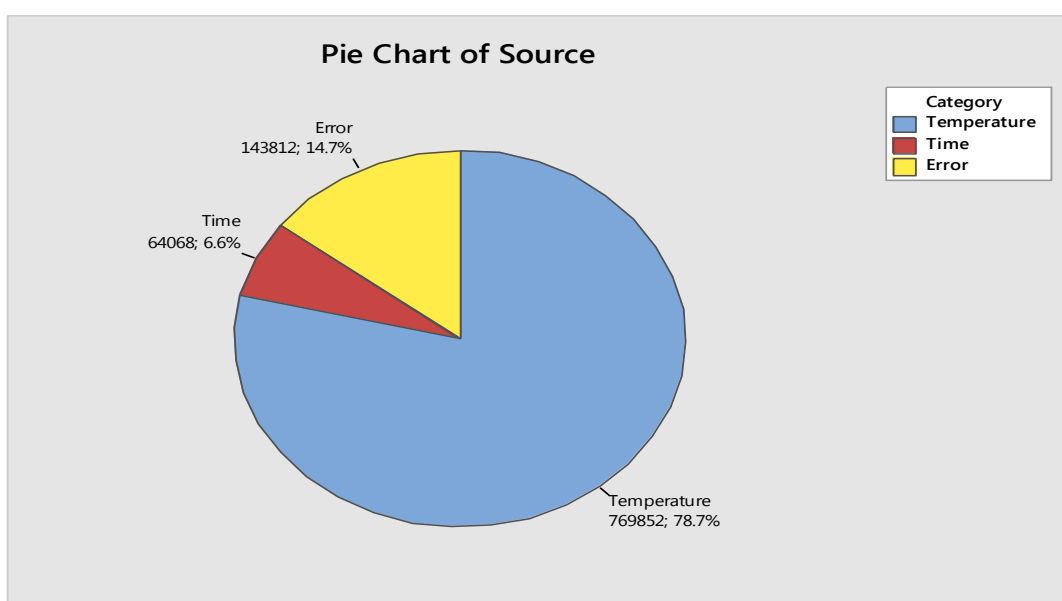


Figure 6.17. Pie chart of the factors; time and temperature on the surface energy.

In Figure 6.18., it can be distinctly observed that T-peel strength has highest values at 100 °C for all ageing times and at 165 °C for 8 min. The samples treated at 165 °C for 16 and 64 min. presented a sharp decrease at the adhesion performance to EPDM. When carrying out the test, it was observed that EPDM cohesion failure occurred in the case of T-peel strength is above 350 N. Therefore, deviation of the results above 350 N was ignored due to reason of deviation arising from EPDM internal elongation characteristics. In addition, it was observed that interphase separation failure was occurred in the removing step of the samples from the press molds for the samples thermally treated above 165 °C for 16 min and 230 °C for 8 min.

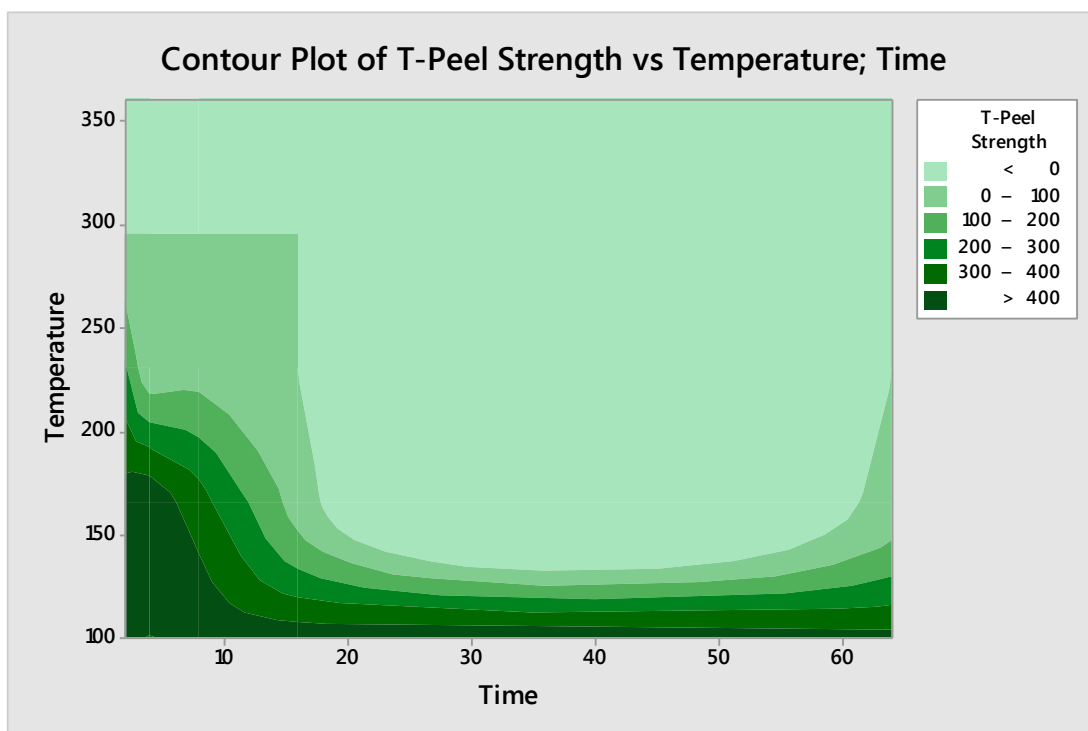


Figure 6.18. Contour Plot of T-Peel Strength after thermal treatments from 100 °C to 360 °C for 2, 4, 8, 16, 64 min. ageing conditions respectively.

The images of the EPDM cohesion and interface adhesion failures are illustrated in Figure 6.19. 100% cohesion failures were observed at 100 °C for all ageing times and at 165 °C for 2 and 4 min. Contrary to this, adhesion failures were occurred at 165 °C for 16 and 64 min. It should be taken into consideration that partially interphase adhesion characteristic was observed at 165 °C for 8 min. Correspondingly this shows that 165 °C for 8 min. ageing condition is the degradation milestone of the Chemosil coating material in terms of adhesion performance.



Figure 6.19. Images of the interface adhesion failures between Chemosil coated aluminum and EPDM surfaces after T-peel strength test. (a) Cohesion failure of EPDM at 100 °C for 2, 4, 8, 16 and 64 min. and 165 °C for 2 and 4 min., (b) Partially adhesion and cohesion failure at 165 °C for 8 min., (c) Adhesion failure at 165 °C for 16 and 64 min.

6.1.1.5. Weight change after T-Peel strength test

Thermal degradation of the Chemosil coating material on the Aluminum surface in different time and temperature combinations was investigated in terms of weight loss. Experiments were carried out based on General Linear Model. Figure 6.20. illustrates that both temperature and time are an effective factor on the response. The interaction of time*temperature was removed from the model due to F-test is zero or undefined. The General Linear Model explains the 90.85 % of the system based on the R-square adjusted value.

Source	DF	Seq SS	Adj SS	Adj MS	F	P
Temperature	4	0.0078086	0.0078086	0.0019521	52.47	0.000
Time	4	0.0013590	0.0013590	0.0003397	9.13	0.000
Error	16	0.0005953	0.0005953	0.0000372		
Total	24	0.0097629				

S = 0.00609977 R-Sq = 93.90% R-Sq(adj) = 90.85%

Figure 6.20. Statistical parameters for weight loss of the thermally treated samples.

The interaction plot shown in Figure 6.21. illustrates that there is no any interaction point affecting the response as a function of increasing time and temperature.

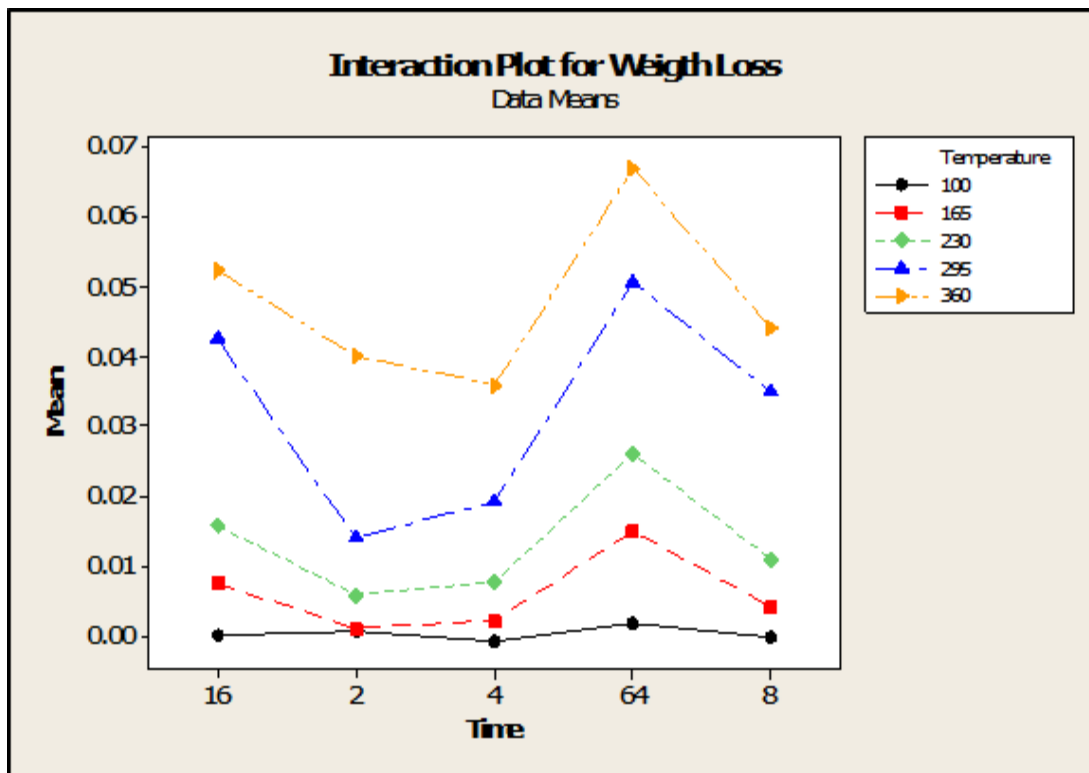


Figure 6.21. Interaction plot of the factors; time and temperature on the response of the weight loss.

Pie Chart analysis is also conducted to see the effect of each individual factor on the response as shown in Figure 6.22. The effects of the temperature and time are 80.0% and 13.9% respectively. In weight loss analysis, temperature is also revealed as the most effective factor on the response. The error percentage of the model is 6.1% as expected from the R-square adjusted value calculated in the General Linear Model analysis.

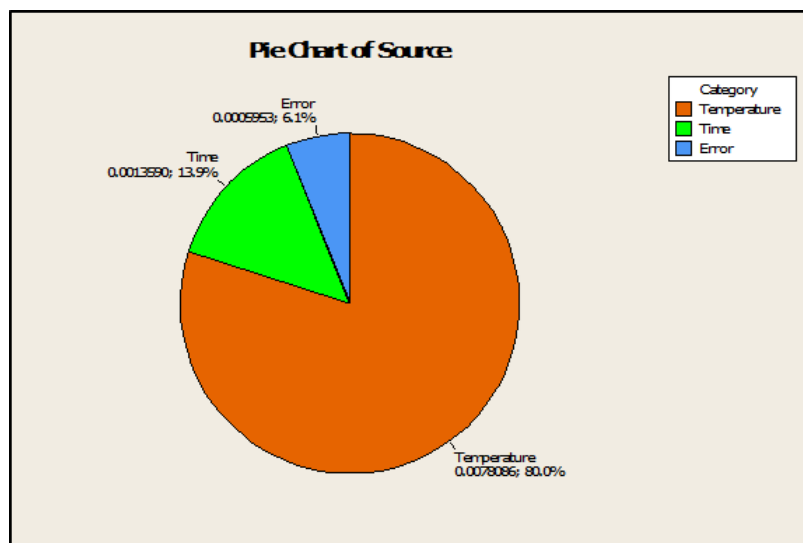


Figure 6.22. Pie chart of the factors; time and temperature on the response of the weight loss.

The rate of the weight loss change increases obviously as a function of increasing time and temperature as shown in Figure 6.23. The increase rate at high temperatures, which is above 250°C, is quite a lot than lower temperatures. As concluded in the results of the T-peel strength test, the adhesion characteristics of the Chemosil coating material is sharply lost after 165 °C for 8 min and noticeably decreased after 100 °C for 8 min. Therefore, FT-IR analysis was carried out to conclude whether weight loss is arising due to degradation of chemical composition of the surface or removal of the volatile components from the surface.

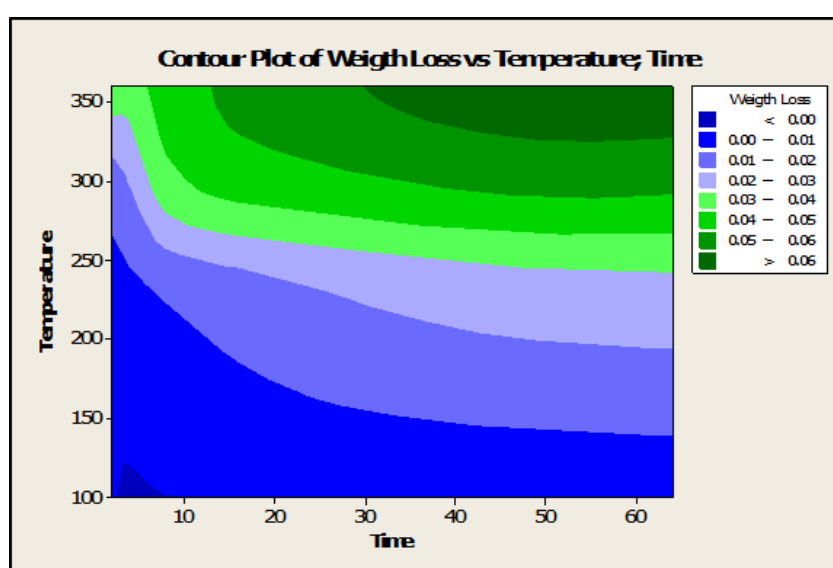


Figure 6.23. Contour Plot of weight loss change after thermal treatments from 100 °C to 360 °C for 2, 4, 8, 16, 64. min. ageing conditions respectively.

6.1.1.6. FTIR analysis

The changes in surface composition of Chemosil coated aluminum substrate before and after the thermal treatment were investigated by FT-IR. The FT-IR spectra's of untreated and thermally treated Chemosil coated aluminum surface for 8 and 64 min. are shown in Figures 6.24. and 6.25. As illustrated in Figure 6.24., the strong peak observed at 1255cm^{-1} on untreated surface exhibits gradually decline in intensity on treated surfaces at 100°C and 165°C for 8 min. respectively. On the other hand, the same peak lying at 1255 cm^{-1} presented decrease in intensity at 100°C and shifted to 1242 cm^{-1} at 165°C for 64 min. compared to untreated surface as shown in Figure 9.25., This peak is attributed to C-O stretching. The absorption peaks at 856 cm^{-1} and 773 cm^{-1} observed on untreated surface shows gradual decline in the intensity on the thermally treated surfaces as temperature increasing from 100°C to 165°C . The same situation is valid for the peaks observed at 1304 cm^{-1} , 1416 cm^{-1} and 1483 cm^{-1} after 8 min at 100°C and 165°C thermal ageing conditions. This absorption area could be correspond to C-H bending. On the contrary, the absorption peak appeared at 1416 cm^{-1} on untreated surface and treated surface at 100°C for 64 min. shifted to 1422 cm^{-1} on the treated surface at 165°C 64 min. This can be attributed that chemical structure of the component is deteriorated at this thermal treatment condition. Furthermore, the absorption peaks observed at 3107 cm^{-1} , 2919 cm^{-1} and 2849 cm^{-1} are also shown decline in intensity on the treated surfaces at 165°C for 8 min. and 64 min. This absorption region corresponds to C-H symmetric/asymmetric stretching vibration.

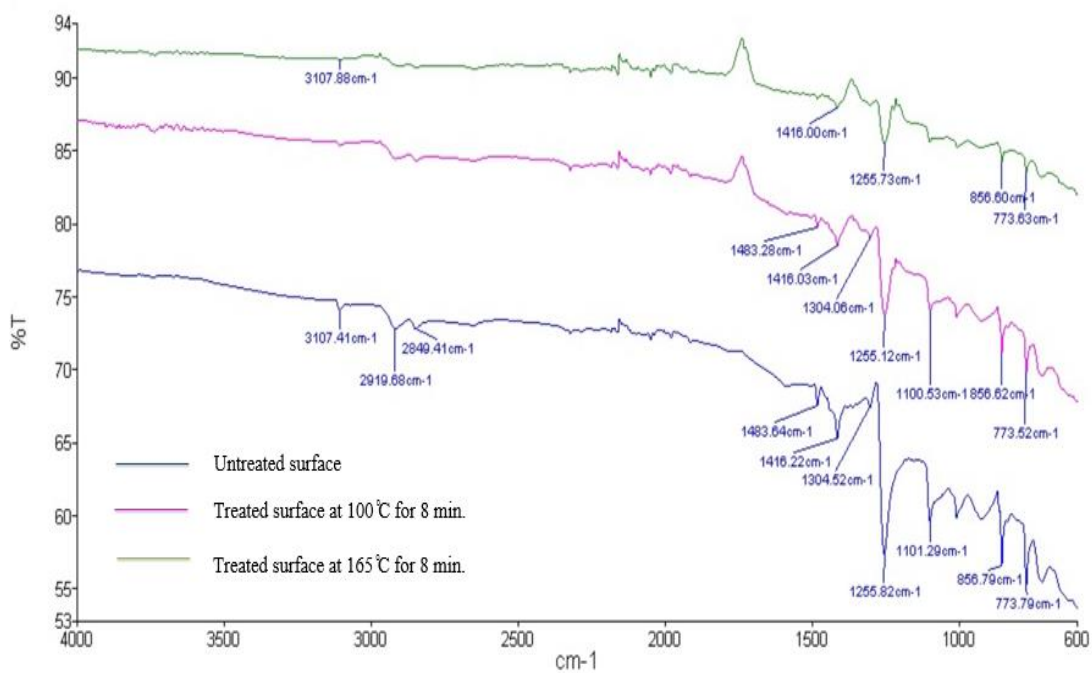


Figure 6.24. Infrared spectra of untreated and thermally treated Chemosil coted aluminum surfaces under the following conditions: at 100 °C and 165 °C for 8 min.

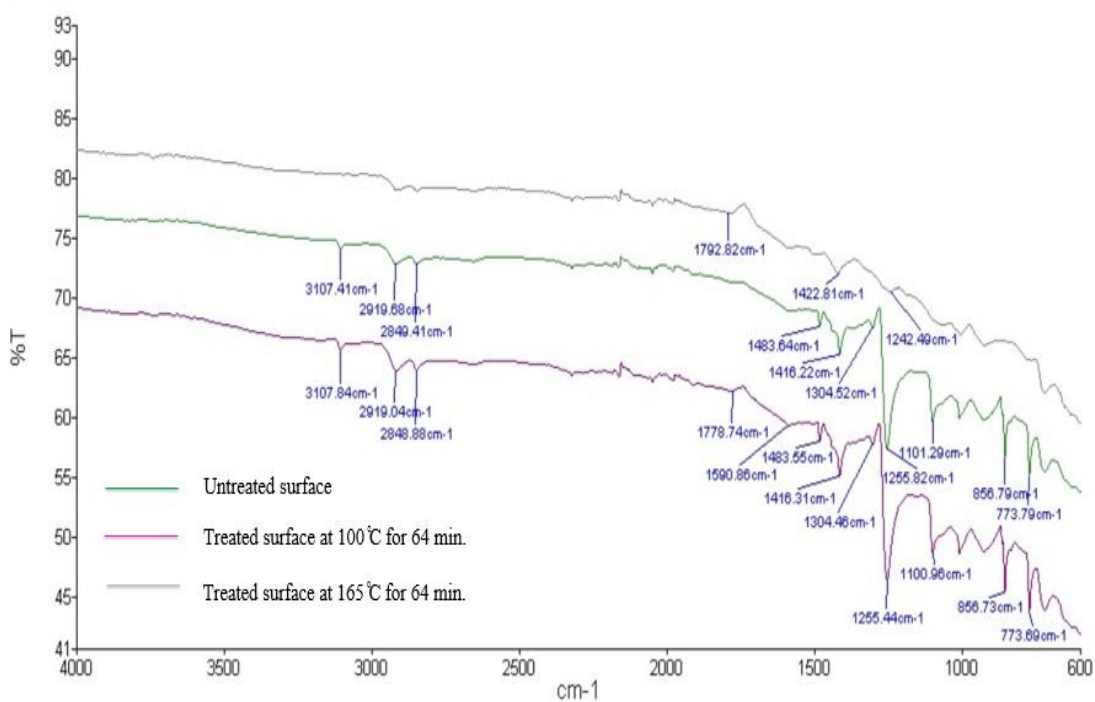


Figure 6.25. Infrared spectra of untreated and thermally treated Chemosil coted aluminum surfaces under the following conditions: at 100 °C and 165 °C for 64 min.

6.1.1.7. Simultaneous thermal analysis (SAT) of the Chemosil

Netzsch Simultaneous Thermal Analyzer (STA) incorporates TGA and DSC were conducted simultaneously to observe the amount of weight change, heat flow rate (caloric reactions/endothermic and exothermic reactions) and most off all thermal degradation behavior of the Chemosil coating material due to decomposition reactions occurred in depending on its temperature. Hence, coating material was exposed to controlled thermal program and continuously its mass is monitored. From the Figures 6.26., it can be easily seen that volatile parts (humidity, volatile organic components) are released approximately up to 150 °C based on TGA curve. That is why; a weight reduction was occurred at this point. It is expected that volatile parts were imposed to physical transitions such as vaporization, evaporation, sublimation, desorption, drying. Since the coating material was dried before STA is carried out, it was seen that there are not too many volatile components available in the coating material. Approximately 15% percent of the volatile parts were released up to 150 °C.

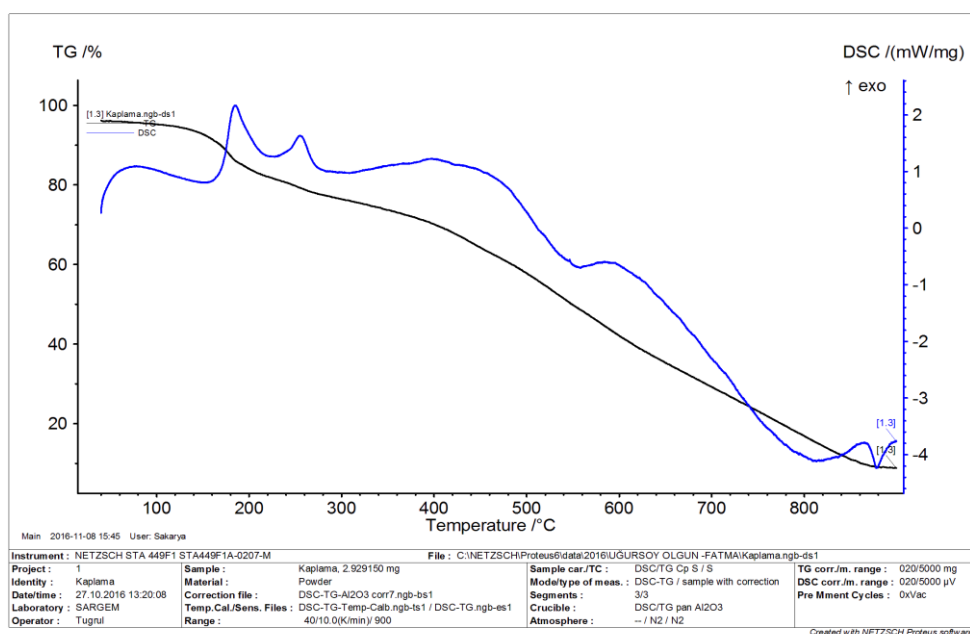


Figure 6.26. Simultaneous thermal analysis of the Chemosil) coating. The blue DSC thermal curve and the black TGA weight loss curve are displayed above.

As illustrated in Figure 6.26., thermal degradation starts after 160 °C in the coating material. Around 200 °C and 260 °C, there are two exothermic peaks in succession. These peaks are predicted to come from thermal degradation of the two types of polymers used in the coating formulation. Tg curves of the polymeric materials are not visible. This could be due to reason of degradation started before Tg. It could be demonstrated that, Tg could be higher than thermal degradation temperature of the polymeric materials.

6.2. Plasma Effect on the Aluminum Surface in Terms of Interface Adhesion

Aluminum surface characteristics have a critical role on bonding to rubber. Plasma surface activation method is an advanced and cost-effective process for adhesion improvement. Physically, plasma surface modification is provided at the Nano level just underneath the surface. In this study, the effect of cold plasma applications on metal-rubber adhesion strength was investigated by T-peel test. The un/treated and un/coated aluminum surface properties were characterized by contact angle (CA) in terms of wettability. In order to understand the effect of plasma modification, the surfaces were characterized by FTIR. This study discusses the mechanisms that are responsible for the adhesion between Chemosil coated / plasma treated aluminum stripe and EPDM based rubber.

6.2.1. Contact angle (CA) / Surface wettability

Plasma treatment physically changes surface while chemically activating the surface. Spreading behavior of the water droplet was observed on the uncoated and Chemosil coated surface. It was understood that the wetting ability to the surface after plasma application at various times varies considerably. Depending on the duration of the plasma application, it gains wetting ability. The critical point here is that the application time is increased without altering the surface morphology and chemical structure. In both cases, the ability to wet with plasma application was increased. As shown in Figure 6.27., the wetting angle on the uncoated dry aluminum surface is reduced from $70^{\circ} \pm 5^{\circ}$ to $10^{\circ} \pm 3^{\circ}$ in a short time by plasma treatment. Initial contact

angle of primer (Chemosil) coated aluminum surface has a hydrophobic surface characteristics. After plasma activation in 1sec. to 10 sec., incredible decrease occurred in contact angle. Contact angle measurement results show that the primer coating wetting angle decrease from 90° to 10°. It is not allowed to increase the surface temperature by more than 60 °C in plasma applications.

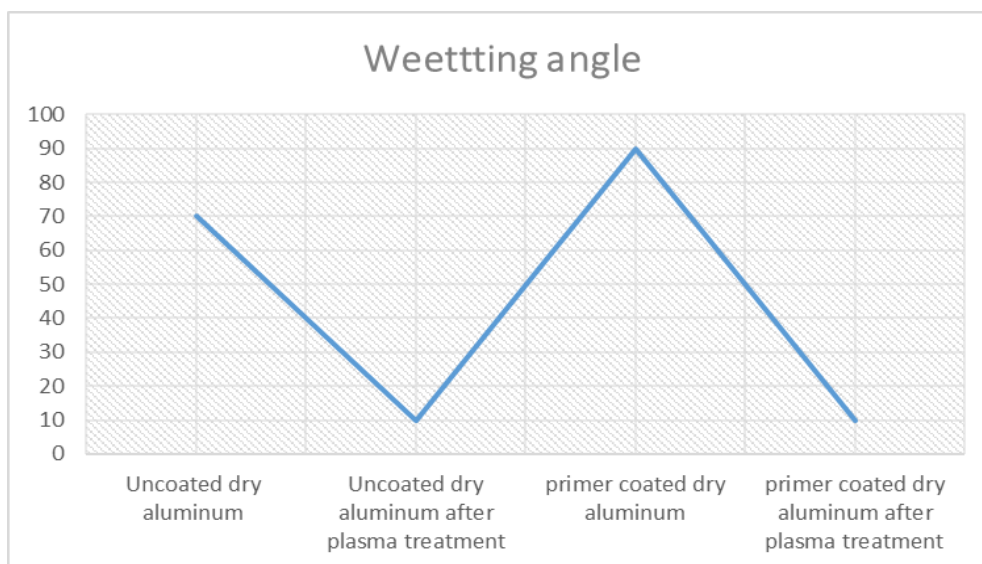


Figure 6.27. Wetting angle change of the uncoated dry aluminum and primer coated dry aluminum surfaces after plasma application

6.2.2. T-Peel strength test

Figure 6.28. shows the T-peel strength forces of interface between EPDM and aluminum having different surface characteristics, which are uncoated rigid aluminum, coated rigid aluminum, uncoated-sanded rigid aluminum, uncoated-plasma treated rigid aluminum, coated-plasma treated rigid aluminum and uncoated lanced aluminum respectively. As shown in Figure 6.29., there is no any adhesion observed at the interfaces where aluminum strip is uncoated. Even aluminum stripe which's surface is treated with sanding operation did not show any interface adhesion. These samples were directly removed from the pressing mold as non-adherent. On the other hand, the interface consisting of EPDM to uncoated-lanced aluminum strip was released from the pressing molds as adhered. After sample is left to be cool at room temperature, it was observed that interface can easily be separated by manually. This is due to EPDM mechanical interlocking was occurred. In other

words, the melted EPDM penetrates from the gaps of the lanced aluminum and spread throughout the gaps. The interface adhesion is only observed at primer (Chemosil) coated aluminum surfaces as expected. The effect of the cold plasma treatment on the Chemosil surface were analyzed here. Thereby, plasma treated and untreated Chemosil coated aluminum surfaces were compared based on their adhesion forces to EPDM. At both cases, adhesion forces are quite high and the interface separation type is cohesion failure in EPDM. EPDM was separated in itself and aluminum surfaces are fully covered by EPDM after T-Peel strength test as illustrated in Figure 6.30 as EPDM coverage percentage on AL surface.

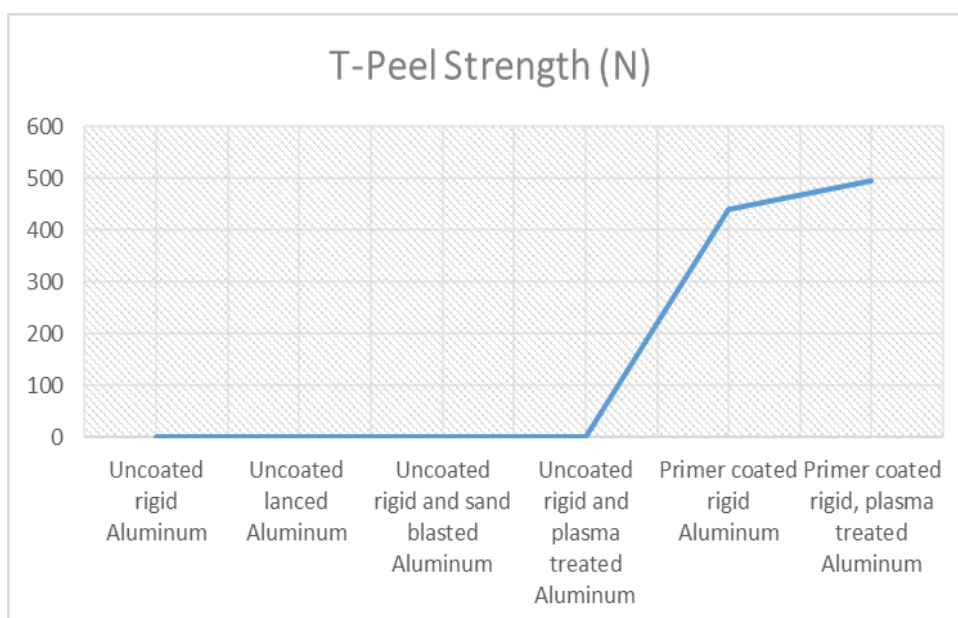


Figure 6.28. T-Peel strength forces of aluminum surfaces with EPDM.

The remaining EPDM on both surfaces (EPDM and aluminum) were analyzed as shown in Figure 6.31. When geometric separation patterns were examined, the separation pattern for the plasma treated surfaces exhibit central v-shaped separation. On the other hand, surfaces without plasma treated showed randomly separation usually from the edges and from a random point on the surface. These patterns were verified on three replicated samples.

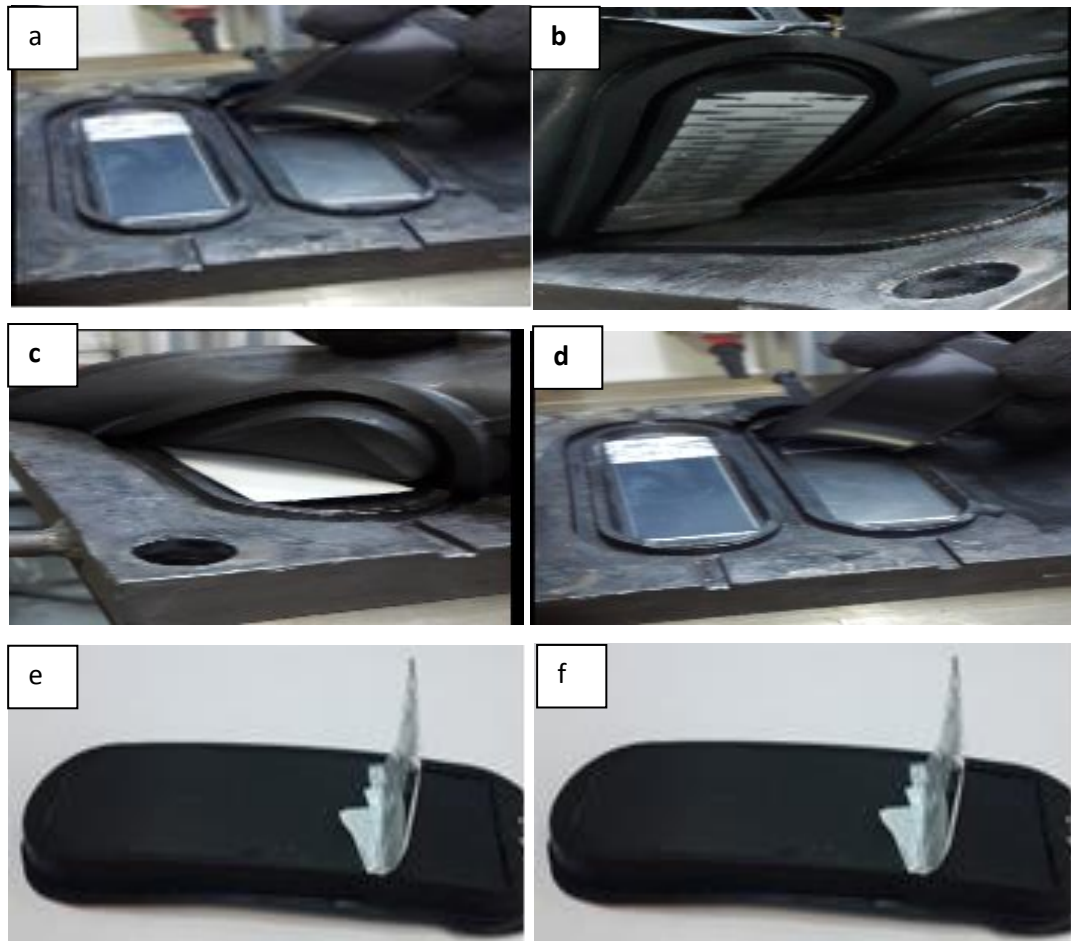


Figure 6.29. Interface appearance of the samples after molding operation (a) uncoated rigid aluminum, (b) uncoated lanced aluminum, (c) Uncoated rigid and sand blasted Aluminum, (d) Uncoated rigid and plasma treated Aluminum, (e) Primer coated rigid Aluminum, (f) Primer coated rigid, plasma treated Aluminum.

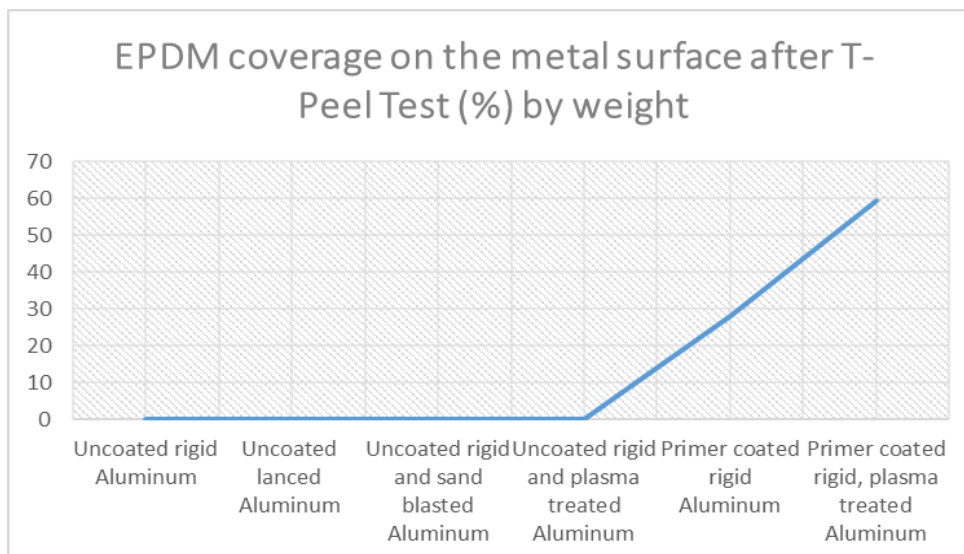


Figure 6.30. EPDM coverage on the metal surface after T-peel test (%) by weight.

EPDM coverage on the AI surfaces after T-peel strength test was also analyzed for the samples that realized interface adhesion to predict the effect of the plasma treatment of the surfaces. For the coated aluminum surface without plasma treatment, EPDM coverage on the aluminum surface is $23.72 \pm 6\%$ as average. On the other hand, EPDM coverage on the aluminum surface, which was plasma treated is $61.43 \pm 8\%$ as average. This also demonstrates that plasma treatment of the Chemosil coated surface affects the EPDM cohesion separation type.

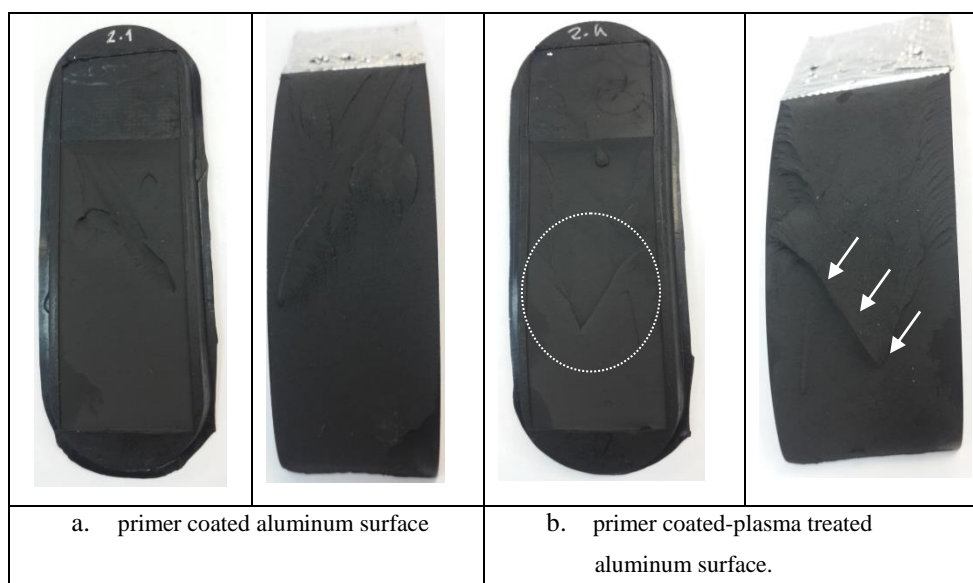


Figure 6.31. Interface images of the coated and coated/plasma treated surfaces after T-Peel Strength test.

6.2.3. FTIR analysis

FTIR analysis was carried out on the surfaces that showed adhesion after T-peel strength test. The aim of this analysis was to predict whether there is any separation occurred from the Chemosil coating layer. Thus, the changes in surface composition of both EPDM and aluminum were investigated after T-peel test. Figure 6.32. shows the infrared spectra of plasma treated and untreated / primer coated aluminum surfaces after T-peel strength test. The infrared peak of the Chemosil coated aluminum surface does not overlap with the surfaces after T-peel strength test. Moreover, the infrared peaks of the both side of the interface, which are EPDM and aluminum, overlap approximately 100 %. Thus, it can be concluded that, EPDM is fully covered on the Chemosil coated aluminum surface and complete EPDM cohesion was occurred at the interface after T-peel test.

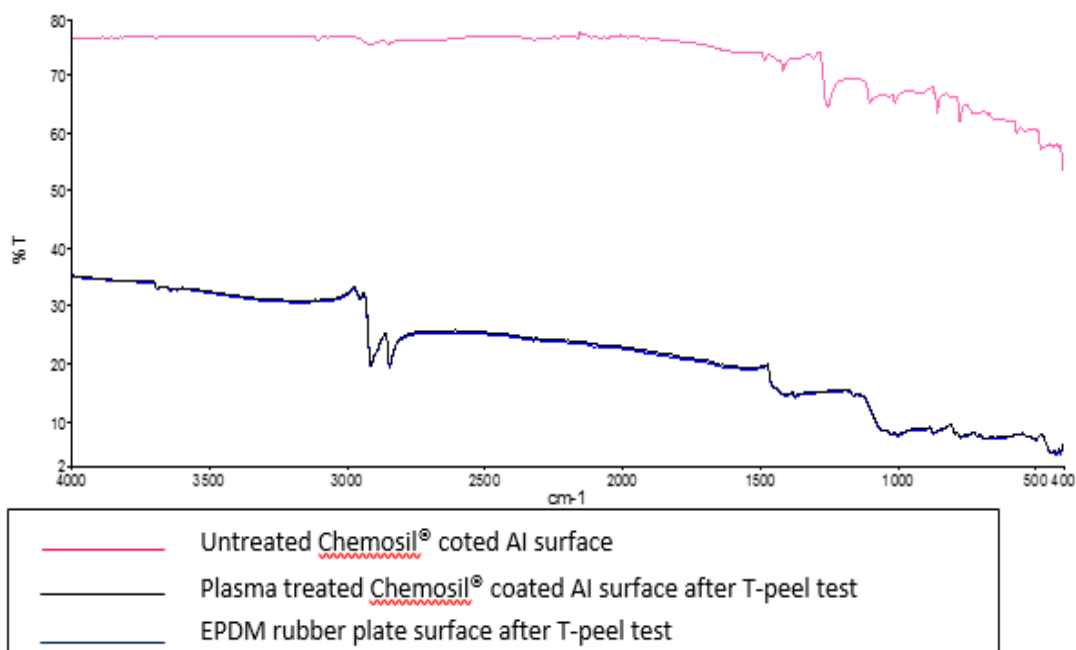


Figure 6.32. FTIR Infrared spectra of plasma treated / untreated primer coated aluminum surfaces.

6.3. Surface Characteristics of the Improved Coating Materials

The selected interface coating materials were applied to the AI strip surface as shown in Figure 6.33. Surface characteristics were analyzed with the following methods.

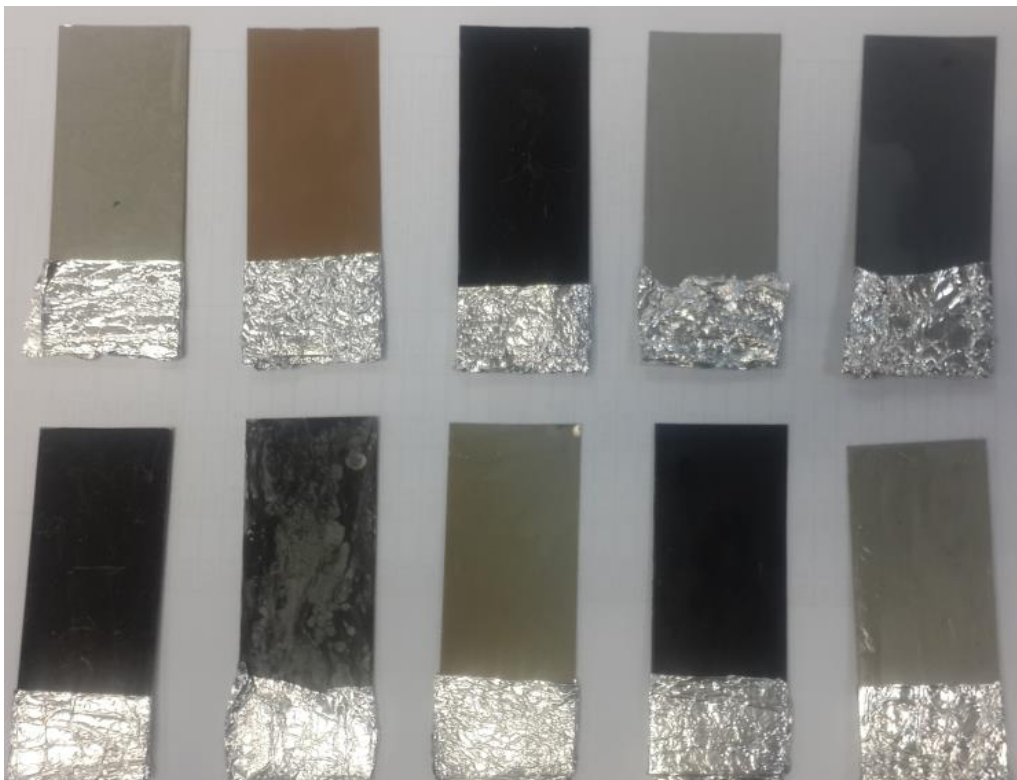


Figure 6.33. Images of the coated aluminum surfaces with improved coating materials.

6.3.1. Wettability analysis

The wettability characteristics of the coating materials were evaluated and compared with each other. Figure 6.34. shows the contact angle measurements of the improved coatings. The expectation for the better interface adhesion is lower contact angle based on the findings observed in Chemosil coating surface characteristics. 3B and 5B showed lower contact angle in comparison of others. On the other hand, 6B exhibited highest contact angle. Based on those results, the effect of the contact angle on the interface adhesion to the EPDM based rubber was discussed in the conclusion section.

When the effect of the content of the coating mixtures is investigated based on coating group codes of A and B, TLA available in the coating mixture 4A provides lower CA. On the other hand, BYK and 1895COST cause higher CA in 2A and 3A respectively. The effect of NL411 is obvious in group B exception in 4B coating mixture. In 4B, this difference could be caused by reaction occurred between TLA and NL411. Because within group of A, TLA was the one, which provides lower CA.

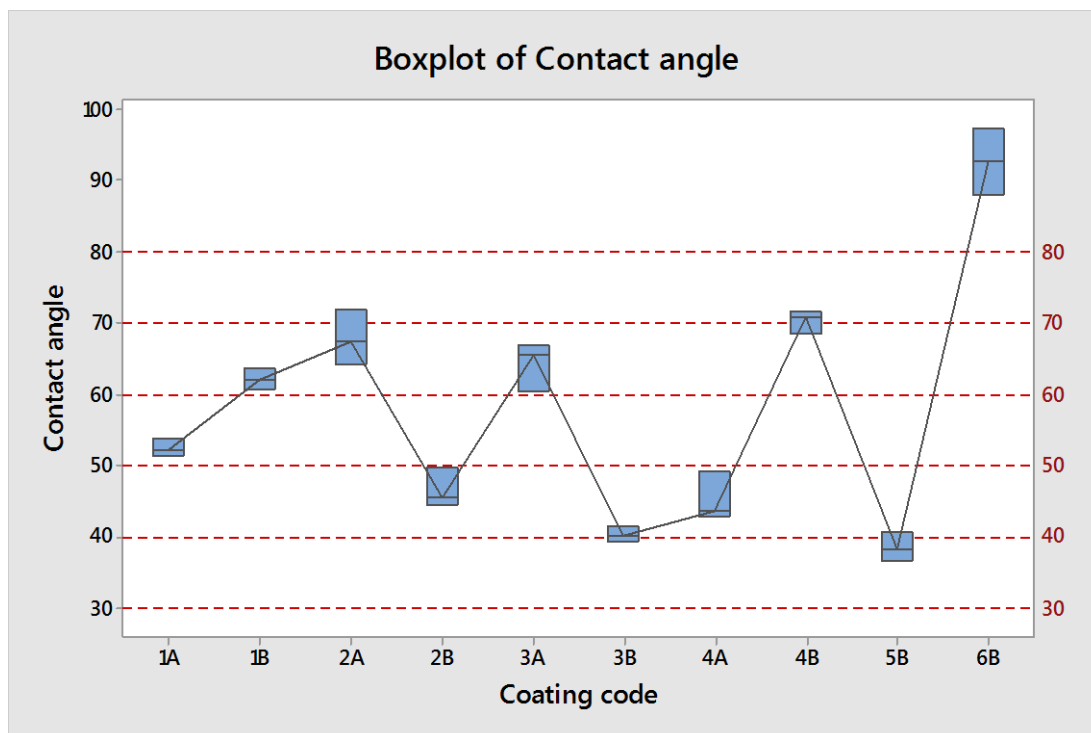


Figure 6.34. Contact angle distribution of the improved coating materials.

6.3.2. Surface morphology analysis

Surface morphologies of the coating materials were investigated under microscope. It is well known that surface morphology influences the interface adhesion characteristics. Figure 6.35. illustrates the morphological structures of the coated aluminum surfaces with different kind of coatings. 2A and 4A have more porous structure. 1A and 3A have similar image in terms of porosity. 1B, 2B and 5B showed similar structure in different color intensities. The image of the 3B and 4B was non-homogenous under microscope. However, 3B and 4B exhibited higher porosity on the surface. The structure of the 6B is approximately similar to the 1B, 2B and 5B.

Since the color of the coating is like light brown, the appearance under the microscope showed difference in comparison of others.

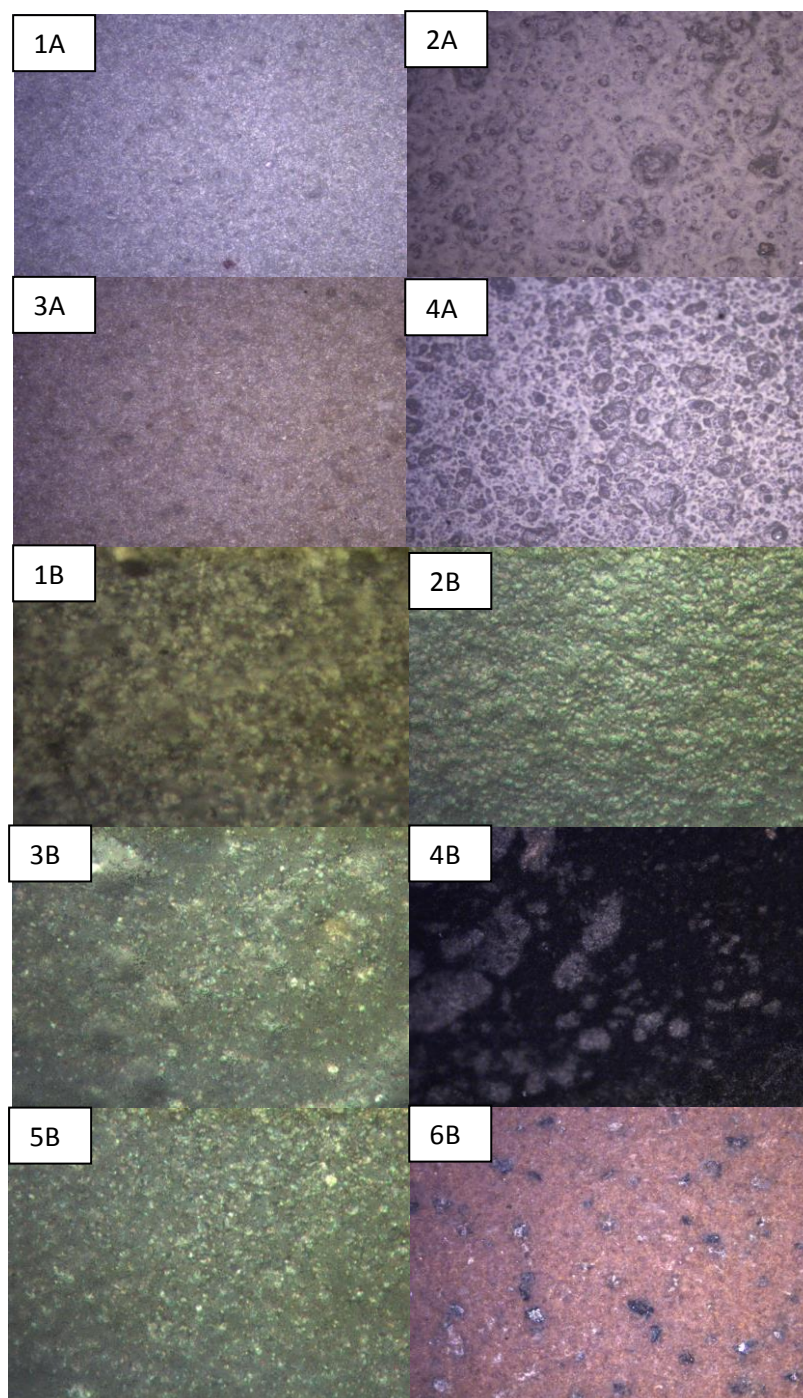


Figure 6.35. Surface morphology images of the improved coated materials of 1A, 2A, 3A, 4A, 1B, 2B, 3B, 4B, 5B and 6B respectively under microscope.

6.3.3. Coating thickness analysis

Coating thickness measurements were carried out on the coated aluminum surfaces with different coating types by using coating thickness gauge (Huatec®). The coating thickness variation within themselves and with each other are illustrated via boxplot graph as shown in Figure 6.36. It was applied to see how the different types of coating materials applied with the same method show the distribution. Correspondingly, it was examined on the graph that the data are regularly distributed and in which range they stack up. Measurements were carried out on 10 samples. Some of the data points are outliers, which are points that do not appear to belong with the rest of the data.

2B coating type shows the better coating thickness distribution in comparison with others. On the other hand, 4B shows highest distribution. 2B is consisting of 211 + BYK + (NL411) and 4B is consisting of 211 + TLA + (NL411). The difference contents of the coating mixtures are BYK and TLA.

The coating thickness deviation on 1A, 2A and 4B coating types are quite high in comparison with others. They are consisting of MER, MER + BYK and 211 + TLA + (NL411) components respectively. The effect of the MER could be taken into consideration.

The mean coating thickness values of the 3A, 4A, 5B and 6B coating types are lower than 50 micron. Moreover, their deviations are not as high as 1A, 2A and 4B. They are consisting of MER + 1895COST, MER + TLA, 211 + (NL411), PF components respectively.

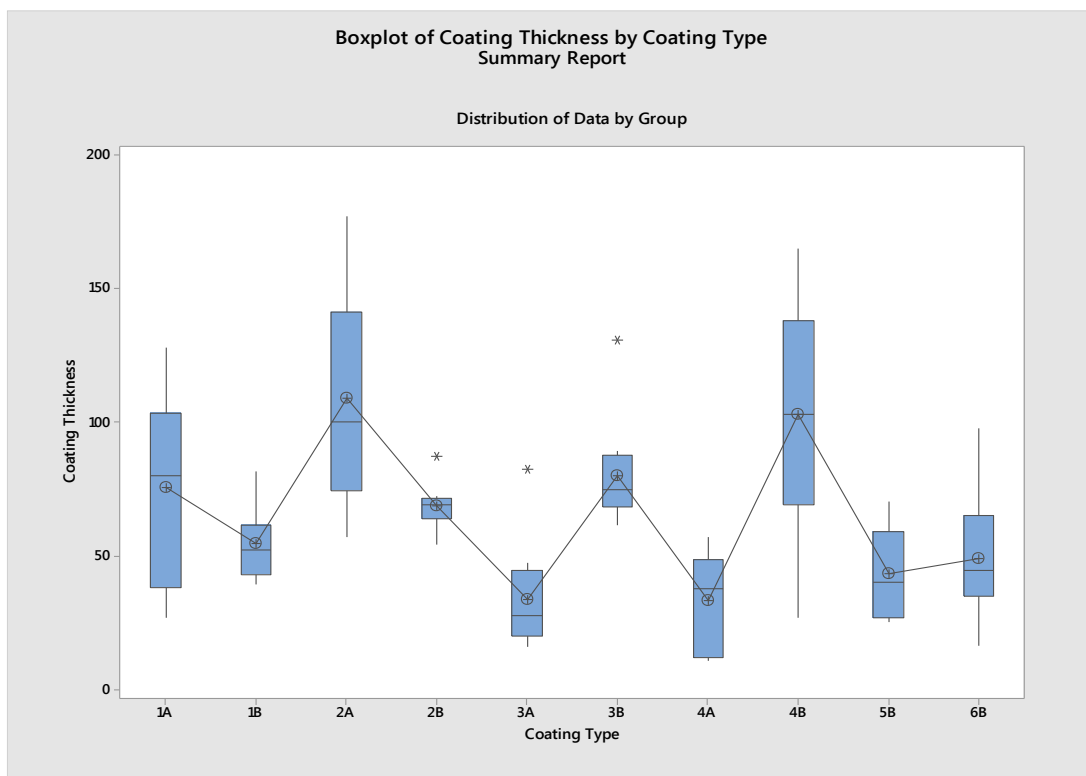


Figure 6.36. Coating thickness distribution of the improved coating materials.

6.3.4. Surface roughness analysis

Surface roughness characteristics were also analyzed via boxplot to be able to see the distribution data and stack up ranges of the coating types. Figure 6.37. illustrates the boxplot graph of surface roughness data.

3B and 4B coating type's exhibits highest surface roughness deviation and values in comparison with others. Their contents include $211 + 1895\text{COST} + (\text{NL411})$ and $211 + \text{TLA} + (\text{NL411})$ respectively. On the other hand, surface roughness values of the rest coating types spread approximately in the range of 0.4 to 1 Ra. The lowest deviations were observed on the coating types of 6B, 5B, 2B and 3A respectively.

Since 1B and 5B exhibited the lowest surface roughness and 3B exhibited highest surface roughness values, the effect of surface roughness on interface adhesion could be taken into account. Moreover, their contents 211 , $211 + (\text{NL411})$ and $211 + 1895\text{COST} + (\text{NL411})$ respectively could be taken in to consideration.

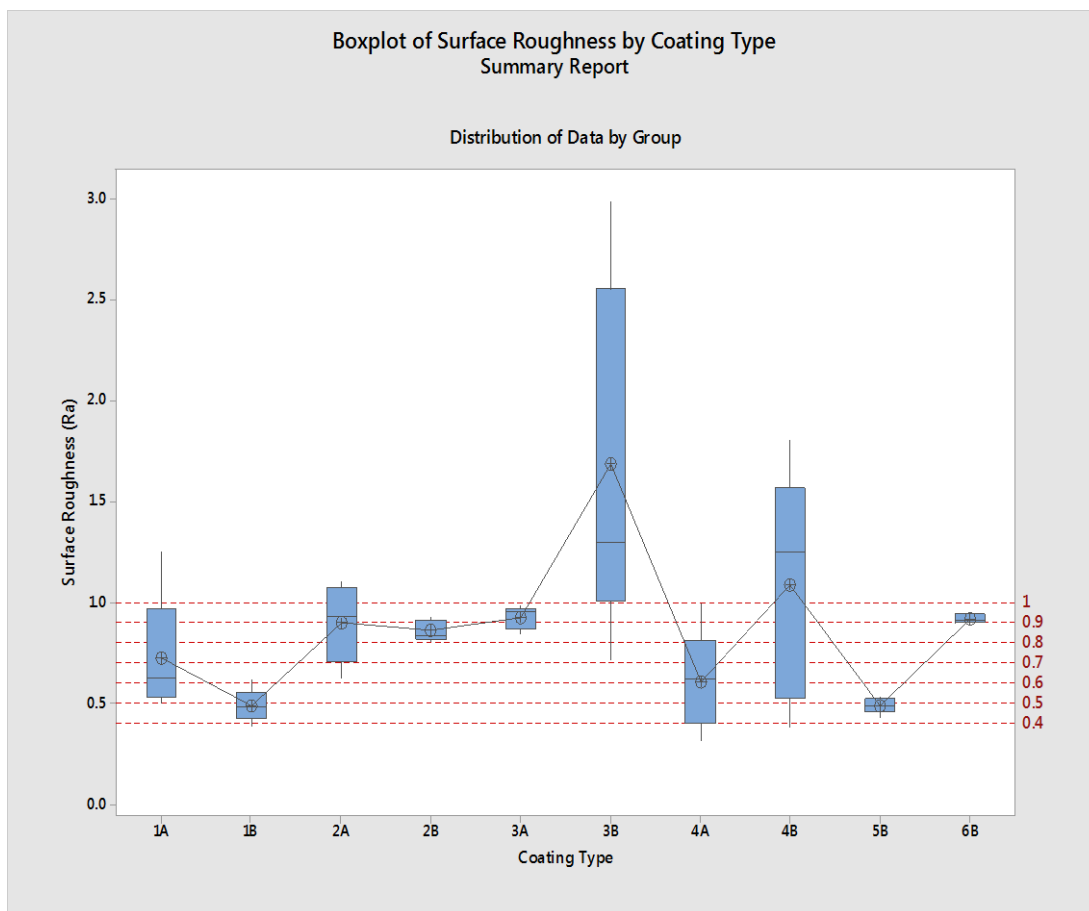


Figure 6.37. Surface roughness distribution of the improved coating materials.

6.3.5. T-Peel strength test

Figure 9.38. shows the T-peel strength forces of the different type of the improved coating materials in comparison of the Chemosil coating at the interface of EPDM based rubber and aluminum alloy strip. Chemosil coated aluminum strip was supplied as coated by supplier. None of the improved coating material could have reached to the interface adhesion force of the Chemosil coated surface.

5B coating type has 261.93 newton peel strength. Its content is included 211 + (NL411) which is also Chemosil coating, is brush applied version. It is known that, the aluminum strip is provided as coated from supplier. In this case, the importance of the coating application process is revealed due to the differences in the peel strengths of the same coatings applied with different coating application methods.

1B coating type is the one, which shows second high peel strength force. It is consisting of only 211, which is primer coat of the Chemosil. This illustrates that, 211 has effective impact on the interface adhesion.

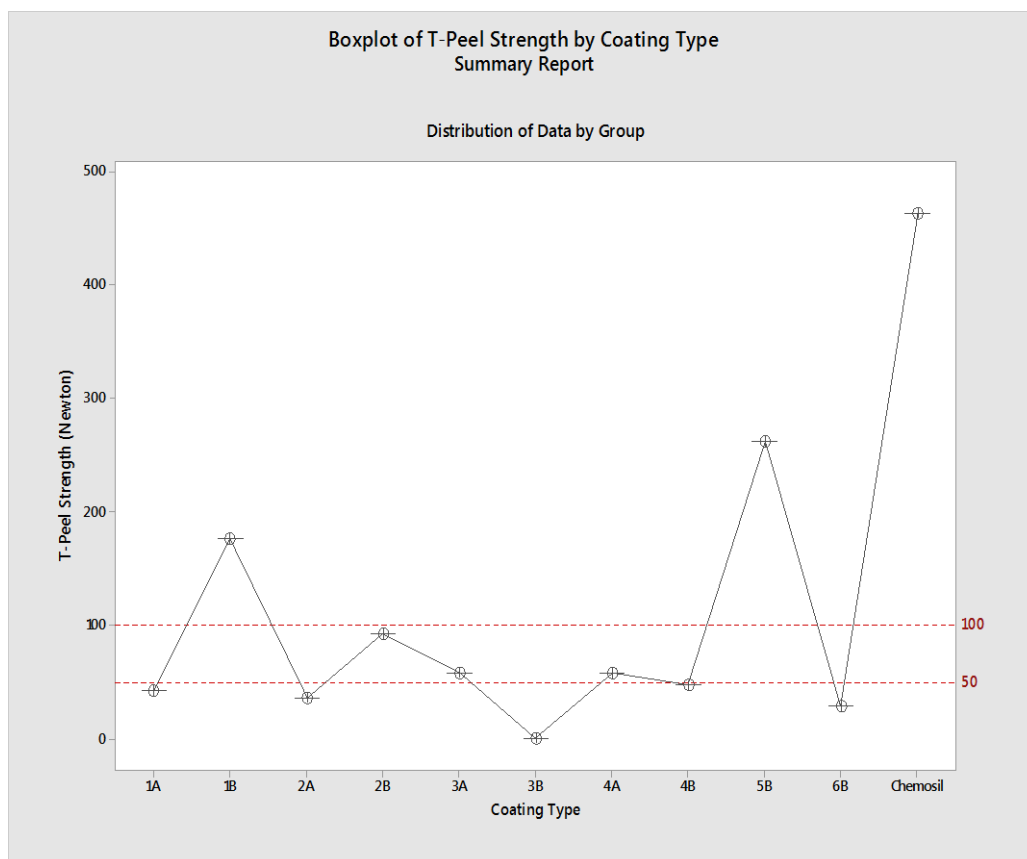


Figure 6.38. T-peel strength forces of the interfaces coated with improved coating materials.

6.3.6. Weight change after T-Peel strength test

Figure 6.39. shows the weight changes of the coated aluminum alloy stripe and EPDM based rubber plates after T-peel strength test. In the case of comparison of the weight changes of the aluminum surfaces after T-peel test, all the coating types except 5B showed decrease in weight. The decrease in weight means that the coating is separated from the aluminum stripe surface. For those coating types, interface adhesion is weak between coating and aluminum stripe. The maximum weight change occurred on the 2A-coated surface and the minimum weight change occurred on 1B-coated surface. 5B-coated aluminum surface exhibited increase in weight after T-peel test. When weight changes of the EPDM rubber plates were compared

after T-peel test, a proportional decline was observed. This could be due to the reasons of migration of the EPDM rubber to the surface of the coated aluminum stripe or evaporation of the some components in the EPDM rubber compound mixture or reactions occurred during the vulcanization process of the compound.

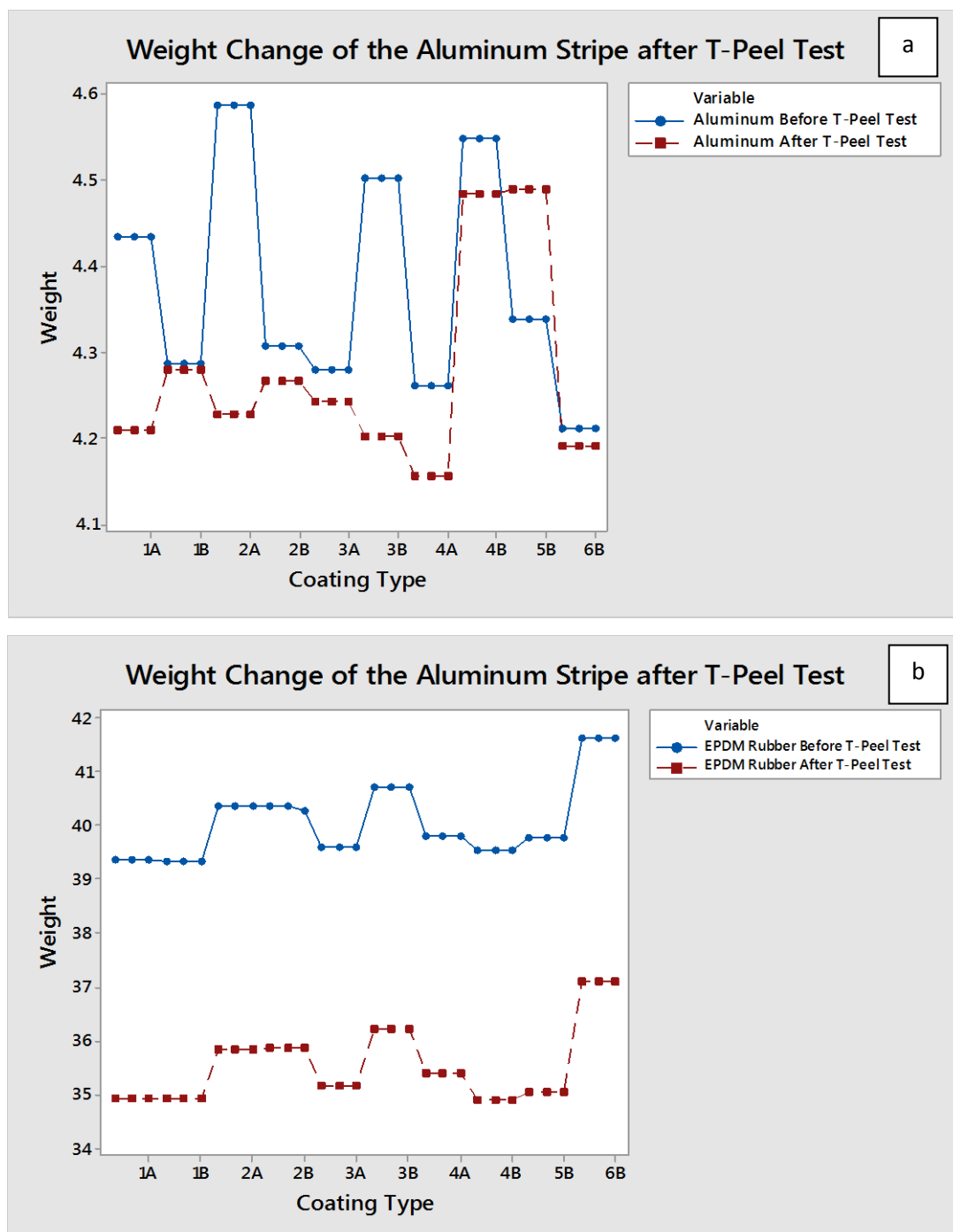


Figure 6.39. Weight changes of the (a) aluminum stripe and (b) EPDM based rubber plate after T-peel test.

6.3.7. Visual evaluation of the interface after T-peel strength test

Table 6.1. illustrates the visual evaluation of the interfaces after T-peel test. The interfaces of the aluminum stripe coating and rubber plate coating were investigated separately. Based on the interface images shown in Figures 6.40. and 6.41. the interface separation shapes were interpreted as following;

- 1A: Approximately half of the coating was separated from the aluminum surface and passed through the rubber plate. There was no rubber residue on the aluminum surface. Interface adhesion force between aluminum-coating is intermediate and rubber-coating is weak.
- 2A: Approximately 2/3 of the coating was adhered to rubber plate. The interfaces of aluminum-coating and rubber-coating exhibited weak and intermediate-good performances respectively.
- 3A: The coating was mostly well adhered to the aluminum surface. There is little regional coating separation on the AI surface. Interface separation was occurred on the rubber-coating surface. As the conclusion, aluminum-coating interface is strong and rubber coating interface is weak-intermediate.
- 4A: The coating was mostly well adhered to the aluminum surface. There is little regional coating separation on the AI surface. Moreover, some of the rubber parts were partially tacked to the coating on the aluminum surface. At the interface of the rubber-coating, separations occurred and adhesion is intermediate-strong. On the other hand, strong interface adhesion performance between aluminum-coating was exhibited.
- 1B: The adhesion between aluminum and coating is strong. On the contrary, the adhesion between rubber and coating is very weak.
- 2B: There are more regional breaks at the interface of aluminum-coating in comparisons of 1B. However, the AI breaks off the surface and shows adhesion to EPDM in these regions.
- 3B: Coating material completely detaches from the AI surface and adheres to the rubber surface. This demonstrates that, rubber-coating interface adhesion is strong. On the other hand, aluminum-coating interface is very weak.

- 4B: Regional coating breaks appear on the aluminum surface. In addition, breaks at the rubber-coating interface is available. Rubber could be migrated to the coating on the aluminum. This suspect is planned to be analyzed in FTIR.
- 5B: Coating material was well adhered to the rubber surface. Rubber to cohesion separation at the rubber interface was observed. Only, a small portion of the coating was passed through to the rubber surface. This is negligible. This could be due to inappropriate substrate cleaning process.
- 6B: The adhesion between aluminum and coating is strong. Regional coating breaks is available on the aluminum surface. This is negligible due to the reason of inappropriate substrate cleaning method. There is no adhesion observed between rubber and coating interface.

Table 6.1. Evaluation of the interfaces after T-peel test in terms of their adhesion ability to EPDM and AL.

Coating Type	Aluminum-coating interface adhesion	Rubber plate coating interface adhesion
1A	Intermediate	Weak
2A	Weak	Intermediate-strong
3A	Strong	Weak-Intermediate
4A	Strong	Intermediate- strong
1B	Strong	Very weak
2B	Intermediate	Intermediate- strong
3B	Very weak	Strong
4B	Intermediate- strong	Weak-Intermediate
5B	Strong	Strong
6B	Strong	Weak



Figure 6.40. Images of the interfaces of “A” series coating applied between aluminum stripe and EPDM based rubber plate after T-peel test.



Figure 6.41. Images of the interfaces of “B” series coating applied between aluminum stripe and EPDM based rubber plate after T-peel test.

CHAPTER 7. CONCLUSION

Within the content of this study, metal to rubber interface adhesion characteristics have been investigated into three categories; effect of thermal treatment on the Chemosil coated aluminum surface, effect of plasma treatment at nano-level on the pure and Chemosil coated aluminum surfaces and adhesion ability of the improved coating materials to the both EPDM and aluminum surfaces.

At the beginning, adhesion properties of Chemosil coating on AL /EPDM interface have been evaluated for the aim of investigating the effect of thermal ageing conditions to be able to find the optimum processing parameters for optimum interface adhesion.

The surface characteristics of the thermally aged Chemosil coated aluminum surfaces have been defined by various analysis. Surfaces have been analyzed by light microscope to observe the morphological changes. The effect of morphological changes has been measured by profilometer to define surface roughness. FTIR analysis has carried out to observe the changes in functional structures. Surface wettability performances have been monitored by increasing time and temperature via contact angle and surface energy measurements. Moreover, the effect of the ageing on the interface adhesion performance has been measured by T-Peel test. The EPDM coverage on the AL surface or vice versa have been analyzed by weight change calculations before and after T-Peel test. To be able to verify findings from surface characterization analysis and see thermal degradation behavior of the Chemosil coating, simultaneous thermal analysis (STA), which incorporates with TGA and DSC has been carried out.

In the wettability analysis of the thermally aged samples in different temperature and time combinations, temperature has been found as effective parameter on the response. This was demonstrated by the pie chart, as the temperature effect is 98, 1 %. On the contour plot, the surface energy exhibited continuous increase as an increasing function of temperature. Hence, it was concluded that low processing time is sufficient to increase surface energy at any processing temperature.

Microscopic analysis illustrated that the first wideness and deepness of the porous structure exhibited change after ageing conditions of 100 °C and 165 °C for 8 min. The most severe change at wideness, deepness and visual color was observed after ageing conditions of 230 °C for 8 min. and 295 °C for 2 min. Morphology of the surface completely changed at 360 °Cs.

The morphological findings were verified by roughness analysis. The first roughness change was observed after ageing conditions of 100 °C and 165 °C for 8 min. The second change was observed after ageing conditions of 230 °C for 8 min. and 295 °C for 2 min. The final change occurred at 360 °C. Moreover, temperature was observed as the effective parameter on the response as it was in morphology analysis.

In the findings of T-Peel test, temperature has been found as the most effective parameter on the response as expected. In the interaction plot, T-peel strength curves of the 295 °C and 360 °C overlapped for the whole ageing times. This demonstrates that there is no significant effect of the temperature on the response after 230 °C ageing condition. Moreover, there is a dramatic decline on the T-peel strength after 165 °C for 8 min.

When the surfaces were evaluated as visually in terms of adhesion and cohesion failures, completely cohesion failure in EPDM was observed at 100°C for all ageing times and at 165°C for 2 and 4 min. The partially interface adhesion characteristic was observed at 165°C for 8 min. In addition, interphase separation failure was occurred in the removing step from the press molds for the samples thermally treated above 165 °C for 16 min and 230 °C for 8 min. As the conclusion, 165°C for 8 min.

ageing condition was demonstrated as the degradation milestone of the Chemosil coating material in terms of adhesion performance.

In contrast to other analyzes, both temperature and time were observed as the significantly effective parameter on the response in the weight change analysis. Weight loss trend exhibited increase as a function of increasing temperature and time on the contour plot. Therefore, FT-IR and TGA-DSC analyses have been carried out to conclude whether weight loss with increasing time and temperatures is arising due to degradation of chemical composition of the surface or removal of the volatile components from the surface.

In the FT-IR analysis, the adsorption peaks at 3107 cm^{-1} , 2919 cm^{-1} , 2849 cm^{-1} , 1483 cm^{-1} , 1304 cm^{-1} , 856 cm^{-1} , 773 cm^{-1} exhibited decrease in the intensity as a function of increasing time and temperature. Furthermore, the peaks at 1416 cm^{-1} and 1255 cm^{-1} shifted to 1422 cm^{-1} and 1242 cm^{-1} respectively at $165\text{ }^{\circ}\text{C}$ for 64 min. compared to thermally untreated surface and thermally treated surfaces at $100\text{ }^{\circ}\text{C}$ for 8 min. The peaks at 1416 cm^{-1} and 1255 cm^{-1} are still available for 8 min but as decreased in intensity. As the result, the radical changes in the chemical structure of the coating occurs at $165\text{ }^{\circ}\text{C}$ and above for 8 min ageing condition.

TGA-DSC analysis was conducted to predict the degradation temperatures of the materials and find explanation for the findings of above analysis. The first severe mass change was observed up to $150\text{ }^{\circ}\text{C}$. This was predicted due to removal of the volatile parts. Around $200\text{ }^{\circ}\text{C}$ and $260\text{ }^{\circ}\text{C}$, two consecutive peaks were observed. These are possibly thermal degradation peaks of the polymeric materials available in the coating formulation. Above these temperature, it can be easily expected that, coating material will lost its adhesion characteristics when thermal degradation of the coating material is completed.

As the summary, all the results of the surface characteristic are compatible with each other. Each one in itself exhibited change at same temperature range, which is around $165\text{ }^{\circ}\text{C}$ for 8 min. Based on the STA curve, coating material is expected to perform

optimum adhesion up to 150 °C since polymeric materials are thermally degraded after this temperature.

In the second step of the study, cold plasma effect was evaluated in terms of interface adhesion characteristics on the un/treated and un/coated aluminum surfaces. Interface adhesion strength was measured by T-peel test. Surface properties were characterized by contact angle (CA) in terms of wettability. Moreover, functional structures occurred or changed on the surface was investigated by FTIR.

The wetting angle on the uncoated dry aluminum surface was reduced from $70^{\circ} \pm 5^{\circ}$ to $10^{\circ} \pm 3^{\circ}$ in a short time by plasma treatment. Initial contact angle of (Chemosil) coated aluminum surface has a hydrophobic surface characteristics. After plasma activation in 1sec. to 10 sec., incredible decrease occurred in contact angle. Contact angle measurement results show that the Chemosil wetting angle decreased from 90° to 10° . This demonstrates that plasma application on both uncoated and coated aluminum surfaces increases the wettability characteristics.

In the T-peel test, there was no adhesion observed on the sample surfaces of uncoated rigid and lanced aluminum, uncoated rigid and sand blasted aluminum, uncoated rigid and plasma treated aluminum. On the other hand, adhesion forces are quite high and the interface separation type is cohesion failure in EPDM on the Chemosil coated and Chemosil coated/plasma treated aluminum surfaces. When geometric separation patterns were examined, plasma treated surface exhibits central separation of EPDM; however, non-plasma treated surface exhibits random separation on each replicated samples. This finding was also demonstrated by EPDM coverage difference as $23,72 \pm 6 \%$ and $61,43 \pm 8 \%$ for untreated and plasma treated surfaces respectively. Moreover, EPDM coverage on the aluminum surfaces was demonstrated by FTIR analysis. The infrared peaks of the Chemosil coated aluminum surface before T-peel test and Chemosil coated aluminum surface after T-peel test do not overlap. On the other hand, infrared peaks of the EDPM and Chemosil coated aluminum surface after T-peel overlap around 100 %.

As the conclusion, cold plasma application to the coated aluminum surface changed the surface characteristics at nano-level, which improves the adhesion characteristics to the EPDM surface. Findings on CA, T-peel test and FTIR analysis demonstrated this improvement.

In the last step of the study, improved coating materials were characterized by different methods such as contact angle measurement, morphological appearance under microscope, surface roughness, T-peel test, weight change after T-peel test. Thereby, interface adhesion mechanism to the aluminum surface and EPDM based rubber was investigated.

Contact angle measurements illustrated that 3B and 4B have lower CA angle in comparison of others. The highest CA was achieved in 6B. Moreover, results were correlated with interface adhesion performances based on T-Peel test results. If the CA is around 40°s (3B and 4B), strong interface adhesion was provided between coating and EPDM based rubber. When CA increased up to 45°s (2B and 4A), intermediate strong adhesion was observed exception group 2A. An extraordinary situation has been observed on this coating type. Although, it has very high CA, intermediate strong adhesion was observed at the interface. This could be caused due to some chemical reactions occurred between contents of the coating mixture or EPDM and coating.

Morphological analysis of the coating materials illustrated different surface images in different structures. When the surfaces were examined in terms of porosity, 2A and 4A in the coating group A and 3B and 4B in the coating group B showed structure that is more porous. However, this porosity could not be correlated with T-peel test results.

Coating thickness measurements were applied to see how the different types of coating materials applied with the same method show the distribution in their coating thicknesses. Based on the results, 2B exhibited stable coating through the surface at

low deviations. 1A, 2A and 4B illustrated heterogeneous coating thickness through the surface at high deviations.

In the surface roughness analysis, 3B exhibited highest surface roughness values, the effect of surface roughness on interface adhesion could be taken into account. On the other hand, surface roughness value could not be an important parameter on the interface adhesion characteristics for 5B due to it has lowest surface roughness value.

Weight change and visual evaluation of the surfaces after T-peel tests were evaluated in correlation with T-Peel test results. 3A, 4A, 1B, 5B and 6B coatings remained as adhered to the AI interface after T-peel test. On the contrary, their weight change showed decrease except 5B after T-Peel test. This could be due to partial adhesion or some kind of reactions occurred during the pressing operation. Based on the T-peel test, 5B has the interface adhesion more than 100N. In case of coating-EPDM interface was evaluated, 3B and 5B coated AI surfaces have EPDM residues. This demonstrates that interface adhesion between coating and EPDM is strong. T-peel test verifies this result since the interface adhesion force has been found around 250 N for 5B. This high interface adhesion force is arising due to strong adhesion on both interfaces; AI-coating and coating-EPDM.

As the conclusion, 3A, 4A, 1B, 5B and 6B coating types have good adhesion to AI surface and they could be improved for adhesion to the EPDM. Moreover, 3B and 5B have good adhesion to EPDM surface and they could be improved for adhesion to the AI with some kind of surface treatment methods. Correspondingly, their surface characteristics could be defined for their processing parameters as it was done on Chemosil coating.

REFERENCES

- [1] Baldan A., 2012. Adhesion phenomena in bonded joints. *International Journal of Adhesion and Adhesives.*, 38: 95-116.
- [2] Grujicic M., Sellappan V., Omar M.A., Seyr N., Obieglo A., Erdmann M., Holzleitner J., 2008. An overview of the polymer-to-metal direct-adhesion hybrid technologies for load-bearing automotive components. *Journal of materials processing technology* 197: 363–373.
- [3] Crowther B., *Handbook of Rubber Bonding*, Rapra Technology Limited, 57-97, 2003.
- [4] Barnes T.A., Pashby I.R., 2000. Joining techniques for aluminium spaceframes used in automobiles Part II: adhesive bonding and mechanical fasteners., *Journal of Materials Processing Technology* 99: 72-79.
- [5] Borsellino C., Bella G. D., Ruisi V.F., 2009. Adhesive joining of aluminium AA6082: The effects of resin and surface treatment. *International Journal of Adhesion & Adhesives* 29: 36–44.
- [7] Lasprilla-Botero J., Alvarez-Lainez M., Acosta D. A., 2017. Water-based adhesive formulations for rubber to metal bonding developed by statistical design of experiments, *International journal adhesion and adhesives.*, 73: 58-65.
- [8] Souid A., Sarda A., Deterre R., Leroy E., 2015. Influence of reversion on adhesion in the rubber-to-metal vulcanization-bonding process., *Polymer testing.*, 41: 157-162.
- [9] Wang F., Xu J., Luo H., Wang J., and Wang Q. (2009). A new organofunctional ethoxysilane self-assembly monolayer for promoting adhesion of rubber to aluminum. *Molecules*, 14, 4087-4097.
- [10] Roucoules V., Siffer F., Ponche A., Egurrola U. & Vallat M. (2007). Strengthening the junction between EPDM and aluminium substrate via plasma polymerisation. *The Journal of Adhesion*, 83, 875–895.

- [11] Airoudj A., Schrodj G., Vallat M., Fioux P., Roucoules V. (2011). Influence of plasma duty cycle during plasma polymerization in adhesive bonding. *International Journal of Adhesion & Adhesives* 31, 498–506.
- [12] Roucoules V., Siffer F., Ponche A., Vallat M.F. Functionalized surfaces by plasma polymerization : A new strategy to reach reversible adhesion between two substrates. Institut de Chimie des Surfaces et Interfaces, C.N.R.S. - UPR 9069 and University of Haute-Alsace 15, Rue Jean Starcky 68057 Mulhouse Cedex, France.
- [13] Kang Z., Zhong C., Wang F., Li Y., Hirahara H., Mori K. (2007). Joining property of EPDM rubber/ cast iron adherend by functional polymeric nanofilm. *Proceedings of MNC2007 micronano China07*, 10-13.
- [14] Petersen J., Fouquet T., Michel M., Toniazzo V., Dinia A., Ruch D., Bomfim J. A. S. (2012). Enhanced adhesion over aluminum solid substrates by controlled atmospheric plasma deposition of amine-rich primers. *ACS Appl. Mater. Interfaces*, 4, 1072–1079.
- [15] Batan A., Brusciotti F., De Graeve I., Vereecken J., Wenkin M., Piens M., Pireaux J.J., Reniers F., Terryn H. (2010). Comparison between wet deposition and plasma deposition of silane coatings on aluminum. *Progress in Organic Coatings*, 69, 126-132.
- [16] Diaz B., Velasco F. (2013). Atmospheric plasma torch treatment of aluminum: improvement wettability of silanes. *Applied surface science*, 287, 263-269.
- [17] Saleema N., Gallant D. (2013). Atmospheric pressure plasma oxidation of AA6061-T6 aluminum alloy surface for strong and durable adhesive bonding applications. *Applied Surface Science* 282, 98-104.
- [18] Williams T. S., Yu H., Hicks R. F. (2014). Atmospheric pressure plasma activation as a surface pre-treatment for the adhesive bonding of aluminum 2024. *Journal of Adhesion Science and Technology*, Vol. 28, No. 7, 653–674.
- [19] Sperandio C., Bardon J., Laachachi A., Aubriet H., Ruch D. (2010). Influence of plasma surface treatment on bond strength behavior of an adhesively bonded aluminum-epoxy system. *International Journal of Adhesion & Adhesives* 30 720–728.
- [20] Ueda R. H. T., Brandao L. C., Lauro C. H. (2010). Analysis of automotive liftgate seals using finite element analysis. *Polímeros*, vol. 20, n° 4, p. 301-308.
- [21] Dick J. S., *Rubber Technology Compounding and Testing for Performance*, Hanser Publishers, 190-502, 2001.
- [22] Massey L. K., *The Effect of UV Light and Weather on Plastics and Elastomers*. Elsevier Inc., 299-369, 2013

- [23] Ebnesajjad S., Ebnesajjad C., Surface Treatment of Materials for Adhesive, Second Edition, William Andrew, 210-286, 2006.
- [24] Rodgers B., Waddell W., The Science of Rubber Compounding. Elsevier Inc., 417-471, 2013.
- [25] Grigore C. B., Coiffet P., Virtual education in rubber technology. Virtual Reality Technology., 174-245, 2007.
- [26] McKeen L. W., The Effect of Long Term Thermal Exposure on Plastics and Elastomers. Elsevier Inc., 1-15, 2014.
- [27] Polaski G., Means J., Stull B., Bonding Elastomers: A Review of Adhesives and Processes, Smithers Rapra Publishing, 103-174, 2005.
- [28] GMW14168, Elastomeric Seals for Glass Sealing, Flocked or Coated (2012).
- [29] Milani G., Milani F. (2013). Kinetic finite element model to optimize sulfur vulcanization: application to extruded EPDM weather-strips. Polymer engineering and science.
- [30] Cho J.R., Han K.C., Kim J.S., Lee S.B., Lim O.K. (2012). Fatigue life prediction and optimum topology design of EPDM weather strip. Finite Elements in Analysis and Design 60, 57–63.
- [31] Picard L., Phalip P., Fleury E., Ganachaud F., 2015. Progress in Organic Coatings., 80: 120-141.
- [32] Thomas, Development of a New Adhesion Promoter for Metal Adhesion on Polymer Substrates for Printed Circuit Board Production Using Functionalized Silica Nanoparticles. Freie Universität, Department of Biology, Chemistry and Pharmacy, Doctor rerum naturalium, 2016.
- [33] Mui T.S.M., Silva L.L.G., Prysiashnyi V., Kostov K.G., 2017. Surface modification of aluminium alloys by atmospheric pressure plasma treatments for enhancement of their adhesion properties. Surface & Coatings Technology 312: 32–36.
- [34] Tendero C., Tixier C., Tristant P., Desmaison J., Leprince P., 2006. Atmospheric pressure plasmas: A review. Spectrochimica Acta Part B 61: 2 – 30.
- [35] Bogaerts A., Neyts E., Gijbels R., Mullen J., 2002. Gas discharge plasmas and their applications. Spectrochimica Acta Part B 57: 609–658.
- [36] Brunelli K., Pezzato L., Napolitani E., Gross S., Magrini M., Dabalà M., 2014. Effects of atmospheric pressure plasma JET treatment on aluminium alloys. Surface Engineering, 30: 636-642.

- [37] Bárdos L., Baránková H., 2010. Cold atmospheric plasma: Sources, processes, and applications. *Thin Solid Films* 518: 6705–6713.
- [38] Merche D., Vandecasteele N., Reniers F., 2012. Atmospheric plasmas for thin film deposition: A critical review. *Thin Solid Films* 520: 4219–4236.
- [39] Bensebaa F., *Interface Science and Technology*. Elsevier Ltd., 1-84, 2013.
- [40] Bauer F., Decker U., Ernst H., Findeisen M., Langguth H., 2006. Functionalized inorganic/organic nanocomposites as new basic raw materials for adhesives and sealants Part 2. *International Journal of Adhesion & Adhesives*, 26: 567–570.
- [41] Zhai L., Ling G., Li J., Wang Y., 2006. The effect of nanoparticles on the adhesion of epoxy adhesive. *Materials Letters* 60: 3031–3033.
- [42] Mohseni M., Mirabedini M., Hashemi M., Thompson G. E., 2006. Adhesion performance of an epoxy clear coat on aluminum alloy in the presence of vinyl and amino-silane primers. *Progress in Organic Coatings* 57: 307–313.

RESUME

Fatma Mıhçı was born in Düzce in 15.09.1988. She has completed pre, middle and high school in Düzce. She graduated from Chemistry Department in Sakarya University in 2012. She enrolled to Umea University in Sweden as Erasmus student in 2011. Her bachelor thesis is about water isotherms of Hydrophilic interaction liquid chromatography (HILIC). She has defended her bachelor thesis in Umea University and graduated by Umea University too. She has started to her carrier as auditor in a Textile Company located in Düzce. Then, she has started to work in her current company Standard Profile since 2012. Since 2012, she has taken different roles in the department of Quality. She has started to work as Laboratory Responsible and then she has promoted to different positions: Laboratory Project Responsible and currently Quality Project Engineer. During this time, she has managed more than 15 projects in different projects. Currently, she has been making master in the department of Nano Science and Nano Engineering in Sakarya University since 2013.